

**UNCLASSIFIED**

---

**AD 255 741**

*Reproduced  
by the*

**ARMED SERVICES TECHNICAL INFORMATION AGENCY  
ARLINGTON HALL STATION  
ARLINGTON 12, VIRGINIA**



---

**UNCLASSIFIED**

NOTICE: When government or other drawings, specifications or other data are used for any purpose other than in connection with a definitely related government procurement operation, the U. S. Government thereby incurs no responsibility, nor any obligation whatsoever; and the fact that the Government may have formulated, furnished, or in any way supplied the said drawings, specifications, or other data is not to be regarded by implication or otherwise as in any manner licensing the holder or any other person or corporation, or conveying any rights or permission to manufacture, use or sell any patented invention that may in any way be related thereto.

ARL-27

AD No. 25574

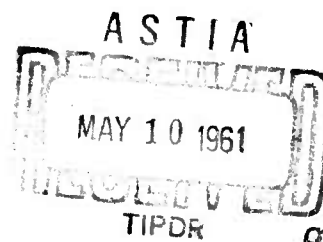
ASTIA FILE COPY

XEROX

**SOCIÉTÉ FRANÇAISE  
ÉTUDES ET DE RÉALISATIONS D'INVENTIONS  
COANDA**



7.60



12, RUE LÉON BLUM, CLICHY (Seine) - FRANCE

MONITORING AGENCY DOCUMENT Nr.

ASTIA DOCUMENT Nr.

ANALYSIS OF THRUST DUE TO THE COANDA PHENOMENON

Henri COANDA

"SFERI-COANDA", 12 rue Léon Blum  
Clichy (Seine) - France

---

TECHNICAL REPORT

Contract Nr. AF 61 (052) - 382

29 October, 1960

" The research reported in this document has been sponsored by

AIR FORCE OFFICE OF SCIENTIFIC RESEARCH

of the AIR RESEARCH AND DEVELOPMENT COMMAND, UNITED STATES AIR  
FORCE, through its European Office. "

## S U M M A R Y

The present report refers to the study of the flow in a Coanda nozzle (in different sections and along the walls) and the comparison between the effective thrust of the nozzle (directly measured on a thrust balance) and the thrust computed on the one hand from the local measurements of pressure forces on the walls, on the other hand from the velocities and pressures in terminal planes.

These tests show that the part located between the slot and the throat and called "lip" of the nozzle, is the active part of the Coanda nozzle.

## GENERAL DESCRIPTION AND OPERATING OF THE COANDA NOZZLE

Present Contract refers to a Coanda nozzle of the 70/84 type.  
(See Figure No. 1).

The important element of the nozzle is the convergent section.  
This convergent section is composed of two distinct parts :

- the first part is the entrance,
- the second part is the fixed lip with a special profile conducting the primary flow,

between these two parts lies an adjustable slot through which the primary air arrives from an annular chamber constructed around the convergent section and constituted by the two said parts screwed on into the other. To control the slot opening it is possible to loosen or tighten the top, or first part, which is therefore called the cap.

The divergent section is a simple conic element which completes the nozzle.

Compressed air is sent into the chamber of the nozzle and emerges from the slot (primary flow). This primary flow is determined by a given slot opening and a given pressure ratio, the air in the chamber being at ambient temperature. The jet of primary air follows the profile of the lip inducing a part of the surrounding air. The resulting mixture passes through the nozzle, the flow rate measured at the exit of the divergent section being the total flow (primary air + secondary air). The mass flow thus created exerts a force on the nozzle. The component of this force in the direction of the axis of the nozzle is called the THRUST (F).

# PURPOSE OF THE RESEARCH PROGRAM

The object of this survey is to analyse the thrust due to the Coanda Effect.

The tests have been performed on a Coanda nozzle of the 70/84 type with a given slot opening of 0.6 mm at two given pressures of primary air.

1.  $\frac{P_1 - P_0}{P_0} = 1.5$  (supersonic slot flow)
2.  $\frac{P_1 - P_0}{P_0} = 0.3$  (subsonic slot flow)

The measurements undertaken were as follows :

1. THRUST MEASUREMENTS F ON A BALANCE (exact value  $\pm 0.030$  kg.)
2. MEASUREMENTS OF STATIC PRESSURES ON THE WALLS - The projection Fx on the axis of the resultant of all the forces due to the pressure (we consider as positive the forces constituting thrust) permits a calculation of the total axial resultant of skin friction forces (Tw) which is the difference between Fx and F, F and Fx working in the same direction and Tw constituting a drag :

Algebraically,  $F = Fx + Tw$ .

The absolute experimental approximations for such measurements depend of the accuracy of the manometer reading that was about  $\pm 0.5$  mm on the mercury scale and  $\pm 1$  mm on the water scale, and during our best measurements the variation of the measured pressures was  $\pm 1.5$  mm of mercury and  $\pm 5$  mm of water, i.e., a total approximation of about :

for  $\frac{P_1 - P_0}{P_0} = 1.5$ , the approximation is  $\pm 0.300$  kg on Fx

for  $\frac{P_1 - P_0}{P_0} = 0.3$ , the approximation is  $\pm 0.170$  kg on Fx

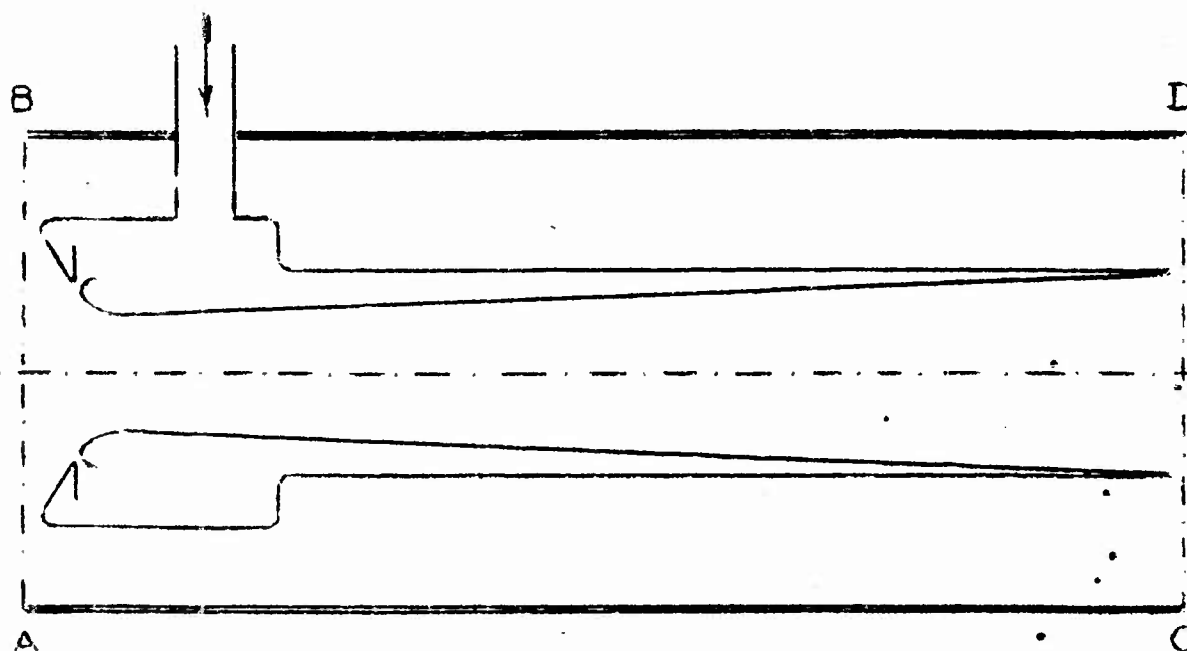
To this absolute approximation, we must add a relative approximation  $\pm 1\%$  due to the integration.

3. MEASUREMENTS IN PLANES I and VI substituted to the entrance plane and to the exit plane.

From measurements of temperatures, static and stagnation pressures, we calculate velocities.

To determine whether the Euler theorem can be applied to analyse the whole flow in such an apparatus, we chose a surface of control whose limits are a cylinder parallel to the axis of the nozzle and two planes AB and CD, perpendicular to the axis, located respectively immediately upstream of the entrance section and immediately downstream of the exit section.

(See Figure No. 2 below)



We determined in each one of these planes the term  $I = MV + PA$  momentum + forces due to the pressure in the jet. (\*)

The thrust calculated corresponds to the difference between  $I$  at exit section ( $I_{CD}$ ) and  $I$  at entrance section ( $I_{AB}$ ), that is to say :

$$F = I_{CD} - I_{AB}$$

(\*) See glossary of symbols - Page B.

After the first measurements made at the entrance section and at the exit section, with the nozzle operating both in an open room and with the nozzle exit section attached to a wall, we were led, neglecting the momentum of the surrounding air, to substitute for AB the section I at the entrance and to substitute for AC, section VI at the exit, because the approximation of the test measurements introduced a greater error than did the influence of the momentum of the surrounding air.

4. SAME MEASUREMENTS IN THE NOZZLE - PORTIONS I to II, II to III and III to VI.

Due to the difficulties of measurements in the section of the nozzle right where the slot lies, we came to separate the survey of the nozzle into 3 portions according to the schematic figure (Figure No. 1) limited by the internal walls of the nozzle and the sections I, II, III and VI, i.e. portion I to II, portion II to III, and portion III to VI, in order to compute separately all the conditions of the total flow :

1. In the convergent section just ahead of the slot or exit of primary air (Portion I to II)
2. In the second part of the convergent (total secondary air (Portion II to III)
3. In the divergent section (the mixture of primary and secondary air) (Portion III to VI).

5. THE SAME MEASUREMENTS WERE MADE IN SECTIONS IV and V, for a more complete survey of the divergent section.

Errors of approximation in measuring static pressure, stagnation pressure, thus in velocities, flow rate, momentum, pressure forces in the section : Due to the variation of the flow, it is not possible to consider a mean value of error on pressure measurements only. - Nevertheless, taking into account the error due to a possible mistake of  $3^\circ$  on the direction of the flow in I and II, the error due to the instability of pressures in III (2 to 3 mm Hg), and the error due to the instability of stagnation pressure in VI, let us admit an error of 3 % on the force PA, Q and V, and therefore greater error on the momentum MV.

## APPARATUS AND TECHNIQS OF MEASUREMENTS

### 1. INSTALLATION FOR MEASURING THRUST - PENDULAR SYSTEM (Figure No. 3)

This apparatus is of similar principle that the one used in the tests performed under Contract No. AF 61 (052) - 158. It consists of a hollow pendular device connected with a balance capable of measuring stresses. (This hollow pendular device has been lengthened so as to increase considerably the sensitivity of the whole system (1.50 m. to 2.50 m).)

The hollow pendular device itself is connected with the feed source of the pressurised fluid, which fluid passes through calibrated flowmeters, and the amount of the fluid (air) coming from the feed is controllable in quantity as well as in pressure by a system of valves. Pressure and temperature gauges complete the installation (See Figure No. 3 - General Installation).

In such a system it was absolutely necessary to be precise with the articulation D (Figure No. 4) so that it would be completely tight, to be extremely sensitive. The compressed air is fed through a lateral inlet (1) into a fixed central tube (2) rigidly fixed on two supports (3). On to this axial tube through which a hole (4) is made, a second tube (5) is placed at the center of which the hollow shaft (6) of the pendulum is attached. The first tube had on its periphery a series of annular grooves (7) which in conjunction with the interior of the second tube (5) are used as expansion chambers (8). Some of these expansion chambers are fitted with (9) floating bronze piston rings. On the right and on the left of the hole, through which the air comes to the shaft of the pendulum (6) are two lubrication points (10).

The apparatus can constantly be brought back to zero, in order to ensure the measurements of greatest accuracy. The zero reading was obtained by the installation of tell-tale red and blue lights which are mounted directly on an arm tightened to the perpendicular re-set, so as to ensure the verticality of the vertical arm tightened to the scale by means of a magnet.

We checked the balance accuracy: the nozzle being at rest, we created an artificial thrust by means of various loads acting on the nozzle through a nylon string on a pulley used as a frictionless perpendicular re-set. The whole system is constantly brought back to zero as with real thrust. The checks were made with increasing and then decreasing loads. This checking states that our thrust measurements are performed with an accuracy of  $\pm 0.030$  kg.

## 2. INSTALLATION FOR MEASURING STATIC PRESSURES ON THE WALL.

We determined on a first nozzle all the pressures pick ups for the survey of the skin pressures,

- all the points of measurements of the static internal pressures along the walls are reported on the general view Figure No. 5. Special view of these connections on the cap and on the lip are shown on Figure No. 6.
- all the points of measurements of the external skin pressures are shown on general view Figure No. 5 (four circular grooves were formed, in each of which two diametrically opposed holes were drilled, one for opening the chamber to the surrounding air, one connected to the pressures gauges).

## 3. INSTALLATION FOR MEASURING STATIC PRESSURES AND STAGNATION PRESSURES IN THE TEST SECTIONS, on a second nozzle.

Pressure probes were made by the E.N.S.A. Laboratory.

Total pressure probes of appropriate geometry permit a determination of both characteristics of the velocity : magnitude and direction.

- For the planes I and VI a special apparatus is constructed with a circular groove on which a special device is able to move the pressure probes millimeter by millimeter with great accuracy so that it is possible to know exactly the point where the measurements are made.

This special device itself can move in the circular groove around the section. (See Figures No. 7 and 7bis).

- For the survey of planes II and III, it was necessary to drill the body of the nozzle to accommodate a large pipe so as to be able to introduce the special apparatus necessary for the survey of the flow inside of the nozzle.

The hole is slightly downstream of the throat in order to introduce a tube inside of which the pressure probes and thermocouples should be introduced to study the flow at the slot and at the throat without disturbing the flow.

Outside of the nozzle the same special device is mounted to move millimeter by millimeter the pressure probes and thermocouples (See Figure No. 7).

- For the planes IV and V, the installation for measurements is the same. (See Figure No. 7).

#### 4. INSTALLATION FOR MEASURING TEMPERATURES.

The thermocouples are Constantan and Manganin wires (1/10 mm). Measurements are recorded by apparatus Kipp Micrograph E.D.3.

As noted above for pressure measurements, a special device was used capable of moving thermocouples millimeter by millimeter with great accuracy (See Figure No. 7)

In plane II<sup>o</sup> other total and static pressure probes and thermocouples were fitted so as to study the jet flow near the wall in proximity of the slot section, but due to the discontinuity of the jet flow in that section all pressures measurements were so much disturbed by the presence of the probes that the resultant measurements must be considered invalid.

However, for the temperature measurements, it was possible to introduce the thermocouples by the entrance, and due to the very small size of the apparatus a good measurement of temperatures was possible.

In plane VI the flow rate of the flow was irregularly distributed and we have surveyed several diameters to obtain the mean value of these measurements.

## RESULTS OF THE INVESTIGATION OF THE FLOW IN VARIOUS PLANES

It is to be noted that all tests were performed at the same slot opening  $b = 0.60$  mm with two feeding pressures  $P_1$ , such that :

$$\frac{P_1 - P_0}{P_0} = \begin{cases} 1.5 & \text{corresponding to primary flow rate } Q_1 = 93 \text{ l/sec.} \\ 0.3 & \text{corresponding to primary flow rate } Q_1 = 38 \text{ l/sec.} \end{cases}$$

at ambient conditions ( $T_0 = P_0$ )

### I. TEMPERATURES MEASUREMENTS.

At first we began by the temperature measurements as we had to know these values for all pressure measurements. Moreover the temperature measurements are the only ones available in plane II' where the slot lies. Due to the construction we measured essentially stagnation temperature through internal sections except for the slot where we could operate in good conditions by introducing thermocouples by the entrance.

In plane II' of the slot, the curve Figure No. 8 points out the masses of air of primary and secondary flow. It is obvious that near the wall, the presence of the wall itself leads us to an important error on the temperature measurements in the jet flow.

In plane III (throat), the temperature measurements are measurements of stagnation temperature (Figure No. 9). From the pressure measurements, we determined the corresponding static temperature (Figure No. 10).

On the whole, these measurements show that the variations of temperature in planes I (entrance), II (convergent section), IV and V (divergent sections), VI (exit), may be neglected, because the errors noticed are lower than the difference between the temperature in the feeding chamber and the surrounding temperature (mean value =  $0.5^\circ\text{C}$ ).

## 2. MEASUREMENTS OF STATIC and STAGNATION PRESSURES IN THE FLOW

Preliminary tests with and without a wall at the exit section had shown that it was not necessary to perform these measurements with a wall attached at the exit section. The curves showing the variations of the effective static pressure plotted versus the radii are reported on figure No. 11 (section I) to figure No. 16 (section VI).

(Concerning the possible errors on these values, see pages No. 4 & 6).

## 3. VELOCITY CALCULATION

The general aspect of the flow in the nozzle is shown Figure No. 17.

The velocities  $V$  have been calculated from the pressure measurements (static and stagnation) and from temperature measurements. - For low velocities (Mach number  $M \leq 0.3$ ) a simplified Bernoulli formula was used :

$$\frac{\Delta}{g} \frac{v^2}{2} = P_t - P_s$$

For higher velocities (Mach number  $M \geq 0.3$ ) the Saint-Venant formula was used :

$$\frac{P_t}{P_s} = \left[ 1 + \frac{\gamma - 1}{2} M^2 \right]^{\frac{\gamma}{\gamma - 1}}$$

The Saint-Venant formula was used in Planes III and IV.

The curves showing the velocities plotted versus the radii are reported on Figure No. 18 (section I) to Figure No. 23 (section VI)

Figure No. 23bis shows the variation of velocities on a diameter of section VI, the nozzle operating in an open room, and the nozzle having the exit section attached to a wall.

The curves (Figures No. 18 to 23) showing the variation of velocities and the curves (Figures No. 11 to No. 16) showing the variation of static pressure have approximately the same general aspect. In sections I and II where stagnation pressure is constant and equal to the atmospheric pressure, velocities are reciprocal to the square root of static pressures. - However, in section VI where the variations of static pressure are very small and about zero (always  $< 2g./cm^2$ ) the velocity varies with the square root of stagnation pressure, which explains the different aspect of Figures No. 16 and No. 23.

#### 4. FLOW RATE CALCULATION.

Before other calculations we consider as essential to confirm the validity of our measurements by applying the fundamental continuity formula. If we assume that the primary flow rate  $Q_1$  is perfectly known (absolute value of error  $\leq \frac{1}{2}\%$ ),  $Q_1$  being the primary flow rate corrected at the surrounding conditions  $P_0$   $T_0$ , and if we measure the flow rates in the various sections (corrected at the surrounding conditions :  $D_I$  in section I,  $D_{II}$  in section II,  $D_{III}$  in section III,  $D_{IV}$  in section IV,  $D_V$  in section V,  $D_{VI}$  in section VI), the continuity formula is to be written :

$$D_I = D_{II} = D_{III} = Q_1 = D_{IV} = Q_1 = D_V = Q_1 = D_{VI} = Q_1$$

To calculate these flow rates we were led to draw the curves  $V$  plotted versus  $R^2$ , whence we compute by graphic summing up the flow rate as

$$D = \int_{R=0}^{R=R_m} \frac{\Delta}{\Delta_0} V 2\pi R dR$$

where  $\Delta$  and  $\Delta_0$  are the specific weights respectively at local conditions and at surrounding conditions. See curves Figure No.24 for section I to figure No. 29 for section VI.

The following table gives the results of the computation of the mean value of the total flow rate in l/sec. at surrounding conditions ( $P_0$   $T_0$ ).

We were able to determine the induction ratio  $\rho$  which is the ratio of  $Q_2$  to  $Q_1$ , i.e.,  $\rho = \frac{Q_2}{Q_1}$

$\frac{P_1 - P_0}{P_0}$	$Q_1$ l/s	$D_I$ l/s	$D_{II}$ l/s	$D_{III} - Q_1$ l/s	$D_{IV} - Q_1^*$ l/s	$D_V - Q_1^*$ l/s	$D_{VI} - Q_1$ l/s	$Q_2$ l/s	$\rho$
1.5	93	616	606	599	631	607	635	617	7.6
0.3	38	297	287	291	308	282	303	292	8.7

\* - In these two planes, which are in the divergent section, the error can be greater and can reach 4 % as the flow begins to be less regular and it was only possible to take measurements on one diameter.

- In planes III and VI, the errors are of the same magnitude as in plane I and II, i.e. about 3 % .

## 5. CALCULATION OF MOMENTUM MV AND OF PRESSURES FORCES PA

We have computed in each section the terms MV and PA with a view to compare the variation of the term I with the resultant of the forces due to the pressure exerted on the walls between two sections (See page No. 6)

These curves are represented on Figures No. 30 to 4I, in which the values corresponding to the variation of  $P_s - P_o$  plotted versus the square of the radii are respectively plotted on the drawings Figures No. 30 to 35 for the sections I to VI, and the variation of the term  $\frac{A}{A_o} V^2$  plotted versus the square of the radii are on the drawings Figures No. 36 to No. 4I for the section I to VI which gives for MV, PA, I, the following table :

	$\frac{P_s - P_o}{P_o}$	MV	PA	I
I	1.5	+ 2.750 kg	- 2.180 kg	+ 0.570 kg
II	1.5	+ 4.750 kg	- 3.290 kg	+ 1.460 kg
III	1.5	+ 16.930 kg	- 6.570 kg	+ 10.360 kg
IV	1.5	+ 11.850 kg	- 3.175 kg	+ 8.675 kg *
V	1.5	+ 7.985 kg	- 1.720 kg	+ 6.265 kg *
VI	1.5	+ 6.460 kg	- 0.170 kg	+ 6.290 kg
I	0.3	+ 0.620 kg	- 0.530 kg	+ 0.090 kg
II	0.3	+ 1.053 kg	- 0.775 kg	+ 0.280 kg
III	0.3	+ 4.130 kg	- 1.155 kg	+ 2.975 kg
IV	0.3	+ 2.500 kg	- 0.710 kg	+ 1.790 kg *
V	0.3	+ 1.670 kg	- 0.420 kg	+ 1.250 kg *
VI	0.3	+ 1.580 kg	- 0.060 kg	+ 1.520 kg

\* for sections IV and V see notice Page No. 12.

Bearing in mind the calculated error in each plane these results are valid with approximation of 3 % on PA and 6 % on MV in the sections I, II, III, VI, and 4 % on PA and 8 % on MV in the sections IV and V.

## RESULTS AND THEIR DISCUSSIONS

### I. THRUST MEASUREMENTS ON THE BALANCE

The results of these measurements are made with an approximation of  $\pm 0.03$  kg.

b = 0.60 mm				
$\frac{P_1 - P_0}{P_0}$	$Q_1$ read l/s	$Q_1$ corrected	$T_r$	" a "
1.5	128.5	92.9	5.520	1.32
I.	112.5	72.3	4.000	1.38
0.75	98	59.1	3.140	1.46
0.5	87	48.5	2.200	1.45
0.3	72.5	37.7	1.400	1.46
0.1	47	22.4	0.540	1.57

We chose, for the other measurements, only two feeding pressures :

$$\frac{P_1 - P_0}{P_0} = 1.5 \text{ and } 0.3$$

2. INTERNAL AND EXTERNAL SKIN PRESSURES on the walls and evaluation of the axial resultant forces Fx of these pressure forces.

Preliminary tests had shown that the surrounding flow was not measurable.

Figure No. 42 shows a general view of the distribution of the pressures along the internal profile of the nozzle.

Figure No. 43 is a detailed view showing how pressures are distributed along the lip profile.

On Figures No. 44, 45 and 45bis, 46 and 46bis, effective pressures  $P_w - P_o$  are plotted versus the square of the distance from the walls to the axis, the elementary forces will be positive if exerted in the direction of the thrust. The area included between the horizontal axis and the curves is reciprocal to the resultant  $F_x$ , elementary forces due to the pressures exerted : on the cap Figure No. 44, on the lip Figures No. 45 and 45bis, on the divergent section Figures No. 46 and 46bis.

The results are :

Curves	$\frac{P_1 - P_o}{P_o}$	Portion	Resultant $F_x$
I0 I0 bis	$\begin{matrix} 1.5 \\ 0.3 \end{matrix}$	cap	$\begin{pmatrix} + 1.310 \text{ kg} \\ + 0.380 \text{ kg} \end{pmatrix}$
I1 II bis	$\begin{matrix} 1.5 \\ 0.3 \end{matrix}$	lip	$\begin{pmatrix} + 8.6 \text{ kg} \\ + 1.970 \text{ kg} \end{pmatrix}$
I2 I2 bis	$\begin{matrix} 1.5 \\ 0.3 \end{matrix}$	divergent	$\begin{pmatrix} - 3.170 \text{ kg} \\ - 0.660 \text{ kg} \end{pmatrix}$

Taking into account the possible errors on these measurements (See page No. 4) we compare the total results  $F_x$  with thrust  $F$  measured on the balance, calculating  $T_w = F_x - F$ .

$\frac{P_1 - P_o}{P_o}$	F in kg	$F_x$ in kg	$T_w$ in kg
1.5	$5.520 \pm 0.030$	$6.740 \pm 0.300$	$1.220 \pm 0.330$
0.3	$1.400 \pm 0.030$	$1.690 \pm 0.170$	$0.290 \pm 0.200$

3. ANALYSIS OF THE THRUST in the whole nozzle in terms of variation of  $I$  (momentum + pressure forces)

From the value of  $I = MV + PA$  given Page No. I3 we calculate the variation  $\Delta I$  between the entrance section I and the exit section VI which gives the following values which we compare with the values of thrust measured on the balance.

In this portion we have :

$\frac{P_1 - P_0}{P_0}$	$\Delta I =$ variation of $I$ kg between I and VI	$F$ kg	Difference $\Delta I - F$		$F_x$ kg	$T_w = F - F_x$	
			in kg	in terms of $F$		in kg	in terms of $F_x$
I.5	+ 5.720	5.520	0.200	4 %	6.740	- 1.220	20 %
0.3	+ 1.430	1.400	0.030	2 %	1.690	- 0.290	17 %

4. ANALYSIS OF THE THRUST IN THE THREE BASIC PORTIONS I II, II III, III VI, in terms of variations of  $I$  ( $\Delta I$ ) between two successive sections which give the following value which may be compared with the values of thrust measured on the balance.

$\frac{P_1 - P_0}{P_0}$	Portions	$\Delta I$ Variation of $I$ between the terminal planes of the portion kg	$F_x$ kg
1.5	{ Portion I VI	+ 5.720	+ 6.740
	{ Portion I II	+ 0.890	+ 0.870
	{ Portion II III	+ 8.900	+ 9.040
	{ Portion III VI	- 4.070	- 3.170
0.3	{ Portion I VI	+ 1.430	+ 1.690
	{ Portion I II	+ 0.190	+ 0.260
	{ Portion II III	+ 2.695	+ 2.090
	{ Portion III VI	- 1.455	- 0.660

Considering that  $\Delta I$  is a fair approximation of  $F$ , the difference  $F_x - \Delta I$  shows that losses due to friction are found essentially in the divergent section.

### CONCLUDING REMARKS

From all the research program carried out in the present contract we can conclude that, in fact we have made a complete investigation on the air flow through a Coanda nozzle; this study points out the two following characteristics : the induction ratio and the thrust augmentation ratio.

- I. Regarding the measurements, it is necessary to notice that all the measurements (no matter what sort of measurements) have a remarkable concordance. However, the work in itself on the Coanda nozzle chosen was not at all easy. Indeed the tests as required by the contract, were performed on a Coanda nozzle 70/84 of an improved type and this for the thrust purpose but with a throat of cross section of small size (diameter  $\phi$  70 mm). In spite of this small dimension, the tests have been performed with a great accuracy due to the sensitivity of all the instruments, more peculiarly of the specially improved balance, and to the great carefulness brought for the measurements and the general observations.
2. If we consider the very encouraging results obtained, it appears that it would be quite important to ascertain the real theory of such nozzles. But, this will need an important study, which would require a special team well trained in aerodynamic and this during a fairly long time. The research would have to be done on nozzles of various dimensions having a perfect geometrical similitude.

3. It had been also observed that the flow at the exit is still distorted, as the primary and the secondary flow seen not to be completely mixed. Consequently it did appeared to us that it could be necessary to improve the mixing, wether by acting on the divergent section length or by adding a new mass of surrounding air. We have therefore fixed at the exit section a single bell (with divergent angle of  $2^\circ$ ) and we then obtained the following thrust augmentation ratio.

NOZZLE 70/84 TYPE

+ a single bell removed at 150 mm. downstream  
the exit section.

b = 0.60 mm				
$\frac{P_1 - P_0}{P_0}$	$Q_1$ read l/s	$Q_1$ corrected	Tr	" a "
1.5	122.5	88.56	6.220	1.55
1	105	67.5	4.460	1.64
0.75	94	56.7	3.500	1.69
0.5	83.5	46.5	2.400	1.65
0.3	70	36.4	1.560	1.68
0.1	46	21.9	0.580	1.72

This puts in evidence that the contact surfaces, between primary and secondary air flow, are not in accordance and that is, probably, due to the small size of the throat section in regard of the lip surface for a given volume of primary air flow.

4. It appears also from our very careful investigations specially on the skin pressure measurements, that the lip is the part of the nozzle producing the maximum of the thrust, and that the divergent section is producing a drag working in the opposite direction.

We have also observed that the divergent section is producing nearly the totality of the losses due to the skin friction.

All this bring us to consider that it seems of great importance to increase the diameter for a given length of the divergent section.

In any case the above considerations show clearly the necessity for more systematic investigations.

This studies has been performed by the SFERI-COANDA team.

#### A C K N O W L E D G E M E N T

This research program and the preparation of the Report were carried out with very valuable supervision of Professor E.A. BRUN, de la Faculté des Sciences de Paris, and using facilities made available by Mr. LEBRUN, Chef du Laboratoire d'Aérodynamique de E.N.S.A., who supervised the tests which were conducted in that Laboratory.

# LIST OF CONTENTS

## Pages

A	Glossary of symbols
B	List of illustrations
2	Summary
3	General description and operating of the Coanda nozzle
4	Purpose of the Research Program
4	1. Thrust measurements F on a balance (exact value $\pm 0.030$ kg)
4	2. Measurements of static pressures on the walls
5	3. Measurements in planes I and VI
6	4. Same measurements in the nozzle - Portions I to II, II to III, and III to VI.
6	5. The same measurements were made in sections VI and V, for a more complete survey of the divergent section.
7	Apparatus and Technics of Measurements
7	1. Installation for measuring thrust - Pendular system
8	2. Installation for measuring static pressures on the wall
8	3. Installation for measuring static pressures and stagnation pressures in the test sections
9	4. Installation for measuring temperatures
10	Results of the investigation of the flow in various planes
10	1. Temperature measurements
11	2. Measurements of static and stagnation pressures in the flow
11	3. Velocity calculation
12	4. Flow rate calculation
13	5. Calculation of momentum MV and of pressures forces PA

Pages

I4	<b>Results and their discussions</b>
I4	1. Thrust measurements on the balance
I5	2. Internal and external skin pressures on the walls and evaluation of the axial resultant forces $F_x$ of these pressure forces
I6	3. Analysis of the thrust in the whole nozzle in terms of variation of $I$ (momentum + pressure forces)
I7	4. Analysis of the thrust in the three basic portions I II, II III, III VI, in terms of variations of $I$ ( $\Delta I$ )
I8	<b>Concluding remarks.</b>

---

# GLOSSARY OF SYMBOLS

a Thrust coefficient =  $\frac{F}{F_o}$

b Slot opening

D General term for air flow rate, corrected for  $P_o$ , To subscript 1 to VI = flow rate through said plane

$$D = \int_{A=0}^{A=\pi R_m^2} \frac{\Delta}{\Delta_o} V dA = \pi \int_{R=0}^{R=R_m} \frac{V \Delta}{\Delta_o} 2R dR$$

dA Surface differential element for a surface limited by R and R + dR  
 $dA = 2 \pi R dR$

dm mass differential element for a cylindrical ring, limited by R and R + dR, length V  
 $dm = 2 \pi \frac{\Delta}{g} V R dR$

dR Radius element

F Thrust developed by the nozzle and directly measured

Fo Theoretical thrust obtained with simple isentropic nozzle

$$F_o = \frac{\Delta}{g} Q_1 U_o \sqrt{\frac{2}{\gamma-1} \left[ 1 - \left( \frac{P_1}{P_o} \right)^{-\frac{\gamma-1}{\gamma}} \right]}$$

Fx Resultant on the axis of the forces due to the pressures on the walls

g acceleration due to the gravity = 9.81 m/sec<sup>2</sup>

h distance from the wall to the axis.  $h = R_m$

I MV + PA

M Mach number

MV General term for momentum

$$MV = \int_{R=0}^{R=R_m} \frac{\Delta}{g} V^2 2\pi R dR$$

PA General term for

$$\int_{R=0}^{R=R_m} (P_s - P_o) dA = \int_{R=0}^{R=R_m} (P_s - P_o) 2\pi R dR$$

P General term for pressure

Po Atmospheric pressure

P1 Pressure of feeding (primary) air

Ps Static pressure in the jet

Pt Stagnation pressure in the jet

Pw Pressure along the skin

Q1 Primary air flow rate, corrected for Po, To

Q2 Total air flow rate, corrected for Po, To

R Radius

Rm Maximum value of R in a section, Rm = h

Tw Skin friction losses

T General term for temperature

Ts Static temperature

Tt Stagnation temperature

To Ambient temperature

Tch Temperature in chamber, generally equal to To

U	Local sound velocity
U <sub>o</sub>	Sound velocity at ambient temperature T <sub>o</sub>
V	Velocity
$\Delta$	Local specific weight of air
$\Delta_o$	Specific weight of air for P <sub>o</sub> , T <sub>o</sub>
$\Delta I$	Variation of I, between two sections
$\gamma$	Ratio of specific heats, here $\gamma = 1.4$
$\rho$	Induction ratio = $\frac{Q_2}{Q_1}$

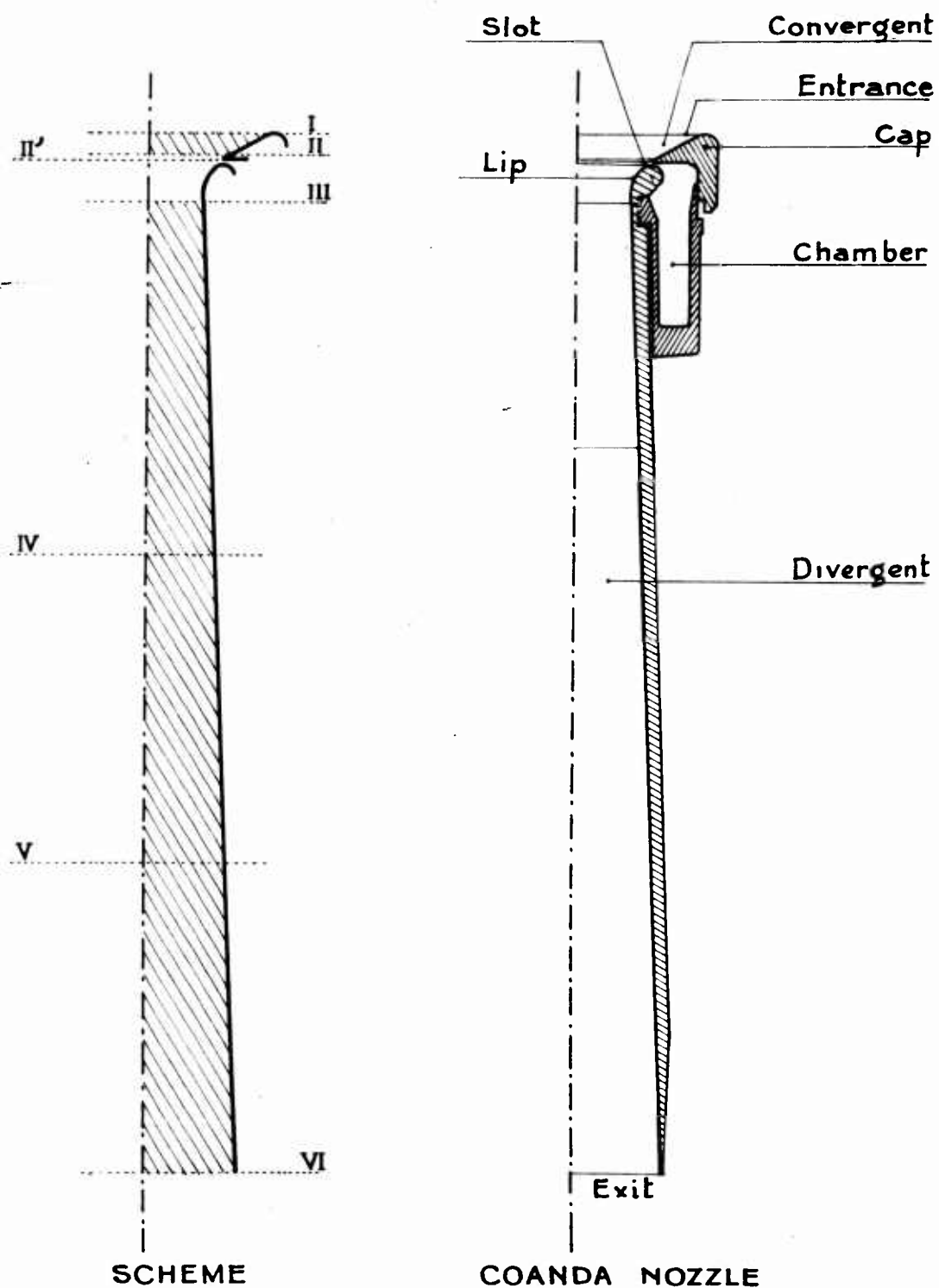
LIST OF ILLUSTRATIONS
-----------------------

No. of Figures	T i t l e
1	General description of a Coanda nozzle
2	Schematic of the entrance and exit planes of survey
3	Pendular system for measuring thrust
3bis	Photograph of pendular system
4	Detail of 3 - Articulation D
5	View of the points of measurements of the static internal and external skin pressures
6	Detail of 5 - Points of measurement on the lip
7	Special device for introducing the measurement instruments
7bis } 7ter }	Photographs of 7 mounted on the nozzle - General view
8	Static temperatures ( $T_s - T_{ch}$ ) in section II' (slot) plotted versus radii R
9	Stagnation temperatures ( $T_t - T_{ch}$ ) in section III (throat) plotted versus radii R
10	Static temperatures ( $T_s - T_{ch}$ ) in section III (throat) plotted versus radii R
<u>11 to 16</u>	Effective pressure ( $P_s - P_o$ ) plotted versus radii R
11	Section I
12	Section II
13	Section III
14	Section IV
15	Section V
16	Section VI

No. of Figures	T i t l e ( continued )
I7	General aspect of the flow
<u>I8 to 23</u>	Velocities V plotted versus radii R
I8	Section I (velocities projected on the axis)
I8bis	Section I (velocities and their projection)
I9	Section II (velocities projected on the axis)
20	Section III
21	Section IV
22	Section V
23	Section VI - mean value
23bis	Section VI on a diameter with and without a wall attached at the exit section
<u>24 to 29</u>	Computation of the corrected flow rate : $V \frac{\Delta}{\Delta_0}$ plotted versus $R^2$
24	Section I
25	Section II
26	Section III
27	Section IV
28	Section V
29	Section VI
<u>30 to 35</u>	Calculation of PA : $(P_s - P_o)$ plotted versus $R^2$
30	Section I
31	Section II
32	Section III
33	Section IV
34	Section V
35	Section VI

No. of Figures	T i t l e ( continued )
<u>36 to 4Ibis</u>	Calculation of $MV: v^2 \frac{\Delta}{\Delta_0}$ plotted versus $R^2$
36	Section I
37	Section II
38	Section III
39	Section IV
40	Section V
4I	Section VI
42	General view of the distribution of the pressure along the internal profile of the nozzle
43	Detail of Figure No. 42, along the lip profile
<u>44 to 46bis</u>	Effective pressures ( $P_w - P_0$ ) plotted versus the square of the distance from the wall to the axis
44	on the cap $\frac{P_1 - P_0}{P_0} = 1.5$ and $0.3$
45	on the lip $\frac{P_1 - P_0}{P_0} = \begin{cases} 1.5 \\ 0.3 \end{cases}$
45bis	
46	on the divergent $\frac{P_1 - P_0}{P_0} = \begin{cases} 1.5 \\ 0.3 \end{cases}$
46bis	

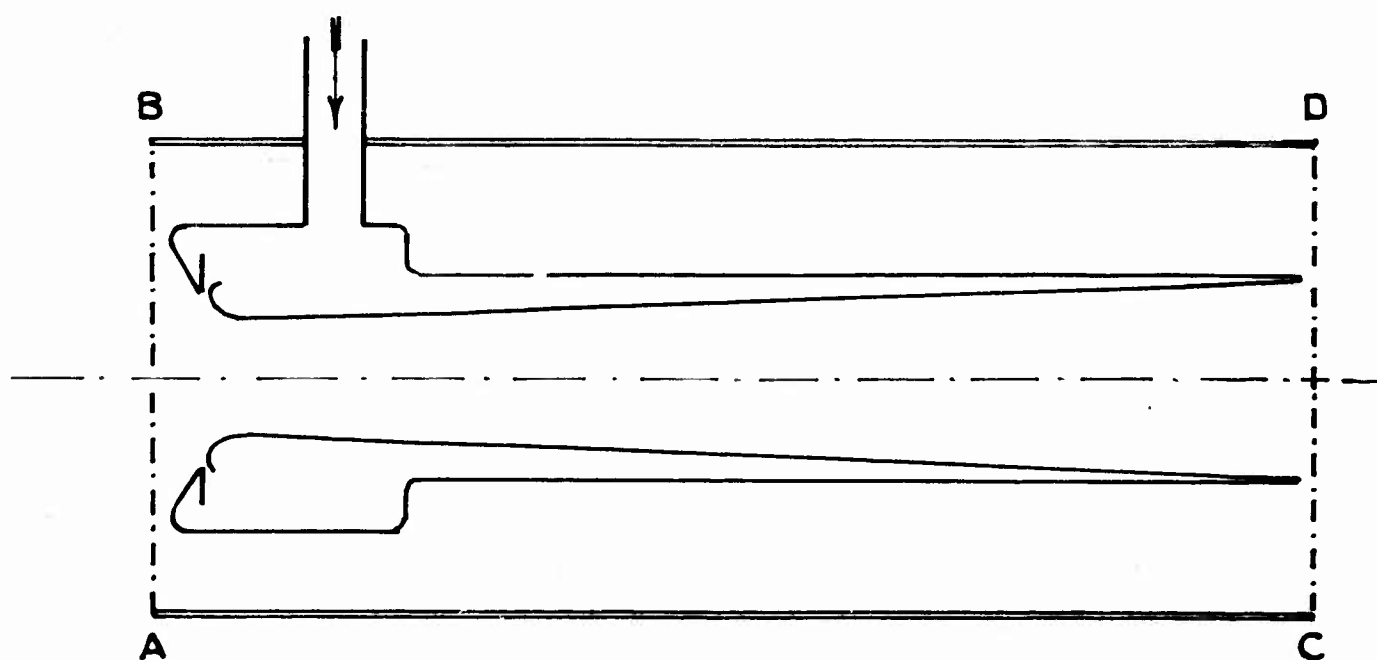
FIG.1



SFERI COANDA

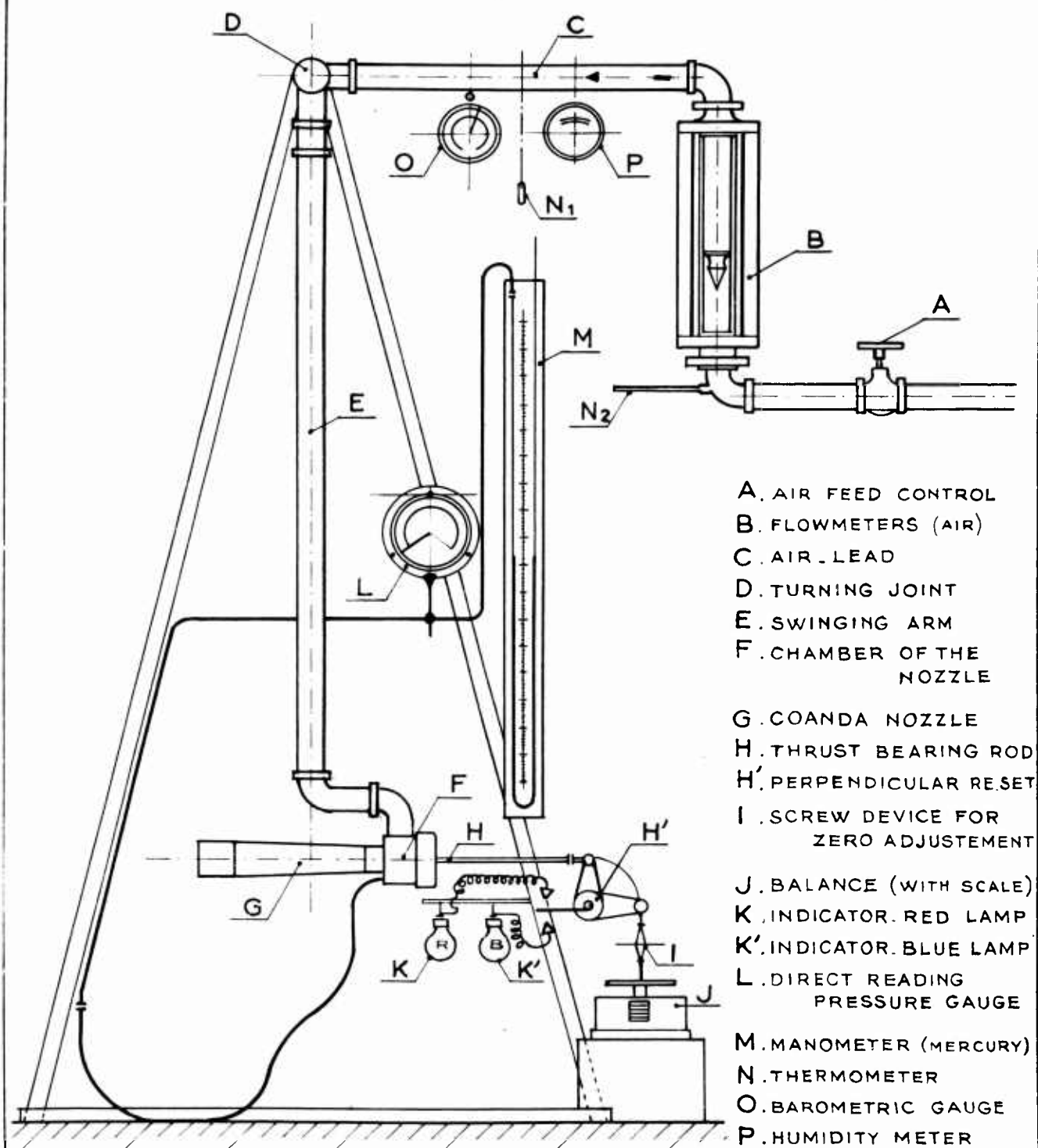
FIG.2

SCHEMATIC OF THE TERMINALS PLANES  
OF THE SURVEY.



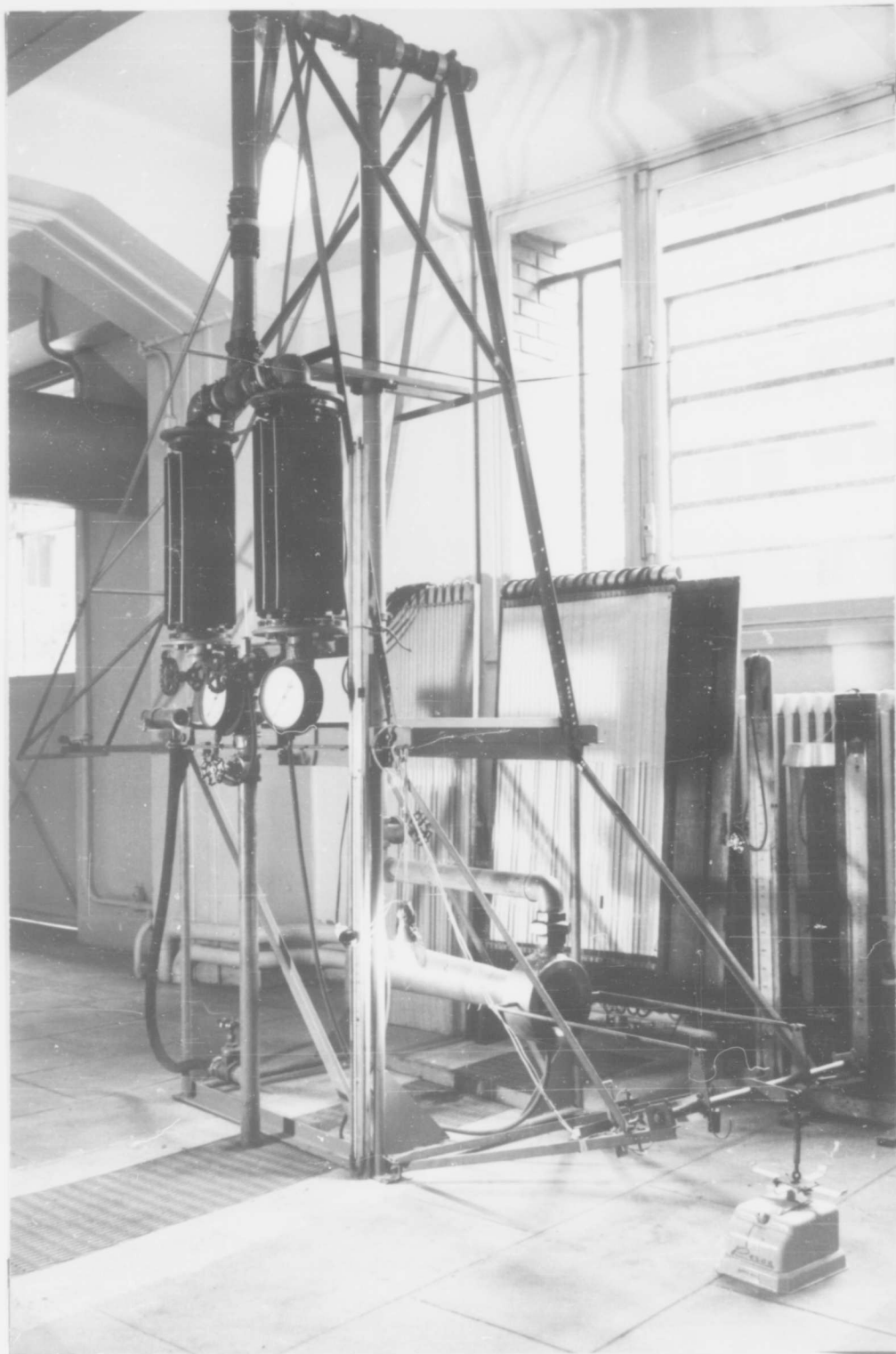
SFERI-COANDA.

FIG.3



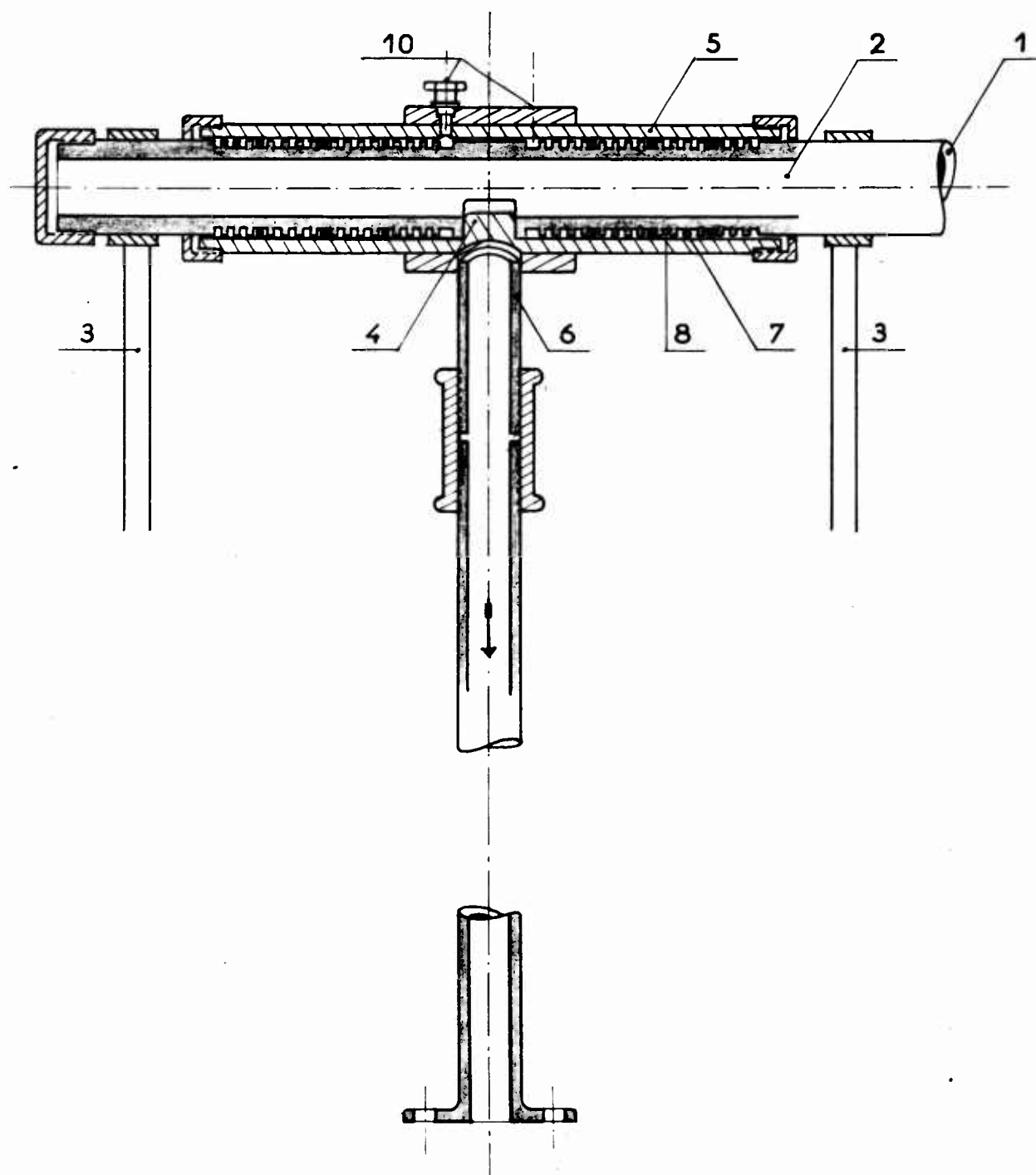
SFERI COANDA

FIG 3 bis



SFERI-COANDA

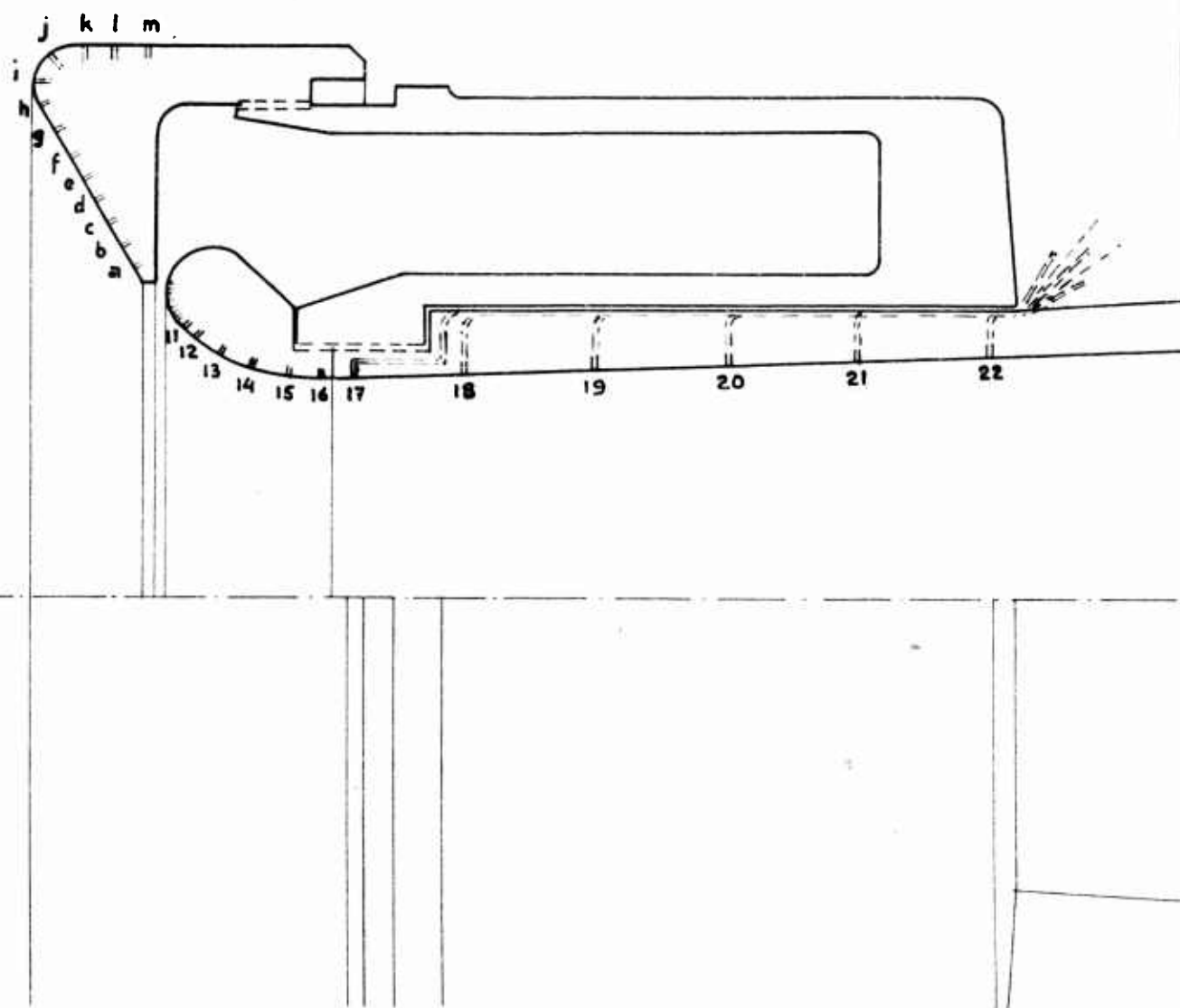
## THE TURNING JOINT D



SFERI COANDA

FIG.5

View of the points of measurements of the static skin pressures on the internal and external walls.

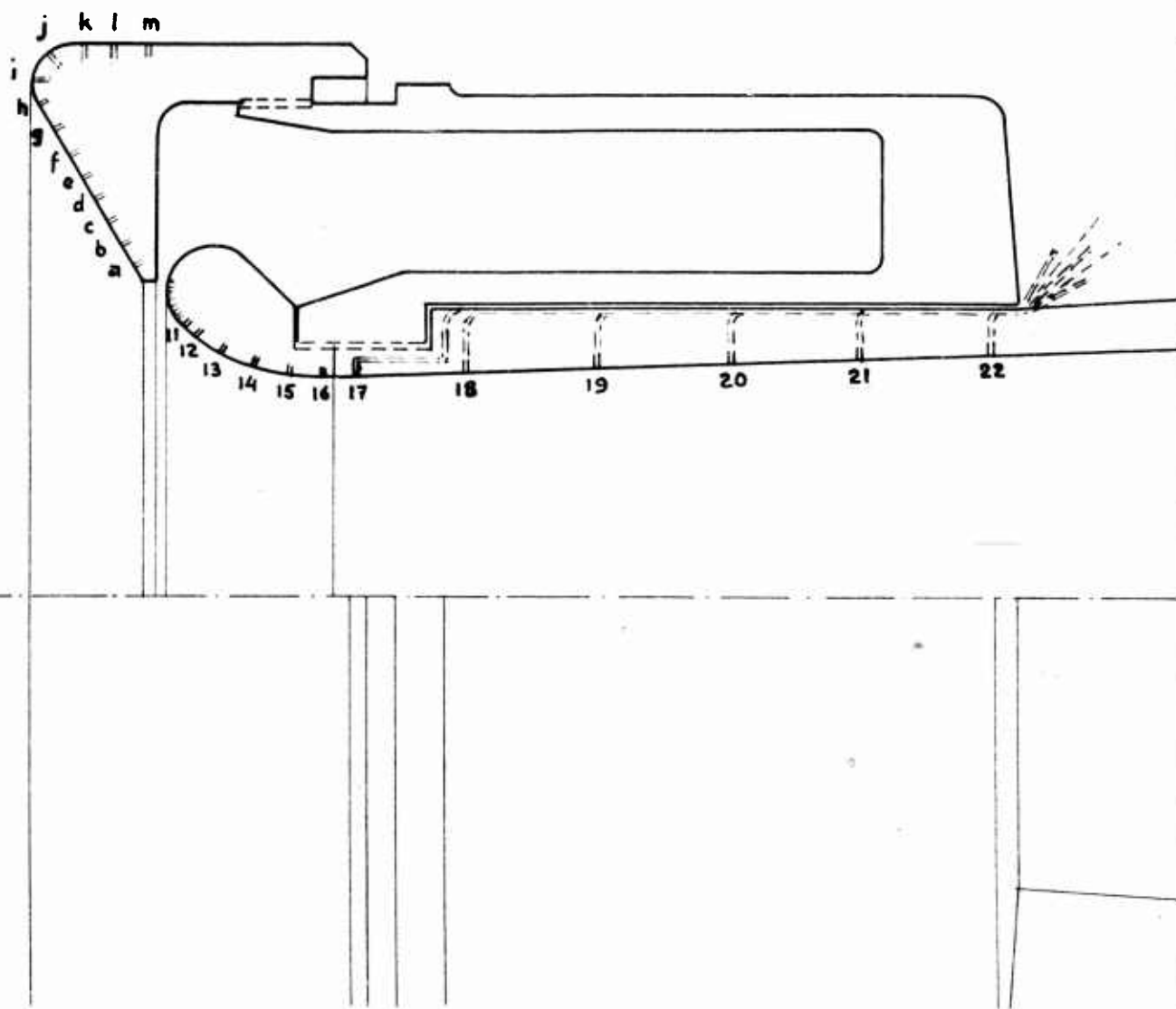


SFERI COANDA.

FIG.5

View of the points of measurements of the static skin pressures on the internal and external walls.

1



SFERI COANDA.

5

2

$\alpha$

22

23

24

3

a



b



25

c



26

4

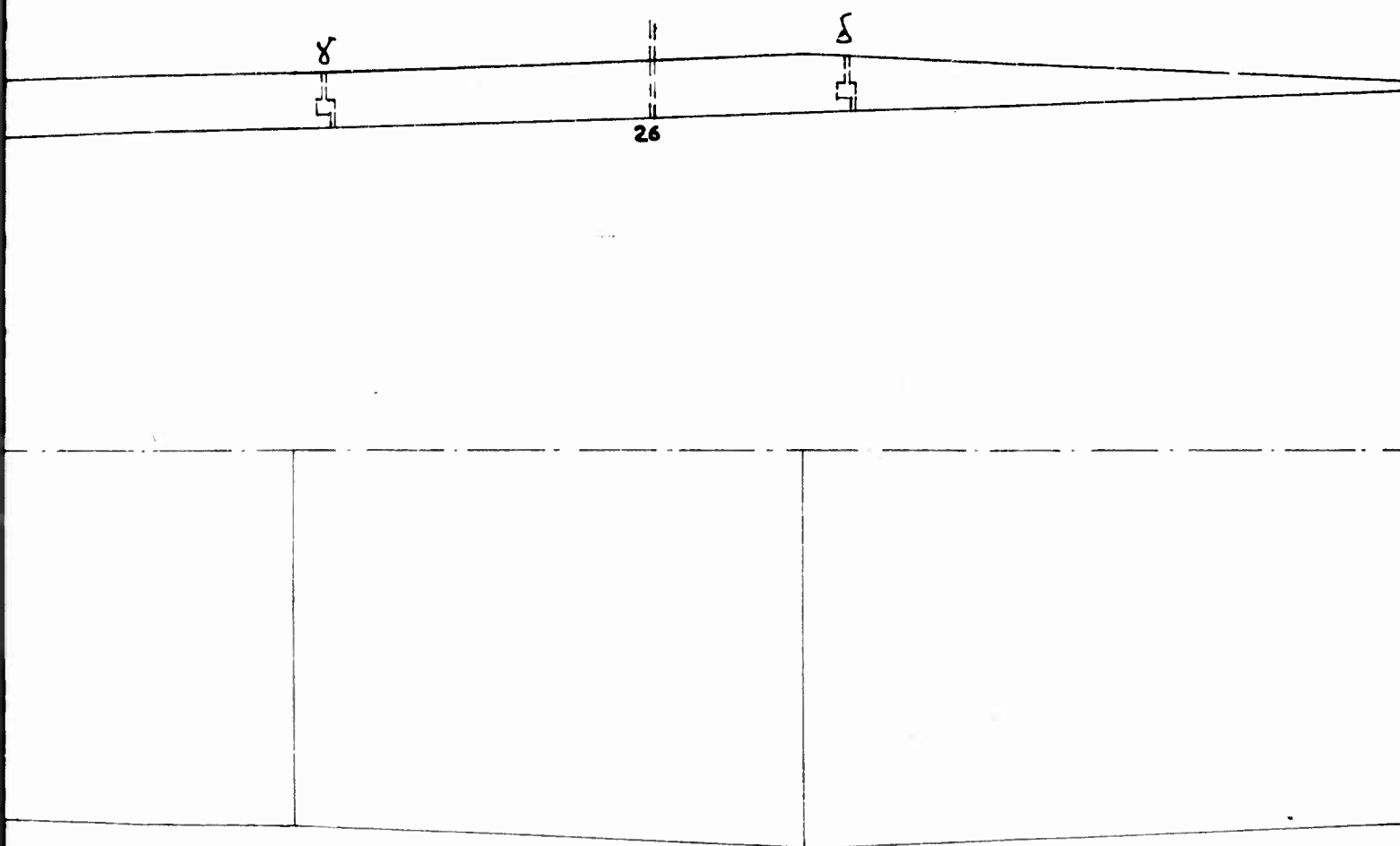
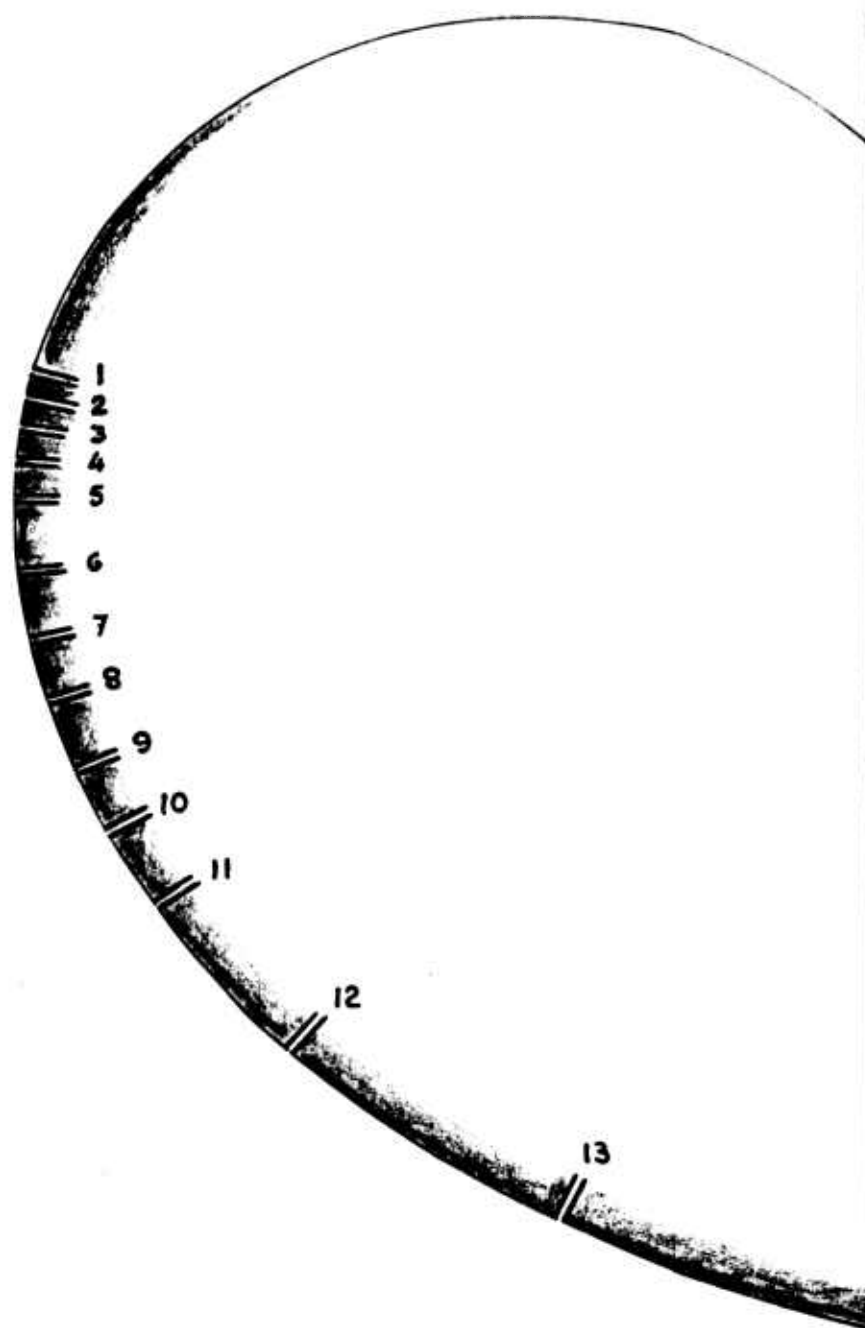


FIG. 6

1



Detailed view of the lip.

SFERI COANDA.

2

14

15

16

17

3

17

18

FIG.7

Special device for introducing the measurement apparatus shown as mounted for the survey of the flow at slot and throat sections.

Special device with  $\frac{1}{100}$  millimetre screwing

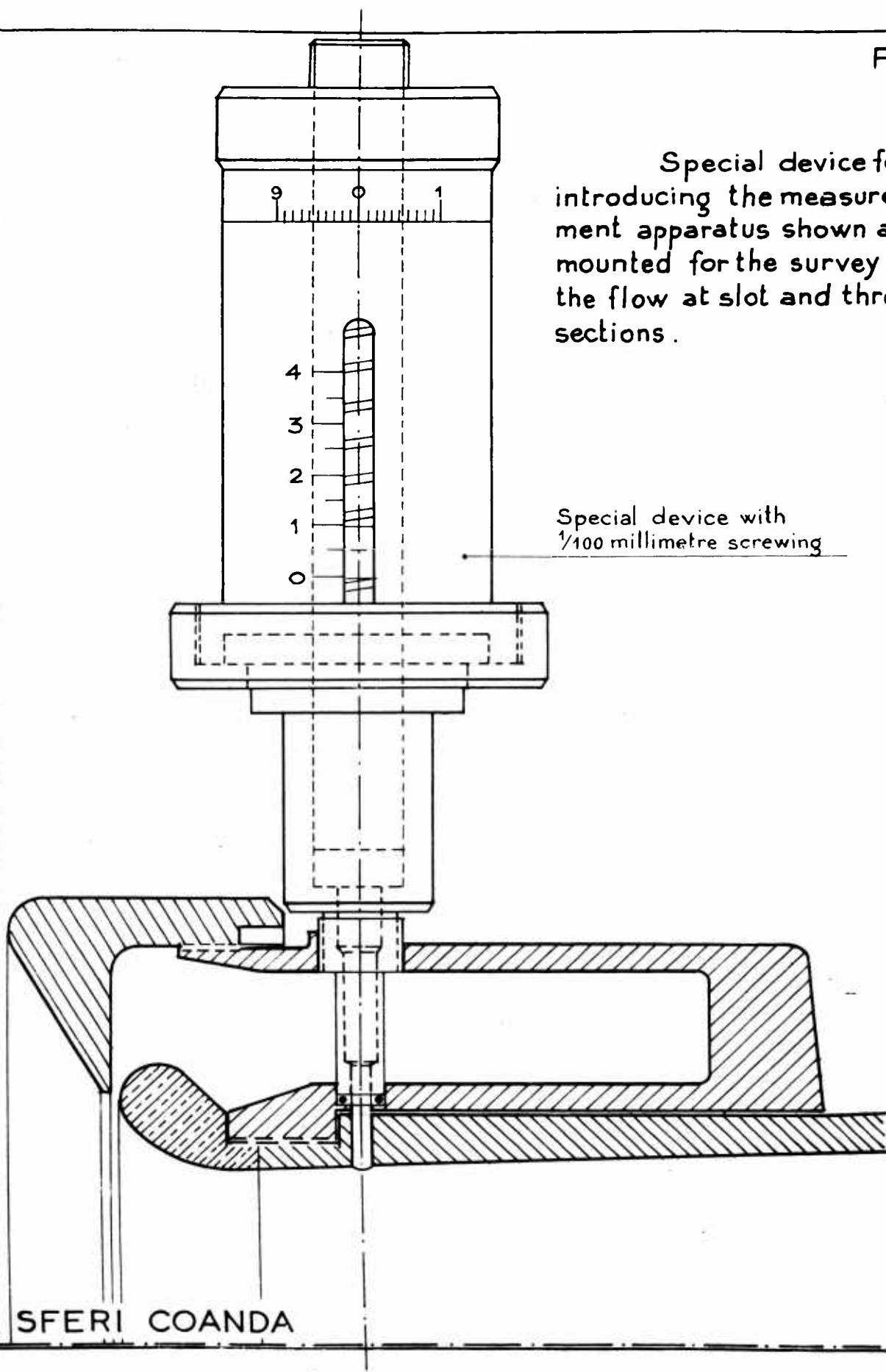
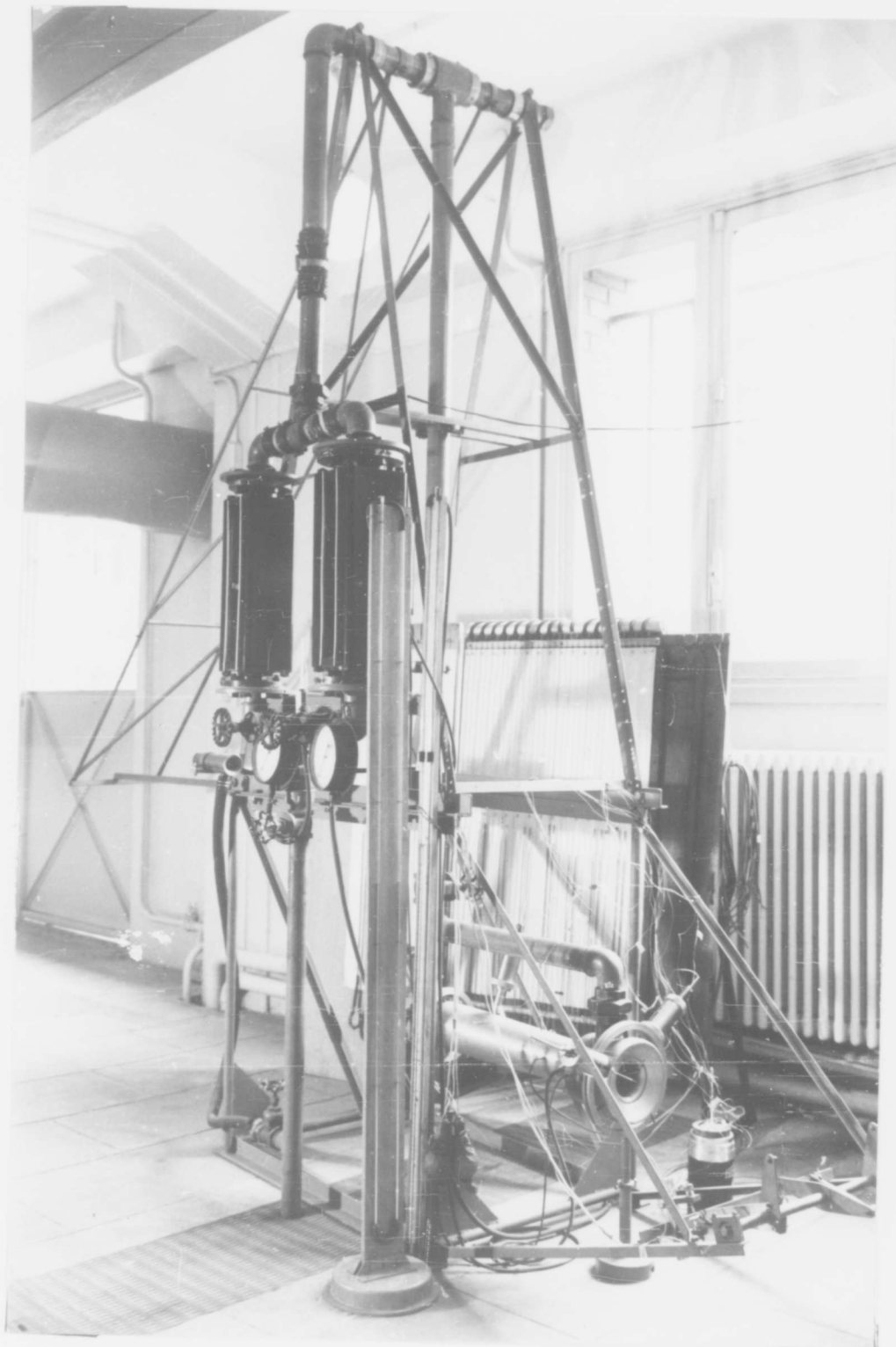
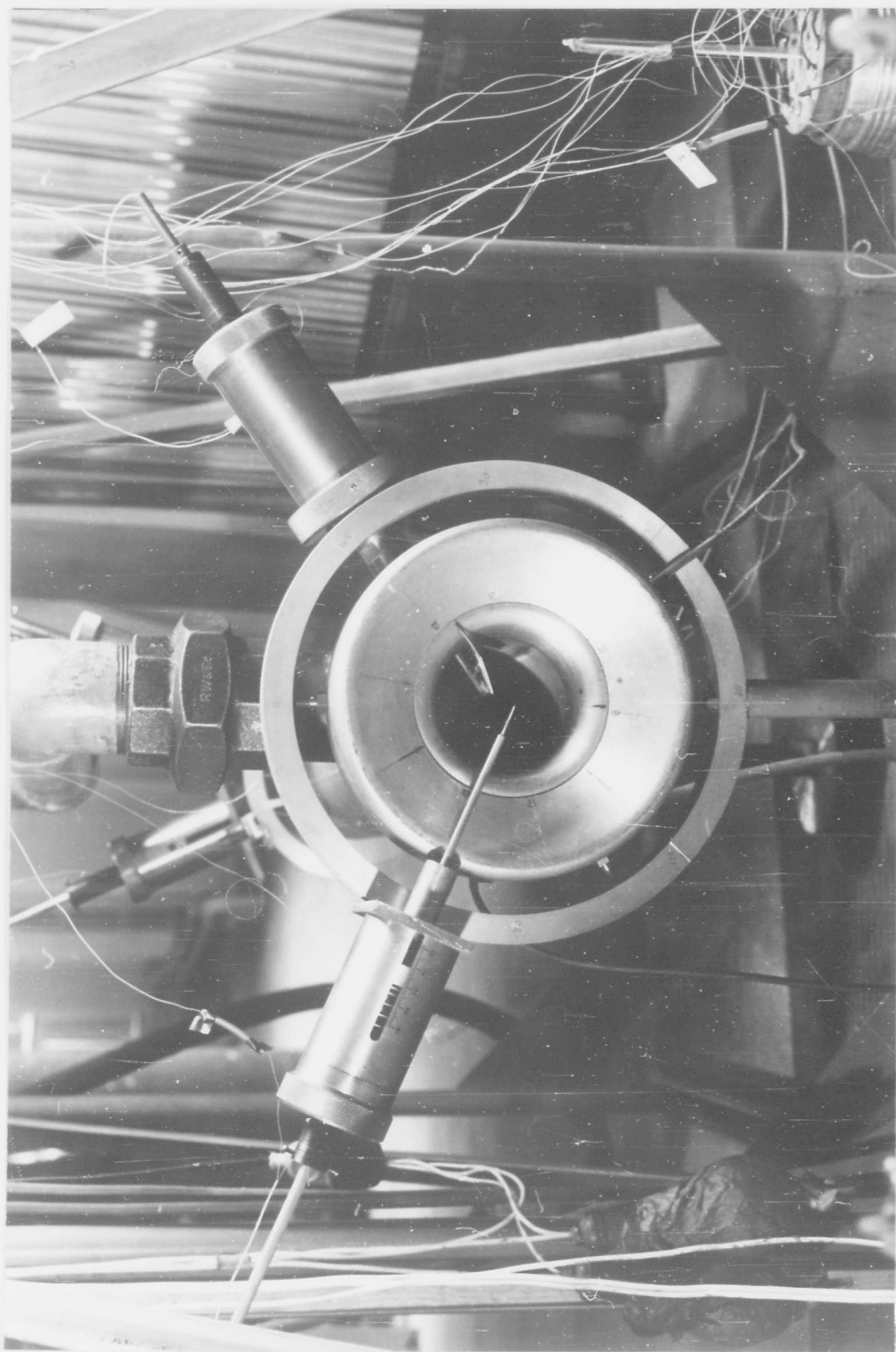


FIG 7 bis



SFERI-COANDA

FIG. 7 ter



SFERI-COANDA.

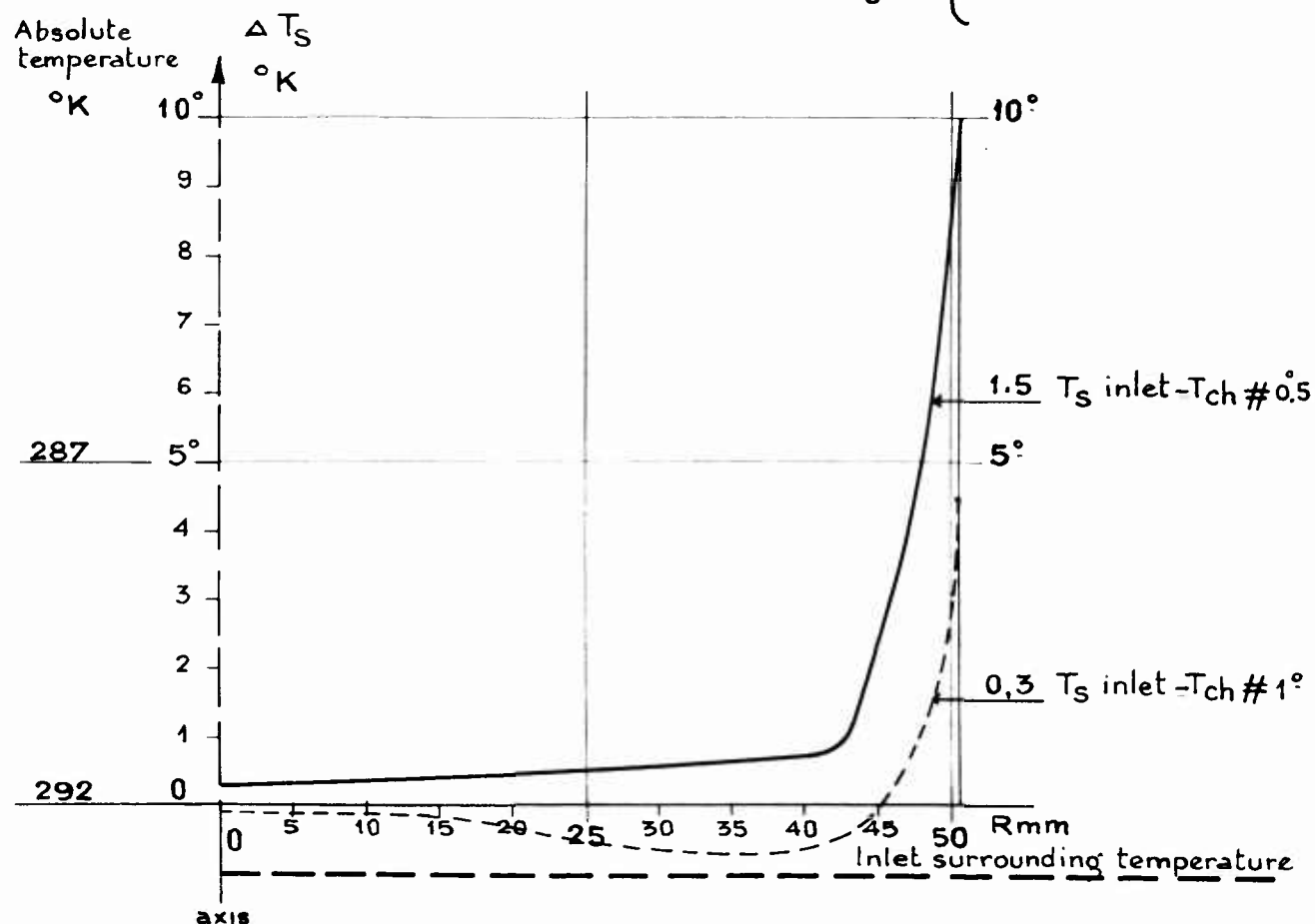
## SLOT SECTION (II')

Approach of the temperature  
 Variation of relative static temperature  
 plotted versus the radii

 $\Delta T_s$  °K versus Rmm

 $\Delta T_s = T_s$  at the point of measurement -  $T$  in the chamber

$$\frac{P_1 - P_0}{P_0} \begin{cases} 1.5 & \text{—} \\ 0.3 & \text{---} \end{cases}$$



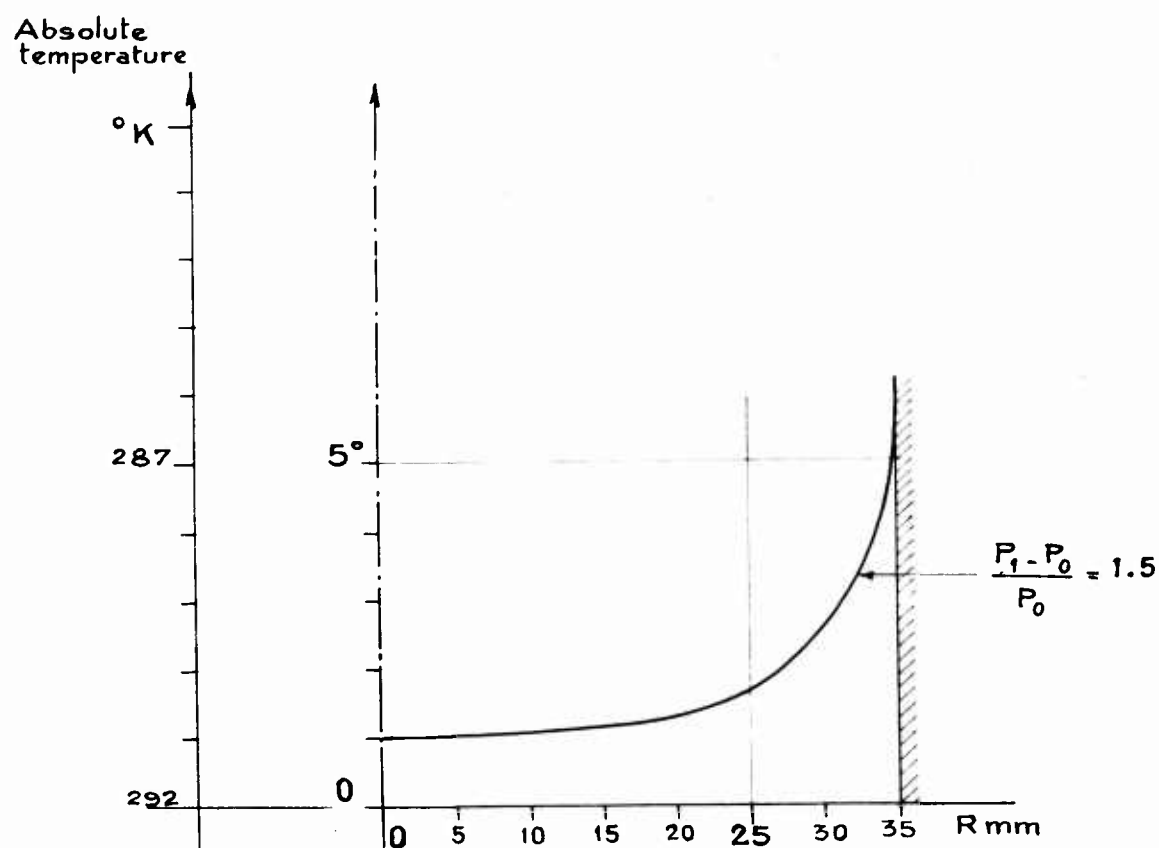
SFERI COANDA

## THROAT SECTION (III)

Variations of total temperatures  
plotted versus the radii

$\Delta T_t$  °K versus Rmm

$\Delta T_t = T_t$  at the point of measurement - T in the chamber

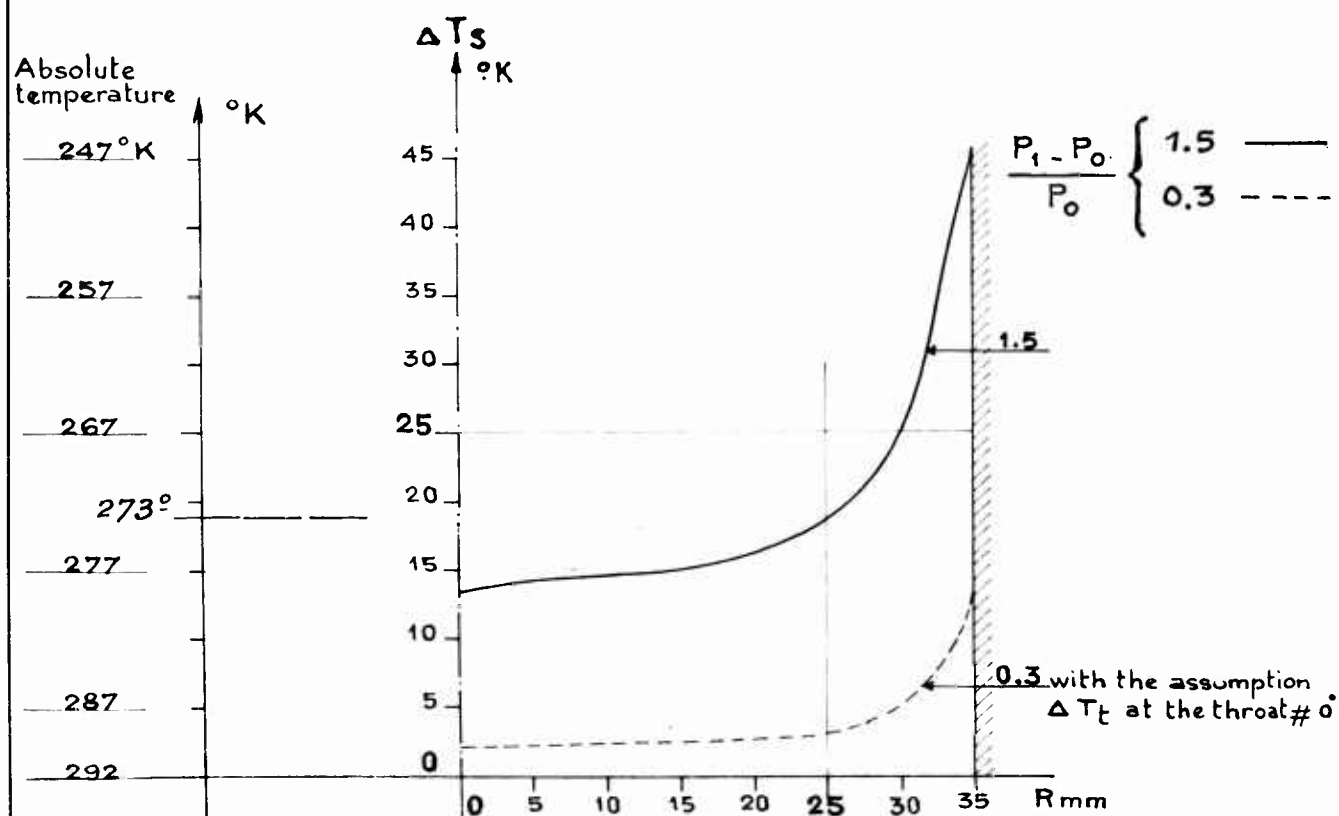


No valable measurement at  $\frac{P_1 - P_0}{P_0} = 0.3$  due to the low value of  $\Delta T_t$

SFERI COANDA

## THROAT SECTION (III)

Approach of the temperature  
 Computed values of static temperatures  
 plotted versus the radii



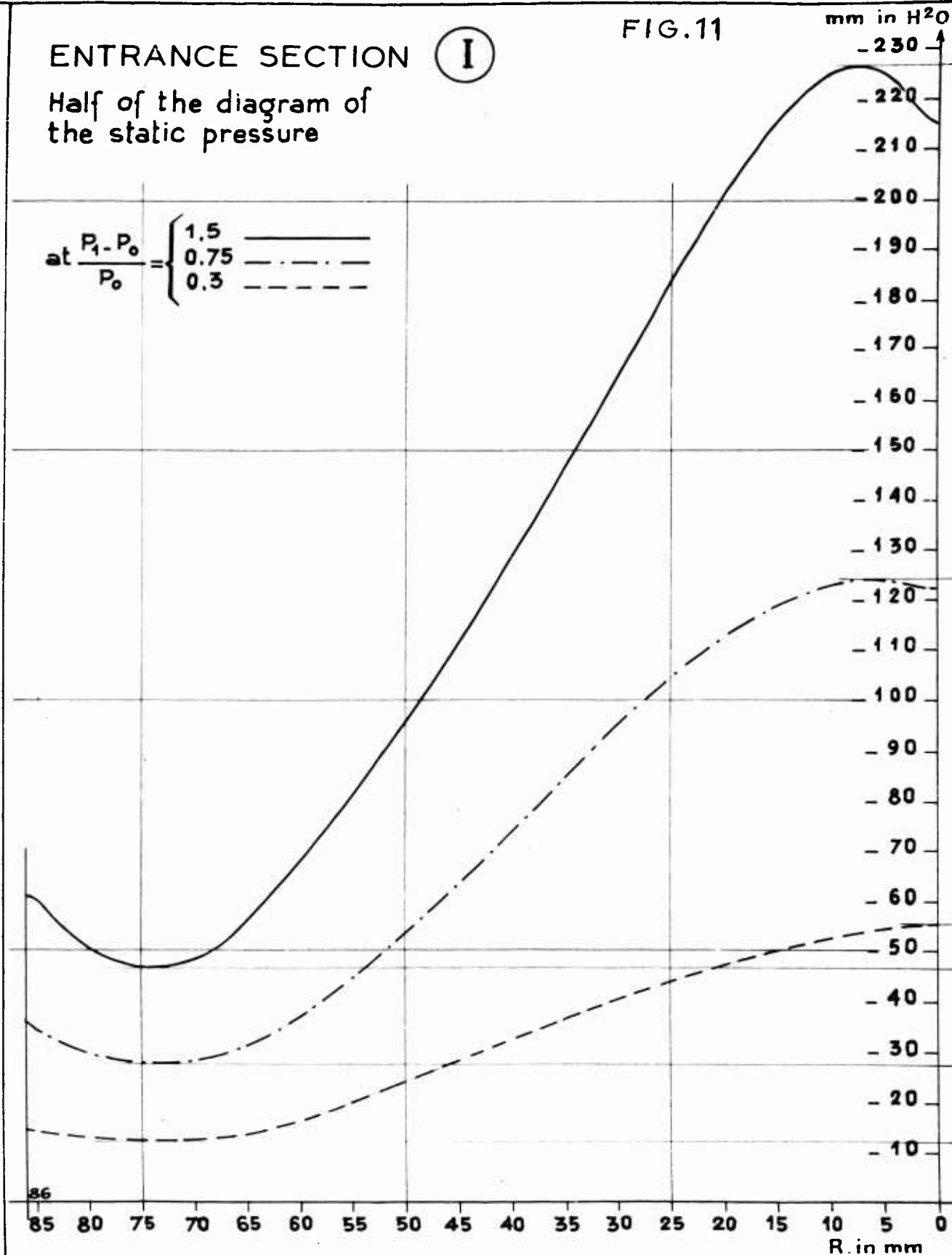
# ENTRANCE SECTION

I

FIG.11

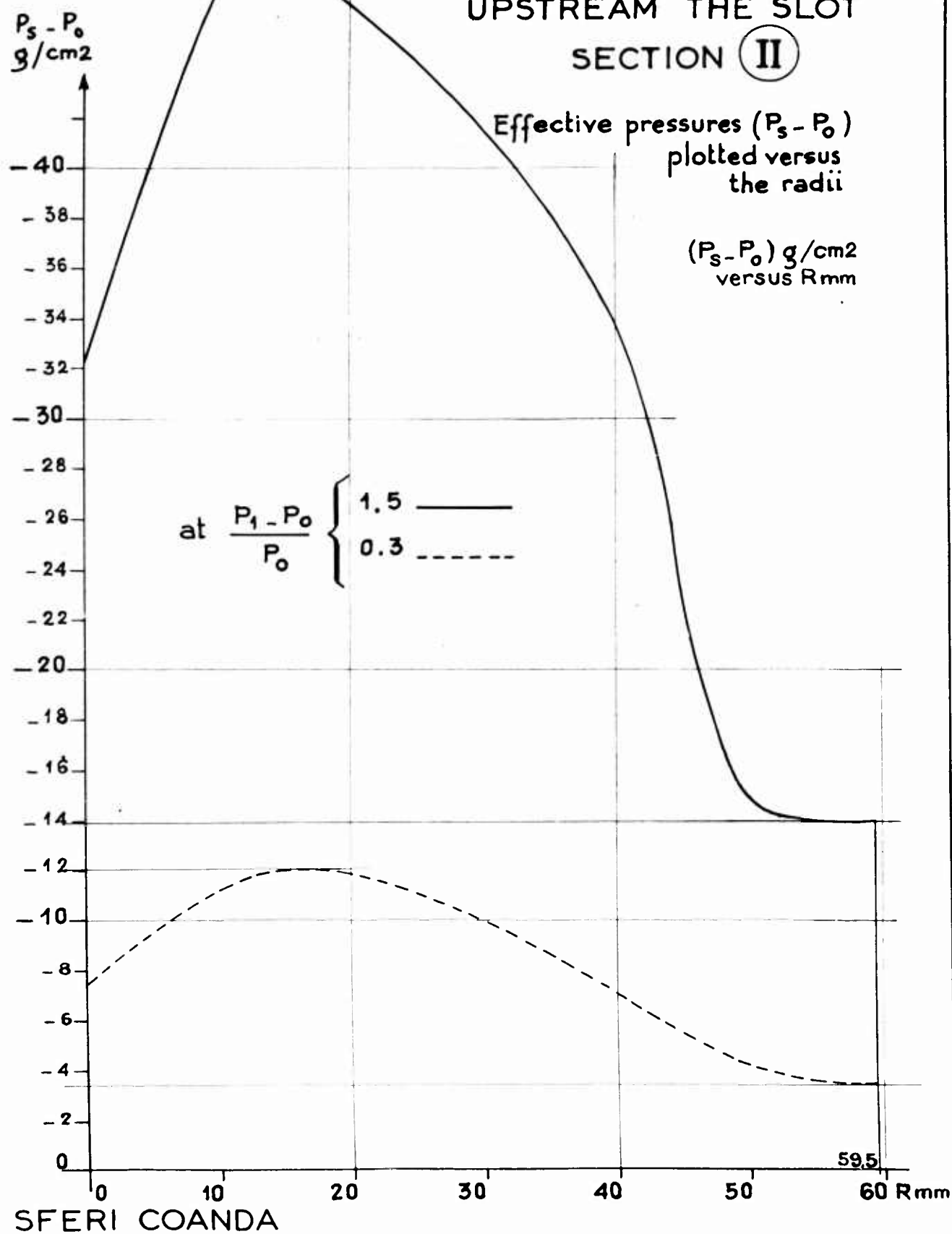
Half of the diagram of  
the static pressure

$$\text{at } \frac{P_1 - P_0}{P_0} = \begin{cases} 1.5 & \text{— — — — —} \\ 0.75 & \text{— · — · — · —} \\ 0.3 & \text{— — — — —} \end{cases}$$



SFERI COANDA

FIG. 12

UPSTREAM THE SLOT  
SECTION (II)

## THROAT SECTION (III)

Effective pressures ( $P_s - P_o$ ) plotted versus the radii

Scale : 1 cm = 1 cm Hg

 $P_s - P_o$   
cm Hg $g/cm^2$ at  $\frac{P_1 - P_o}{P_o} \begin{cases} 1.5 \text{ ———} \\ 0.3 \text{ - - - -} \end{cases}$ 

- 15 - 204

- 10 - 136

- 5 - 68

0

0

5

10

15

20

25

30

35 R mm

SFERI COANDA

## UPSTREAM SECTION IN THE DIVERGENT

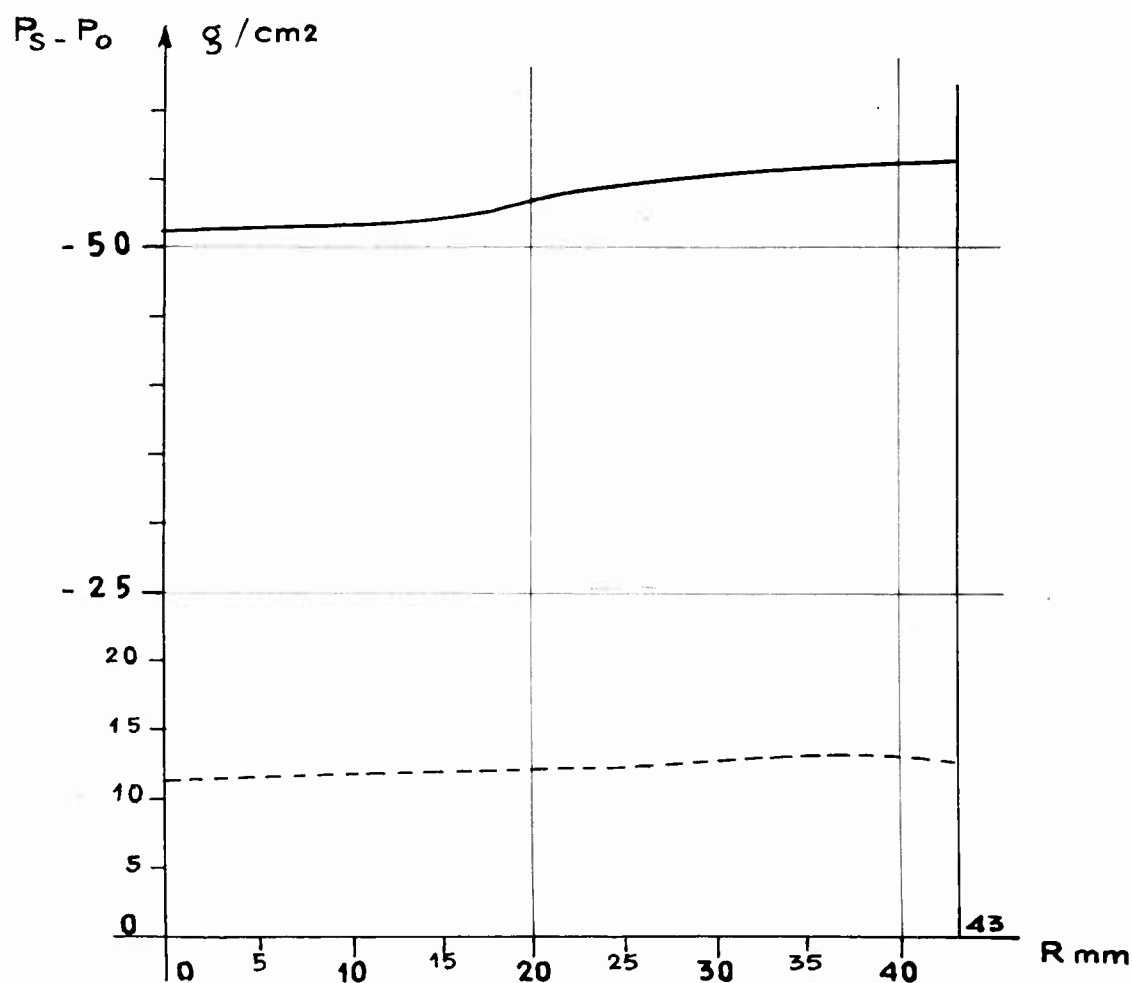
IV

Effectivesstatic pressures  
plotted versus radii

$P_s - P_o$  g/cm<sup>2</sup> versus R mm

Scale: 1cm = -5 g/cm<sup>2</sup>

at  $\frac{P_1 - P_o}{P_o}$   $\left\{ \begin{array}{l} \text{———} 1.5 \\ \text{-----} 0.3 \end{array} \right.$

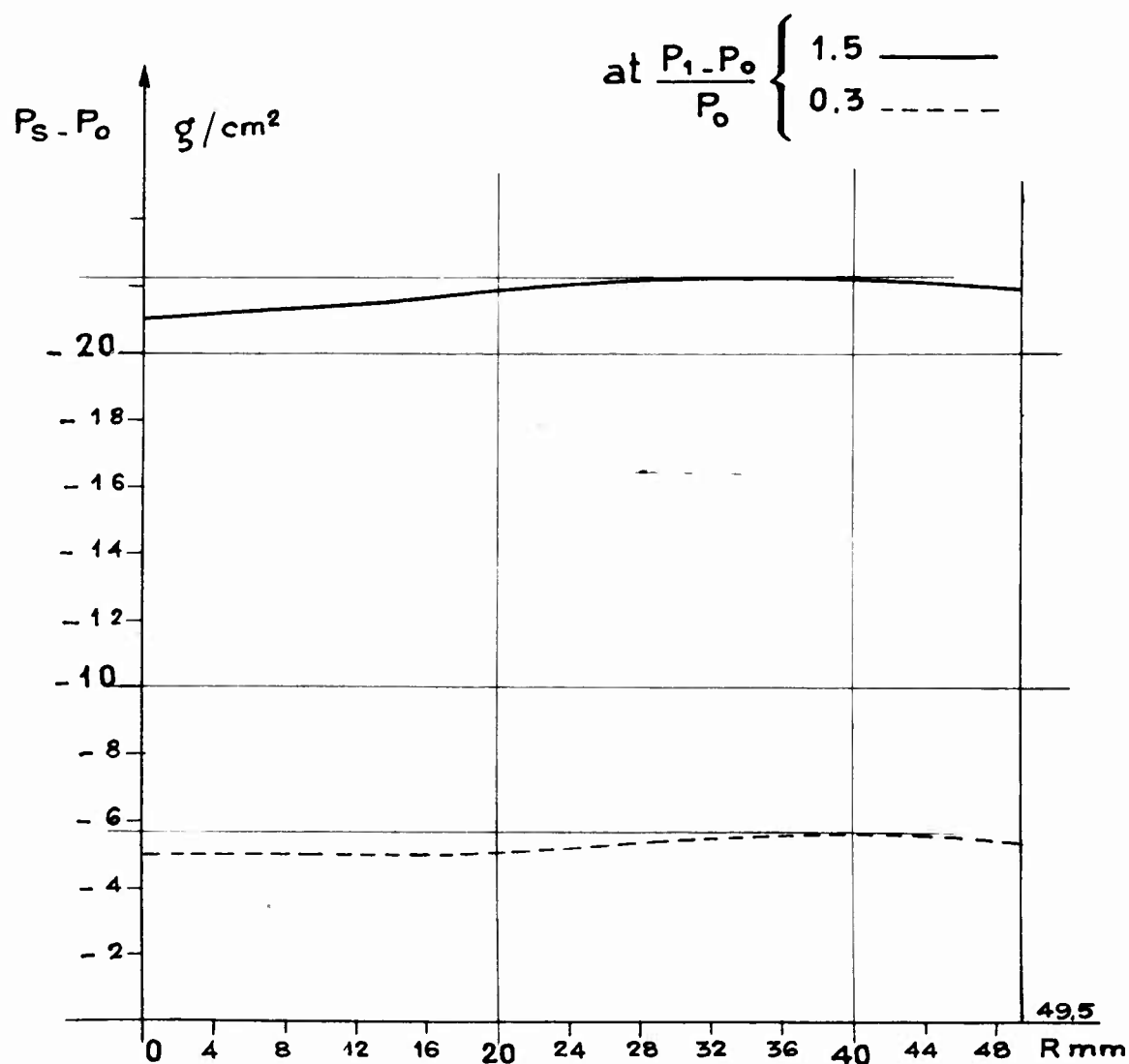


SFERI COANDA

FIG.15

## DOWNSTREAM SECTION OF THE DIVERGENT (V)

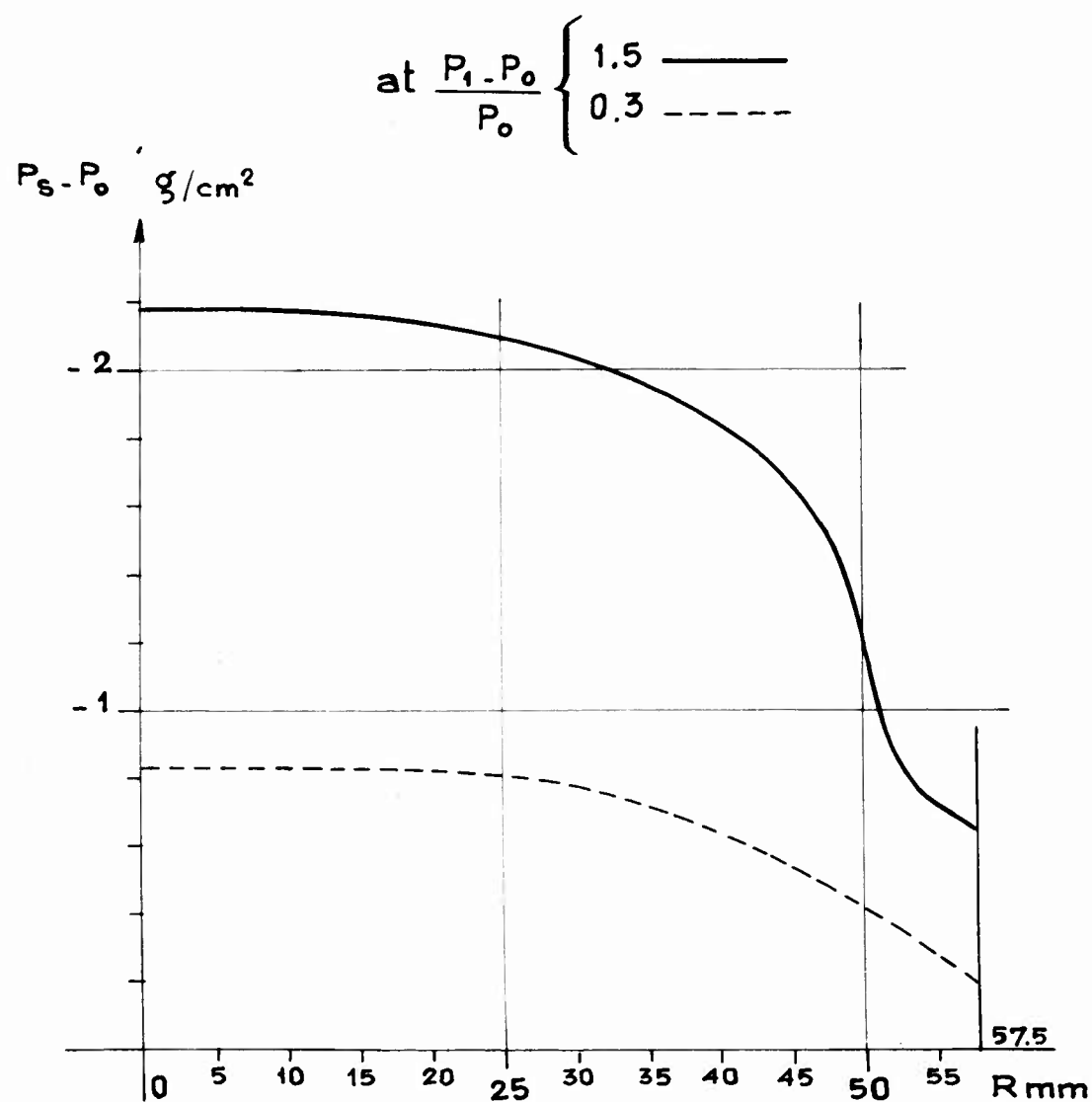
Effective static pressures plotted versus radii

 $P_s - P_0$  g/cm<sup>2</sup> versus R mmScale : 1 cm = 2 g/cm<sup>2</sup>

SFERI COANDA

## EXIT SECTION (VI)

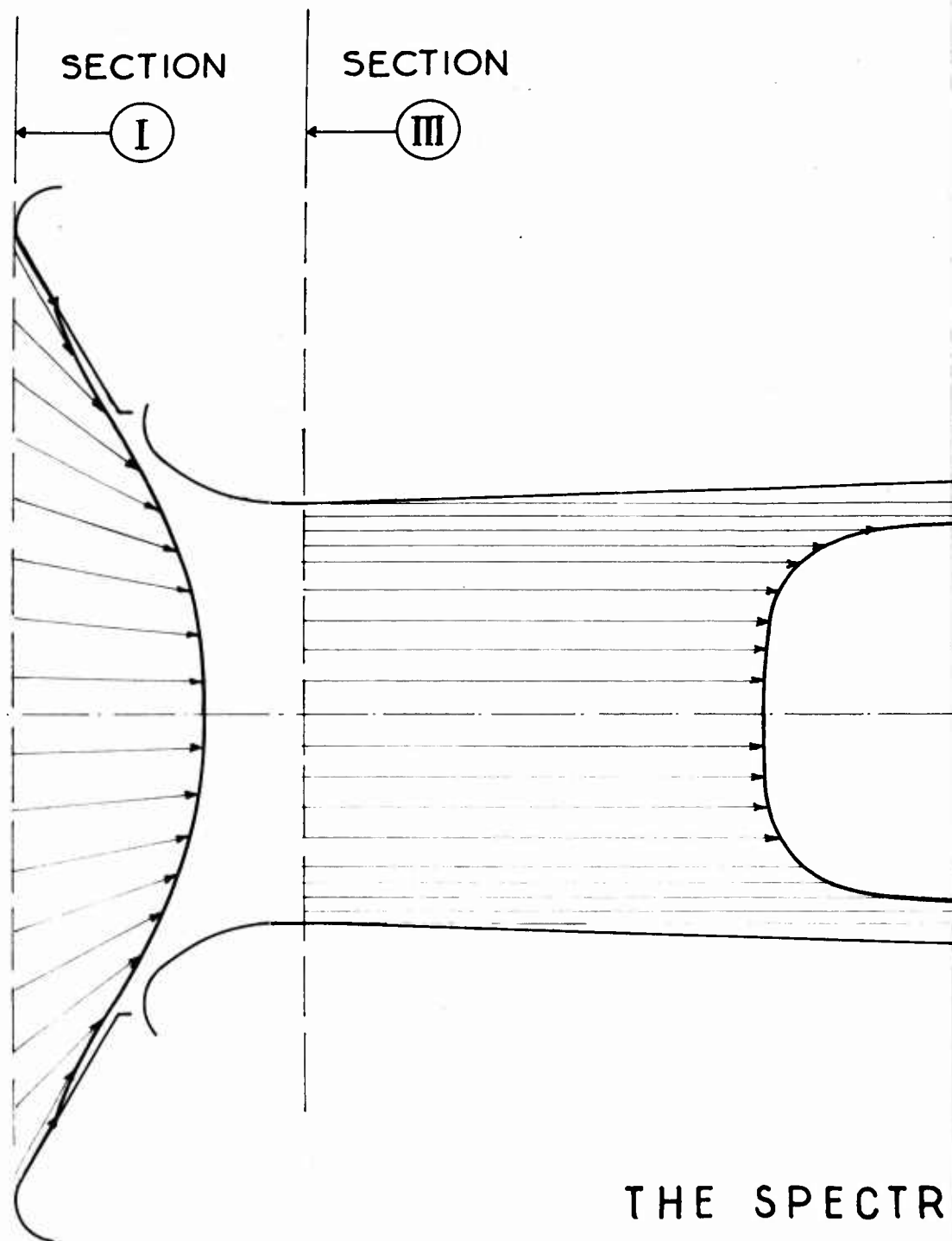
Effective static pressures plotted versus radii

 $P_s - P_0$  g/cm<sup>2</sup> versus R mm

SFERI COANDA

FIG.17

1



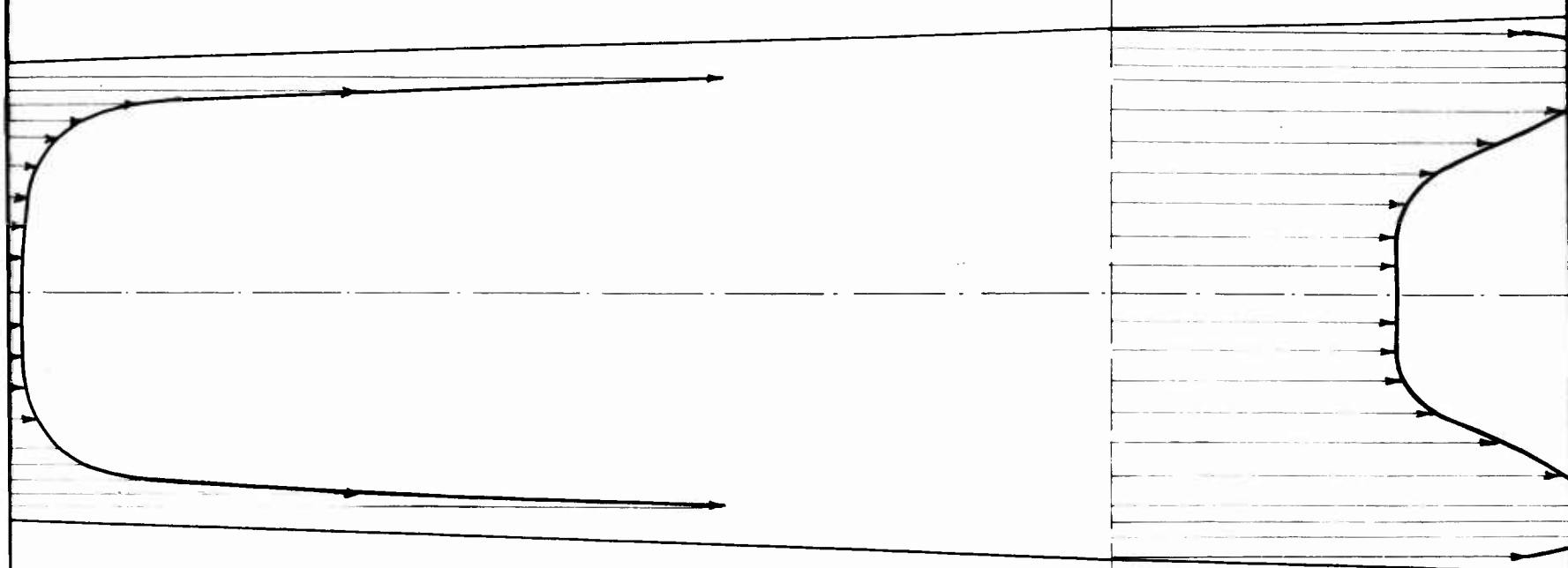
SFERI COANDA

THE SPECTR

2

SECTION

IV

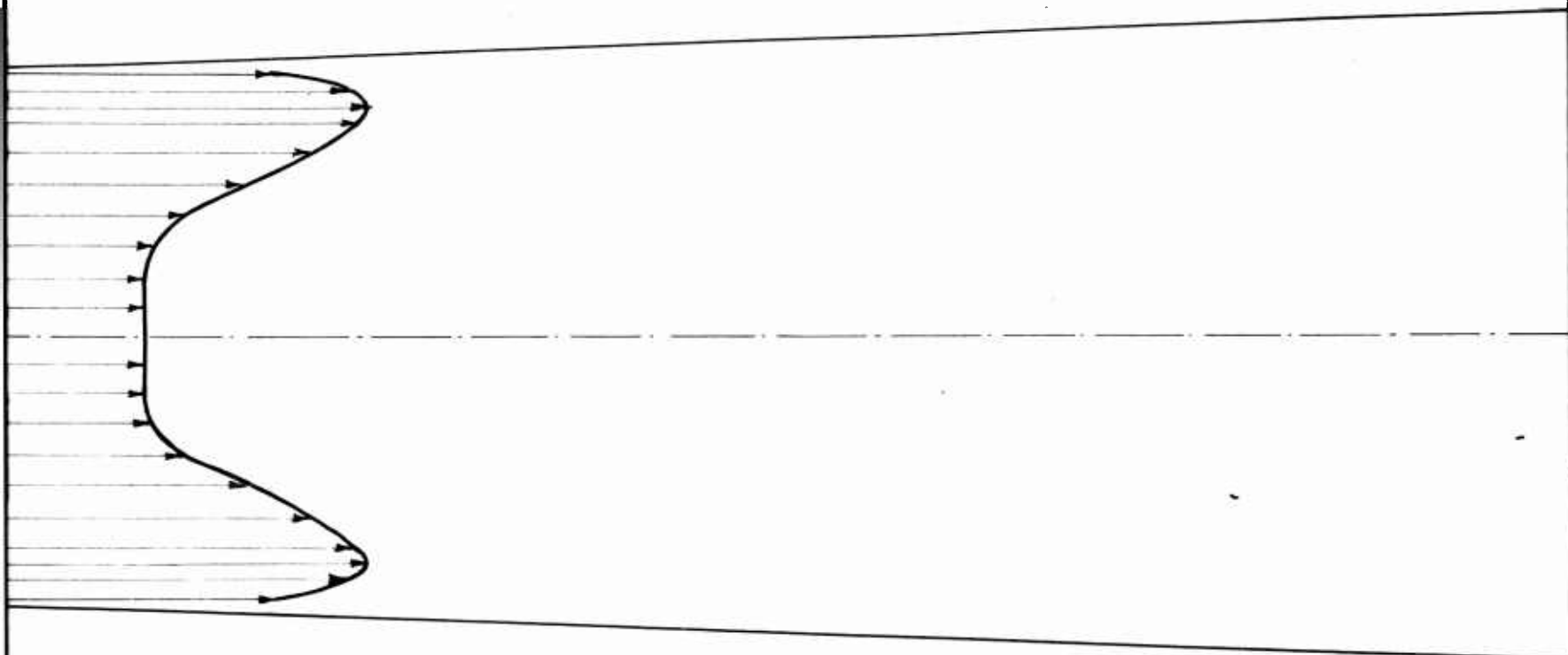


SPECTRUM OF THE DIRECTIONS AND THE INTENSITIES

Scale : 1 cm = 20  $\frac{m}{s}$

ON

3



TENSITIES OF THE VELOCITIES IN DIFFERENT SECTIONS

$$1 \text{ cm} = 20 \frac{\text{m}}{\text{s}} \quad \text{at} \quad \frac{P_1 - P_0}{P_0} = 1.5$$

4

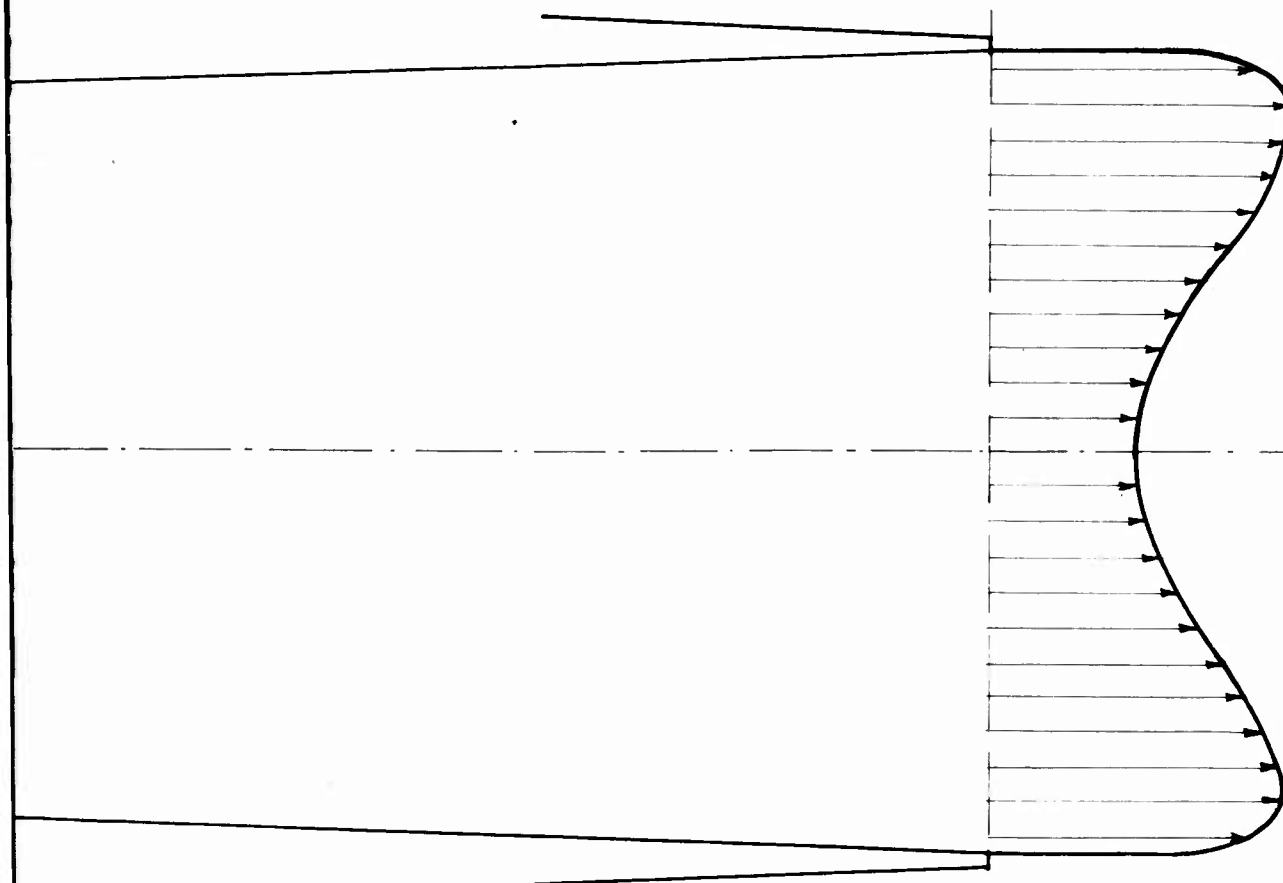
SE

DIFFERENT SECTIONS OF THE NOZZLE

SECTION

VI

5

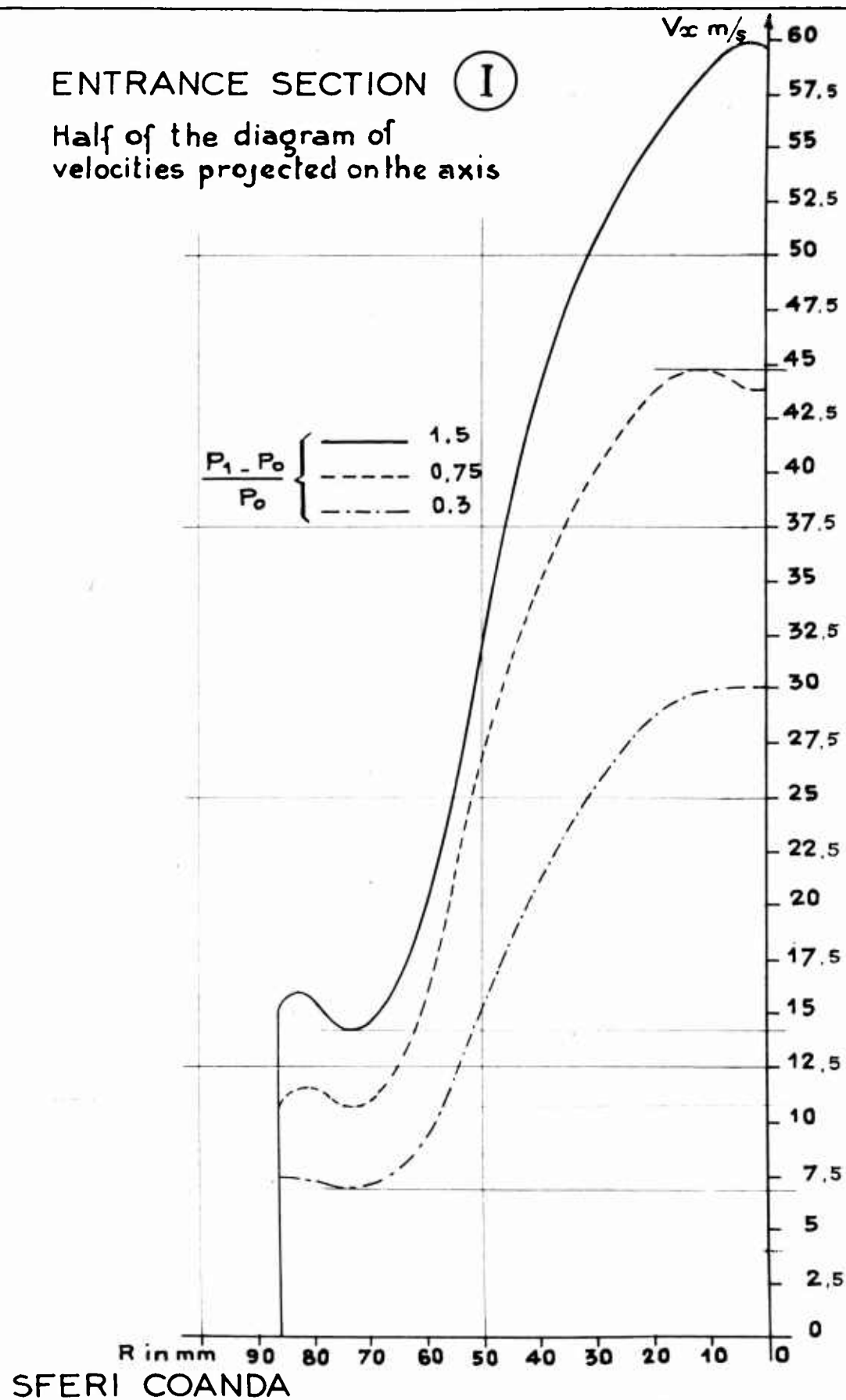


F THE NOZZLE

FIG. 18

## ENTRANCE SECTION (I)

Half of the diagram of  
velocities projected on the axis



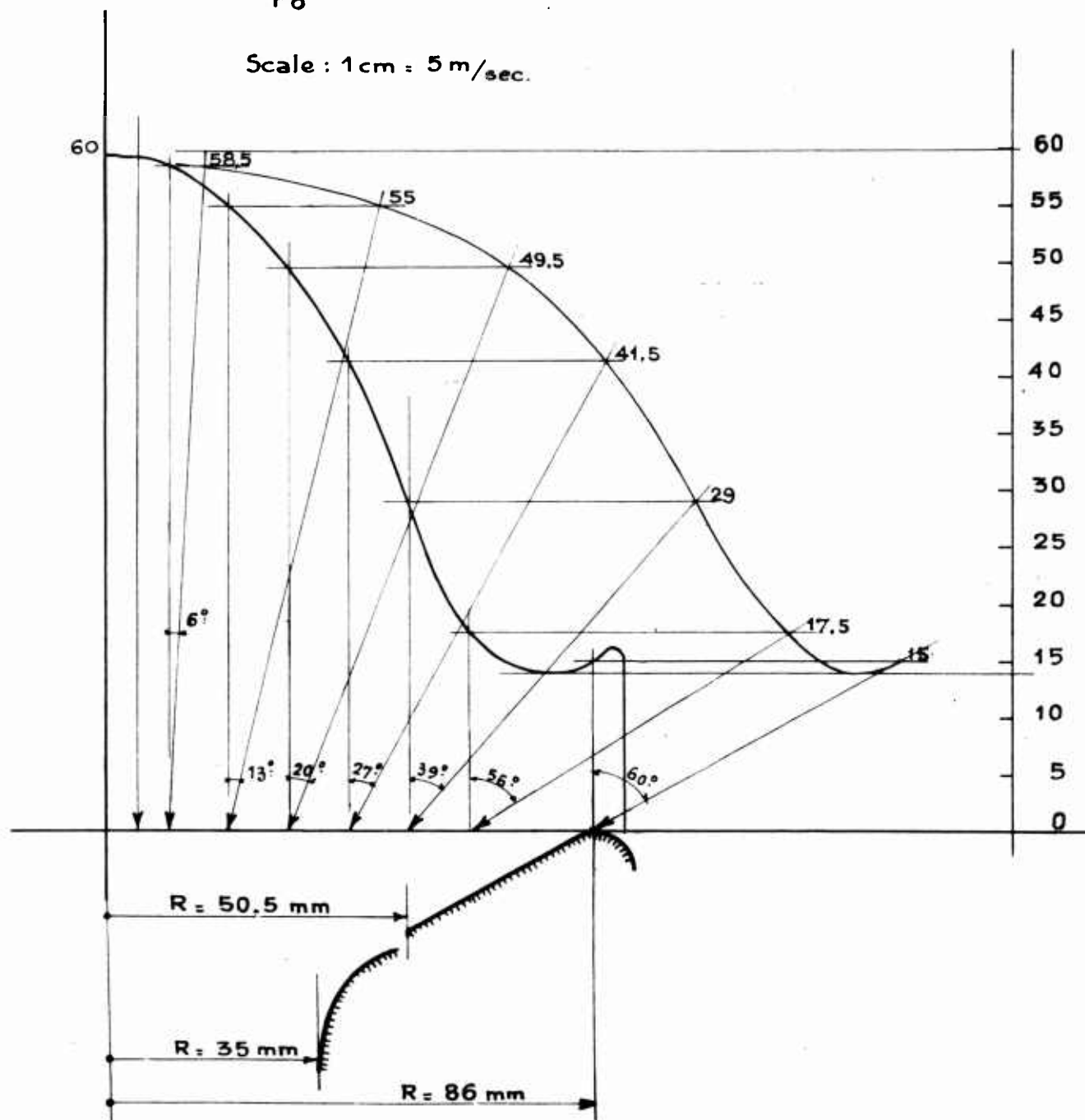
SFERI COANDA

- Half of the spectrum of velocities at the entrance (I)  
(in magnitude and direction.)
- Half of the diagram of their projections on the  
direction of the axis.

$$\frac{P_1 - P_0}{P_0} = 1.5$$

Opening . 6 mm.

Scale : 1 cm = 5 m/sec.



SFERI.COANDA

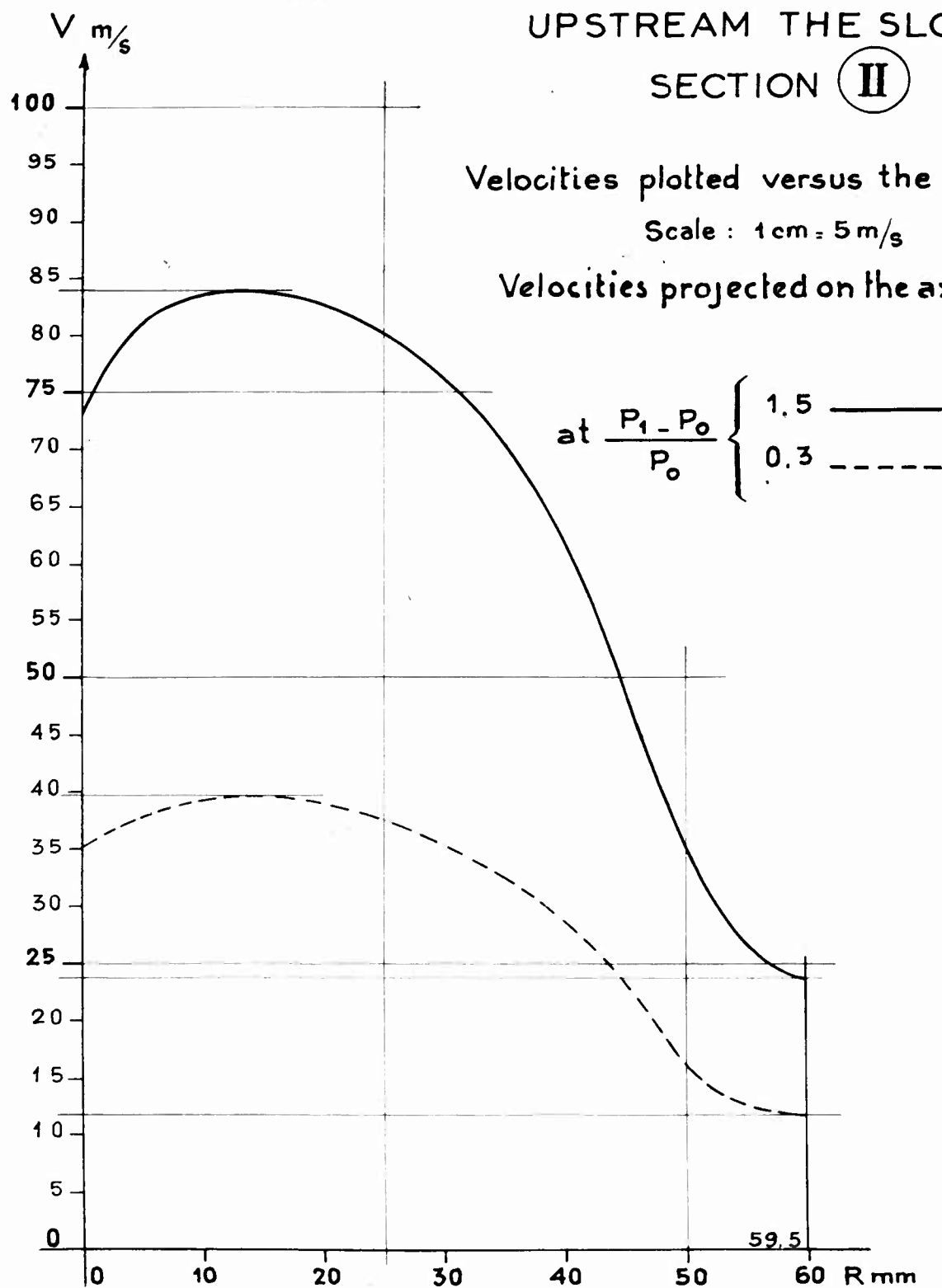
FIG.19

UPSTREAM THE SLOT  
SECTION II

Velocities plotted versus the radii

Scale : 1 cm = 5 m/s

Velocities projected on the axis

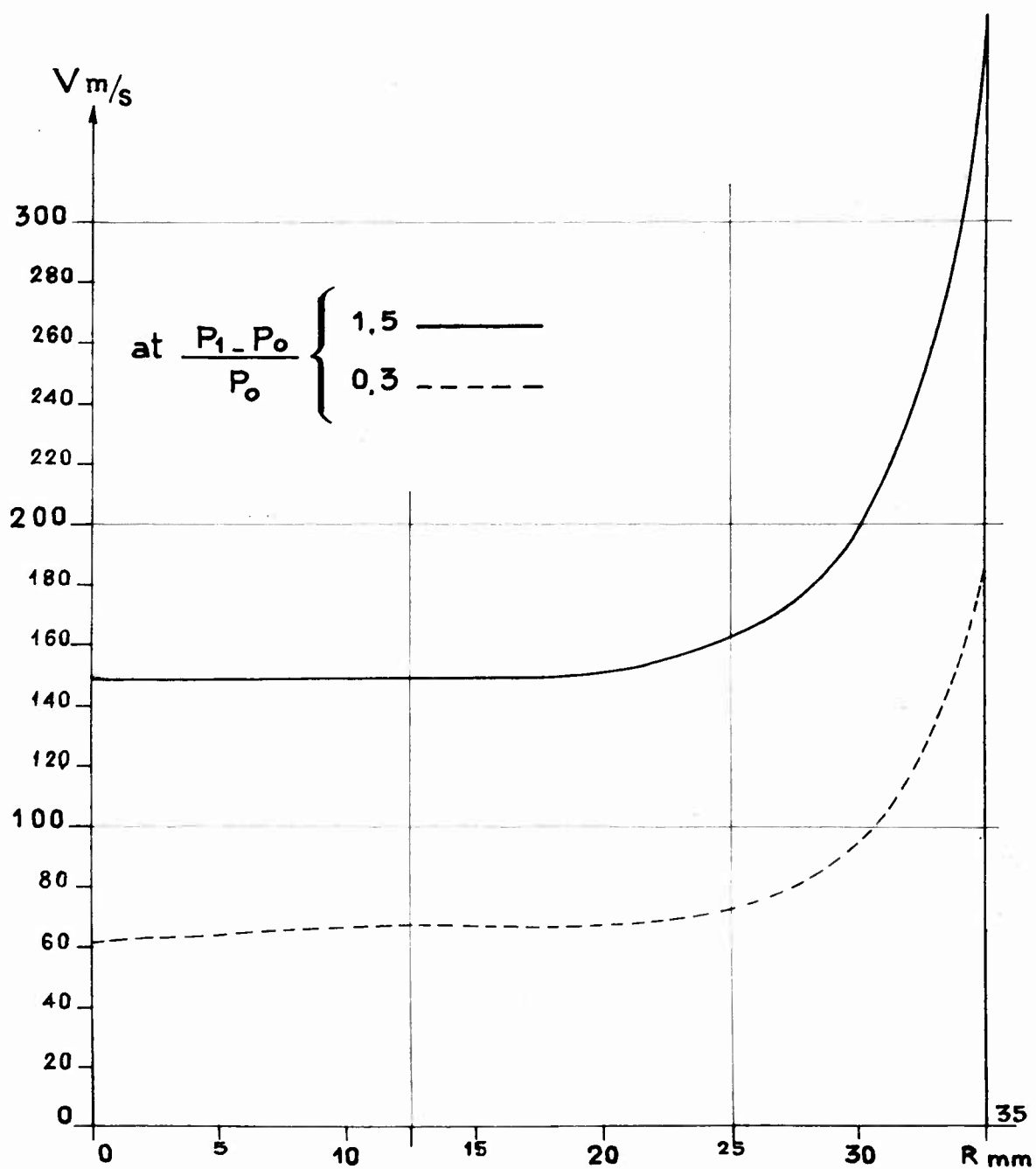


SFERI COANDA

FIG.20

THROAT SECTION (III)  
Velocities plotted versus radii

Scale : 1 cm = 20 m/s



SFERI COANDA

# UPSTREAM SECTION IN THE DIVERGENT

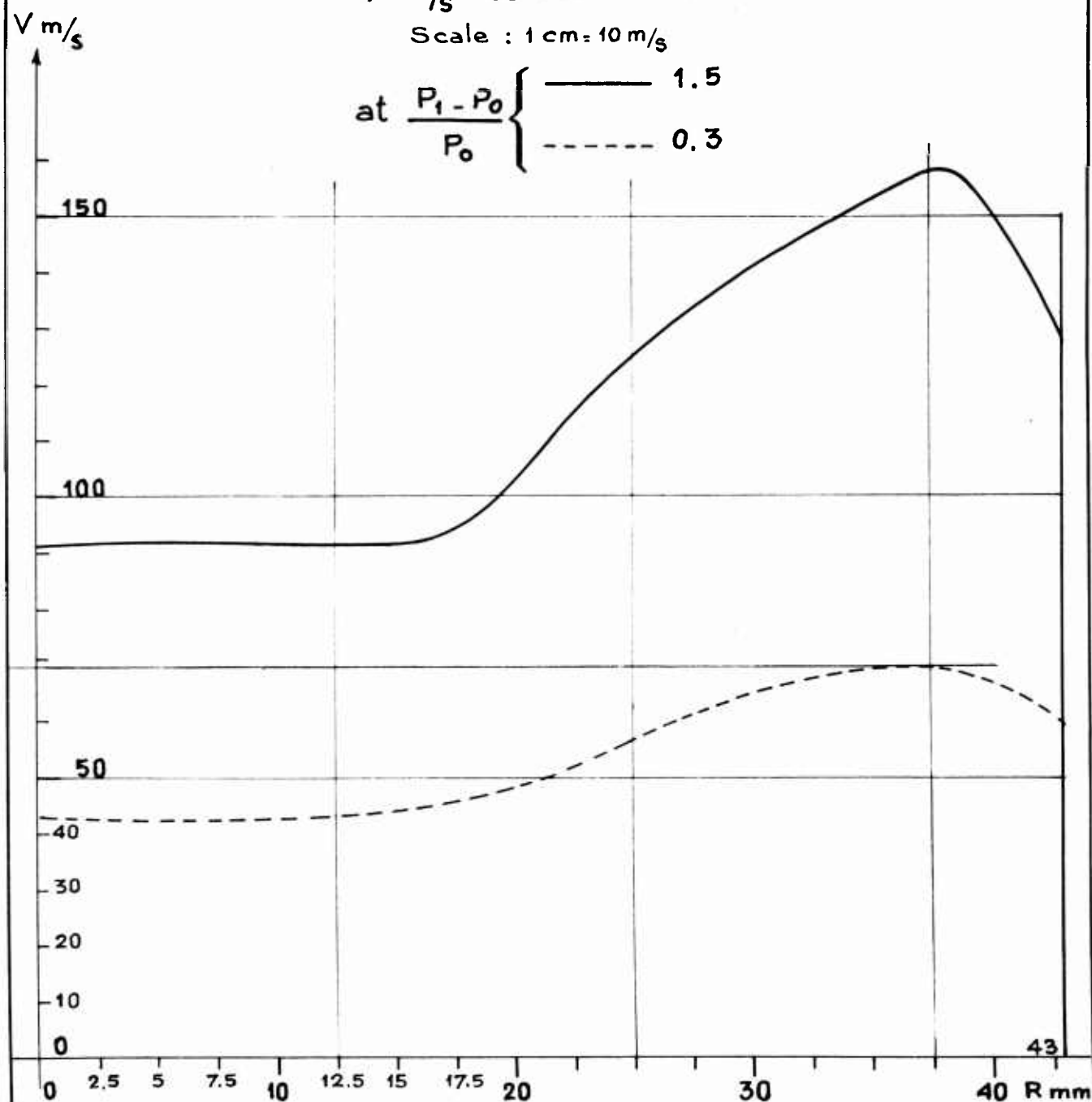
IV

Velocities plotted versus radii

$V$  m/s versus  $R$  mm

Scale : 1 cm = 10 m/s

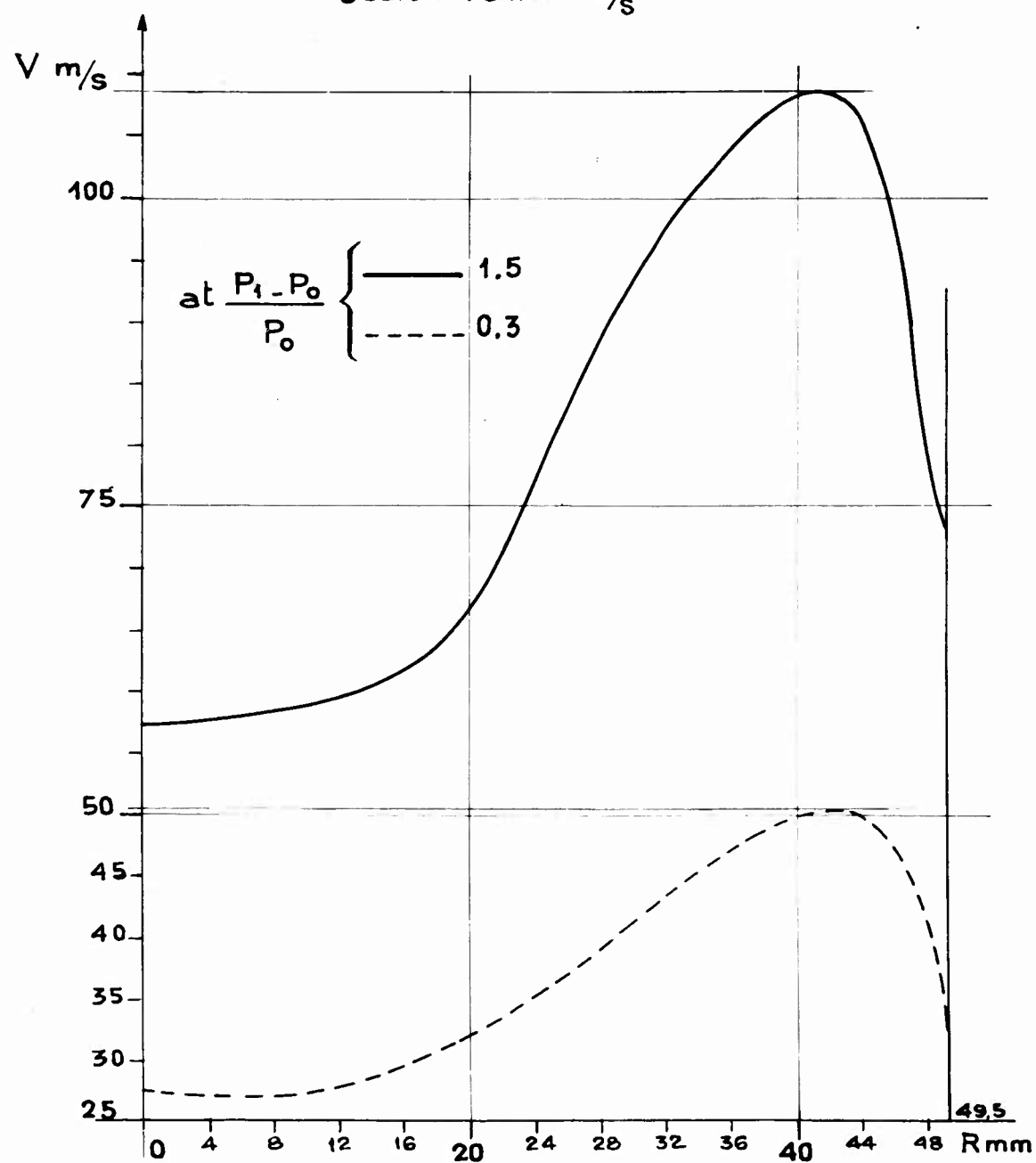
at  $\frac{P_1 - P_0}{P_0} \left\{ \begin{array}{l} \text{———} 1.5 \\ \text{-----} 0.3 \end{array} \right.$



SFERI COANDA

$V$  m/s versus  $R$  mm

Scale : 1 cm = 5 m/s

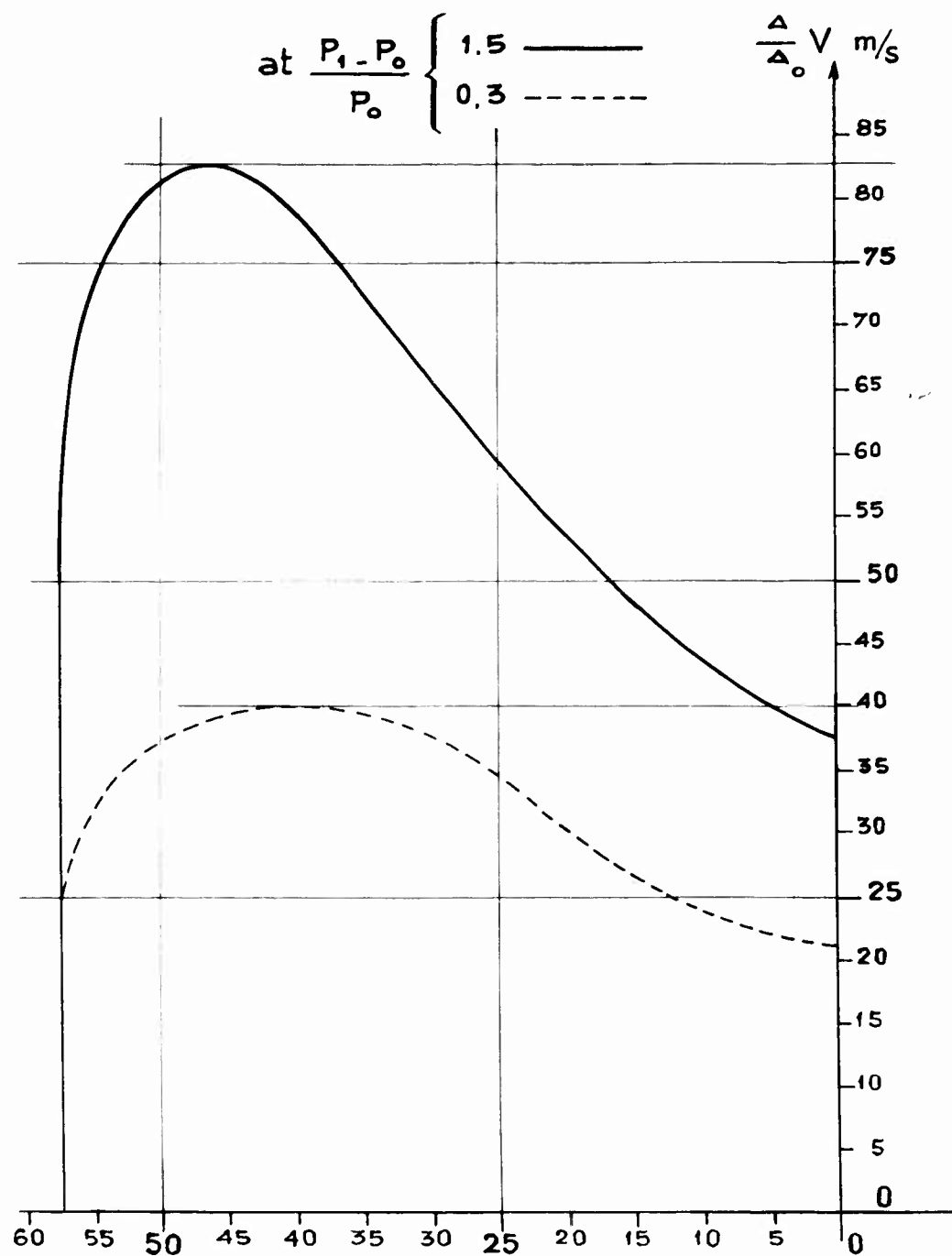


SFERI COANDA

## EXIT SECTION (VI)

Velocities plotted versus radii  
Mean values

at  $\frac{P_1 - P_0}{P_0} \begin{cases} 1.5 \text{ ———} \\ 0.3 \text{ - - - -} \end{cases}$



Scale : 1cm = 5 m/s

SFERI COANDA

Velocities plotted versus radii

FIG.23 bis

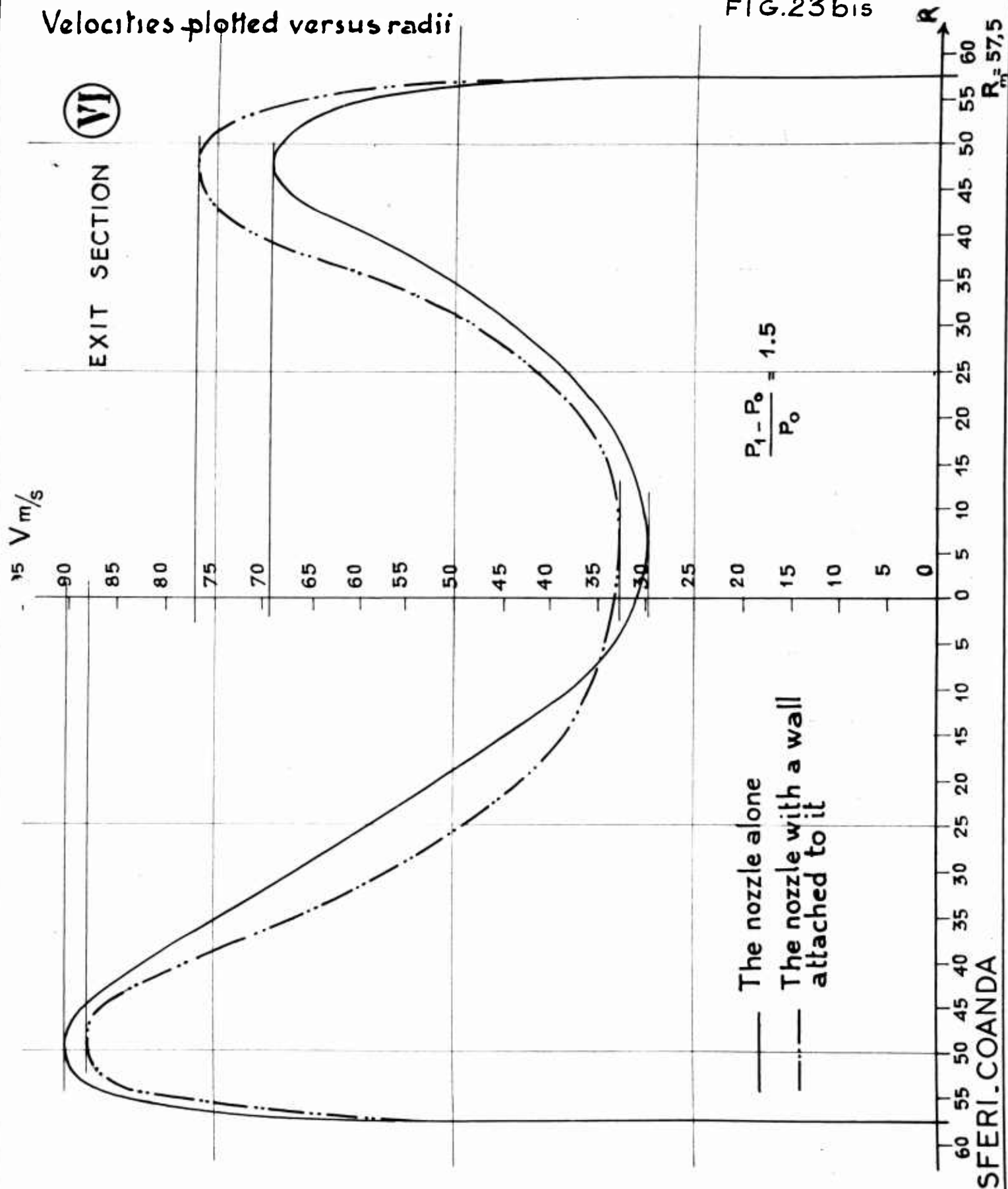


FIG.24

# ENTRANCE SECTION (I)

## Computation of the air flow discharge

Scale :  $1 \text{ cm}^2 = 1.25 \pi \text{ l/s}$

at  $\frac{P_1 - P_0}{P_0} \begin{cases} 1.5 \text{ ———} \\ 0.3 \text{ - - - -} \end{cases}$

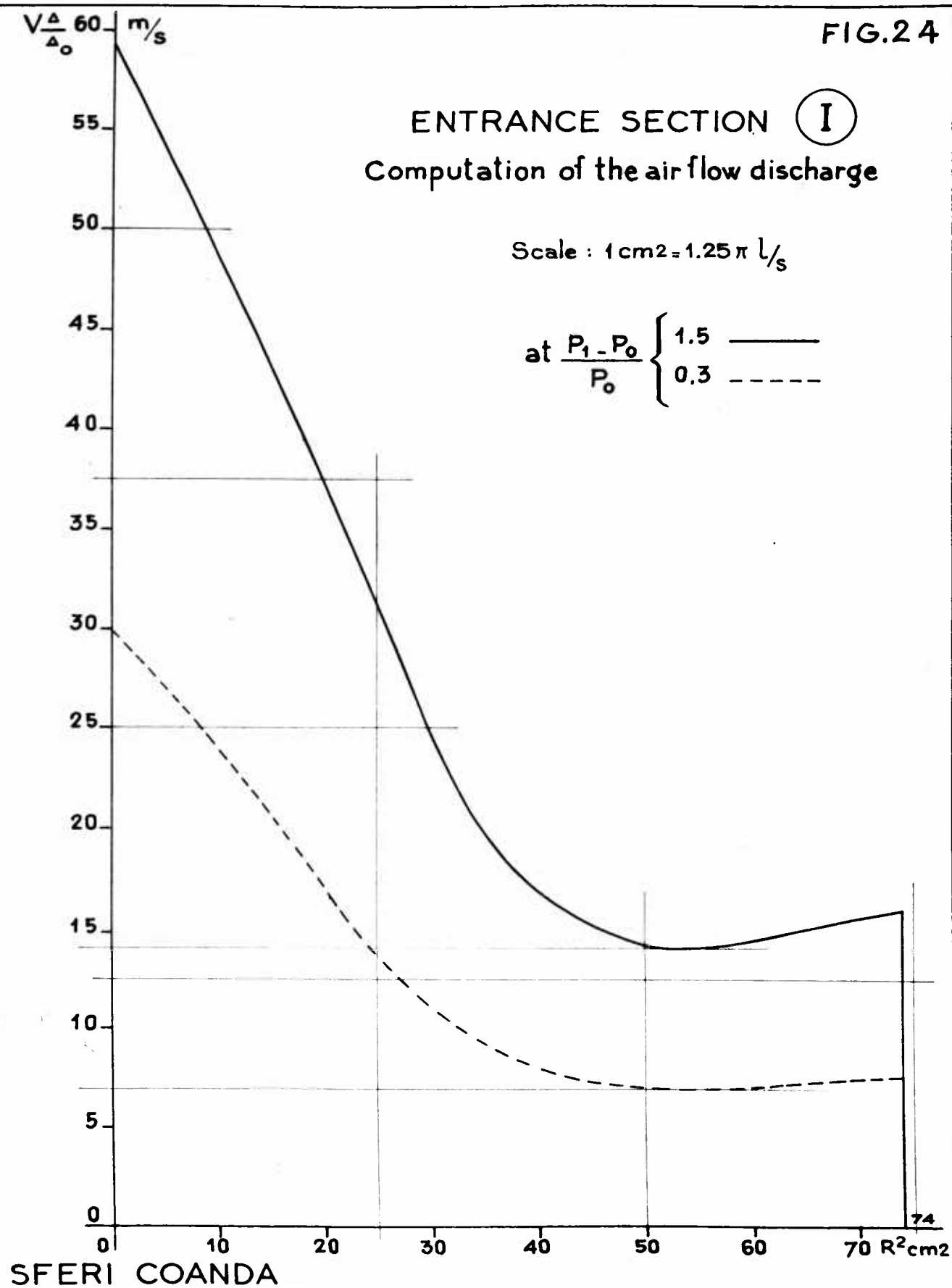
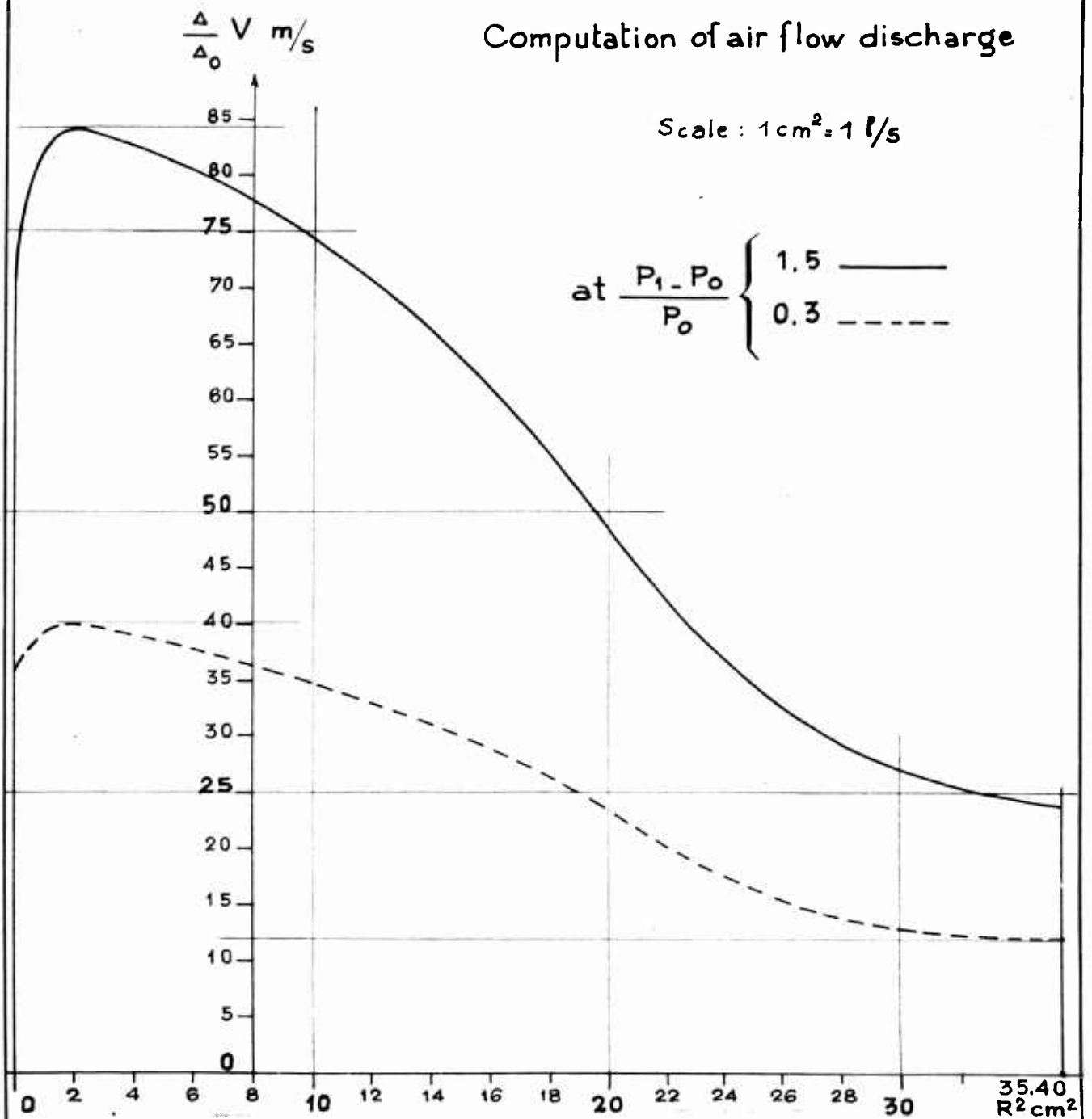


FIG 25  
UPSTREAM THE SLOT  
SECTION (II)

Computation of air flow discharge

Scale :  $1 \text{ cm}^2 = 1 \text{ l/s}$

at  $\frac{P_1 - P_0}{P_0} \begin{cases} 1.5 \text{ ———} \\ 0.3 \text{ - - - -} \end{cases}$



SFERI COANDA

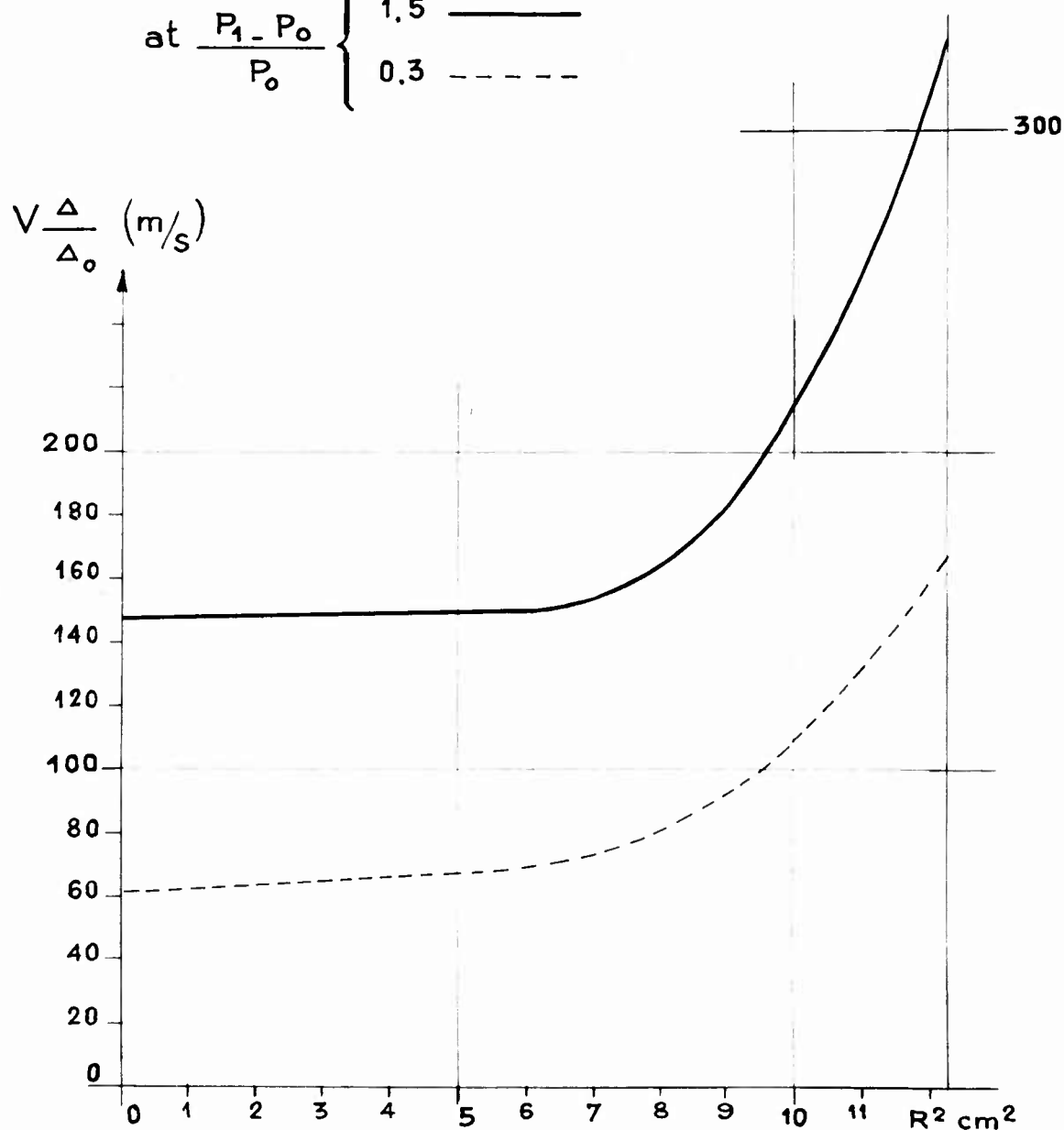
FIG.26

## THROAT SECTION (III)

Computation of the corrected  
air flow discharge

Scale :  $1 \text{ cm}^2 = 2 \pi \text{ l/s}$

at  $\frac{P_1 - P_0}{P_0} \begin{cases} 1.5 \text{ —————} \\ 0.3 \text{ - - - - -} \end{cases}$



SFERI COANDA

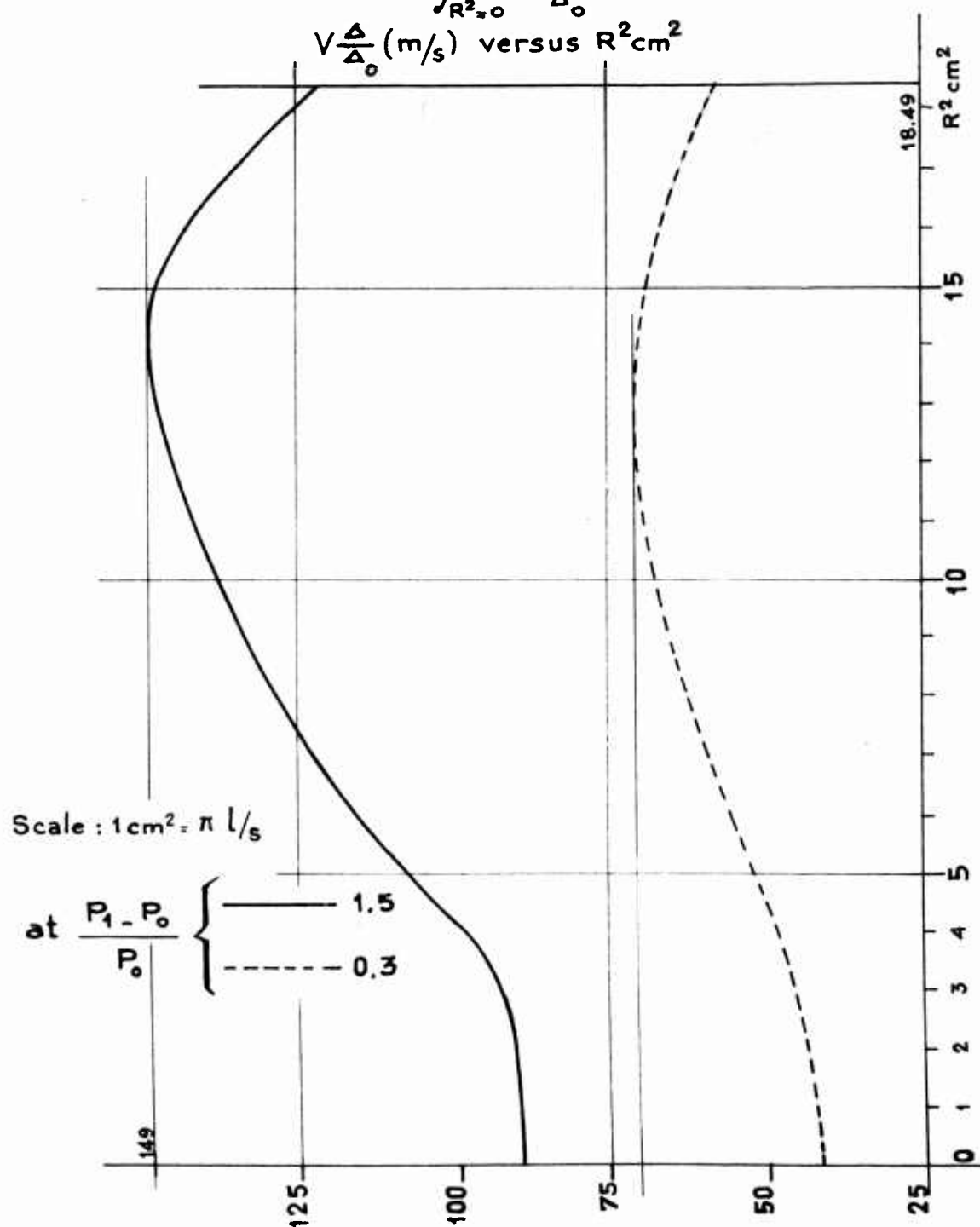
FIG.27

## UPSTREAM SECTION IN THE DIVERGENT (IV)

Computation of the corrected air discharge through the

$$\text{section} \int_{R_{z=0}^2}^{R_m^2} \frac{\Delta}{\Delta_0} V dA$$

$$V \frac{\Delta}{\Delta_0} (\text{m/s}) \text{ versus } R^2 \text{ cm}^2$$



SFERI COANDA

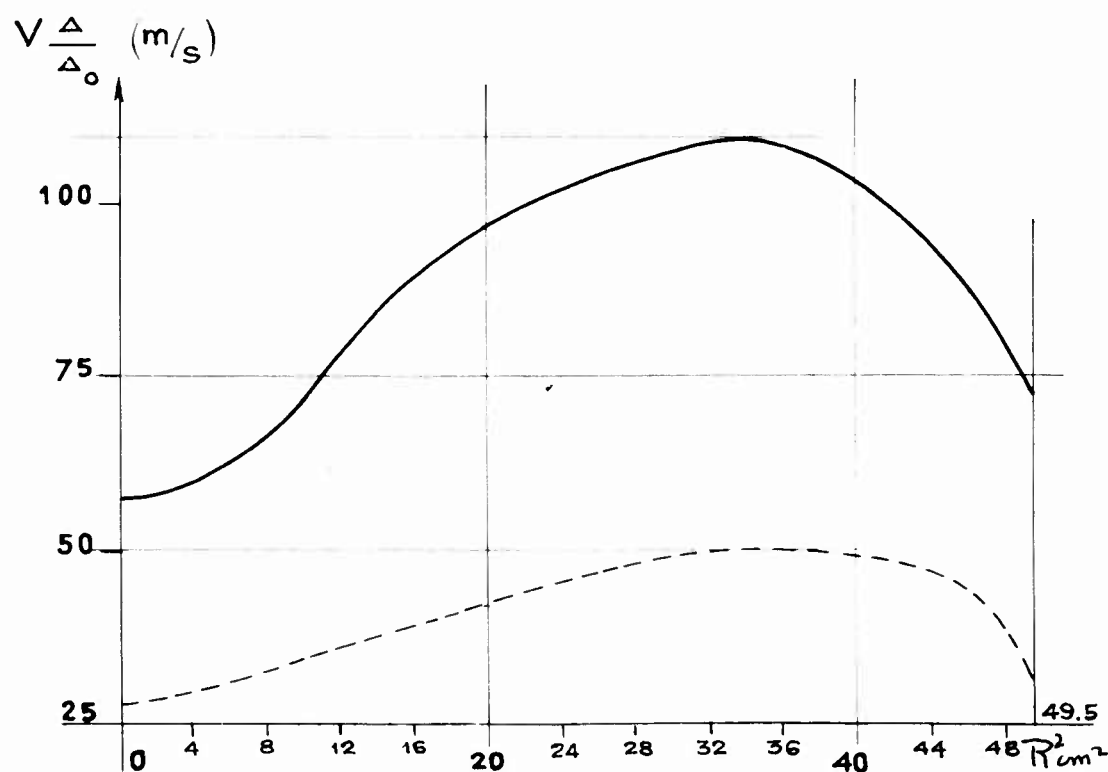
## DOWNSTREAM SECTION OF THE DIVERGENT

V

Computation of the corrected air discharge  
through the section  $\int_{R^2=0}^{R^2=(R_m)^2} \frac{\Delta}{\Delta_0} V dA$

Scale :  $1 \text{ cm}^2 = \pi \text{ l/s}$

at  $\frac{P_1 - P_0}{P_0} \begin{cases} 1.5 \text{ ————} \\ 0.3 \text{ - - - -} \end{cases}$

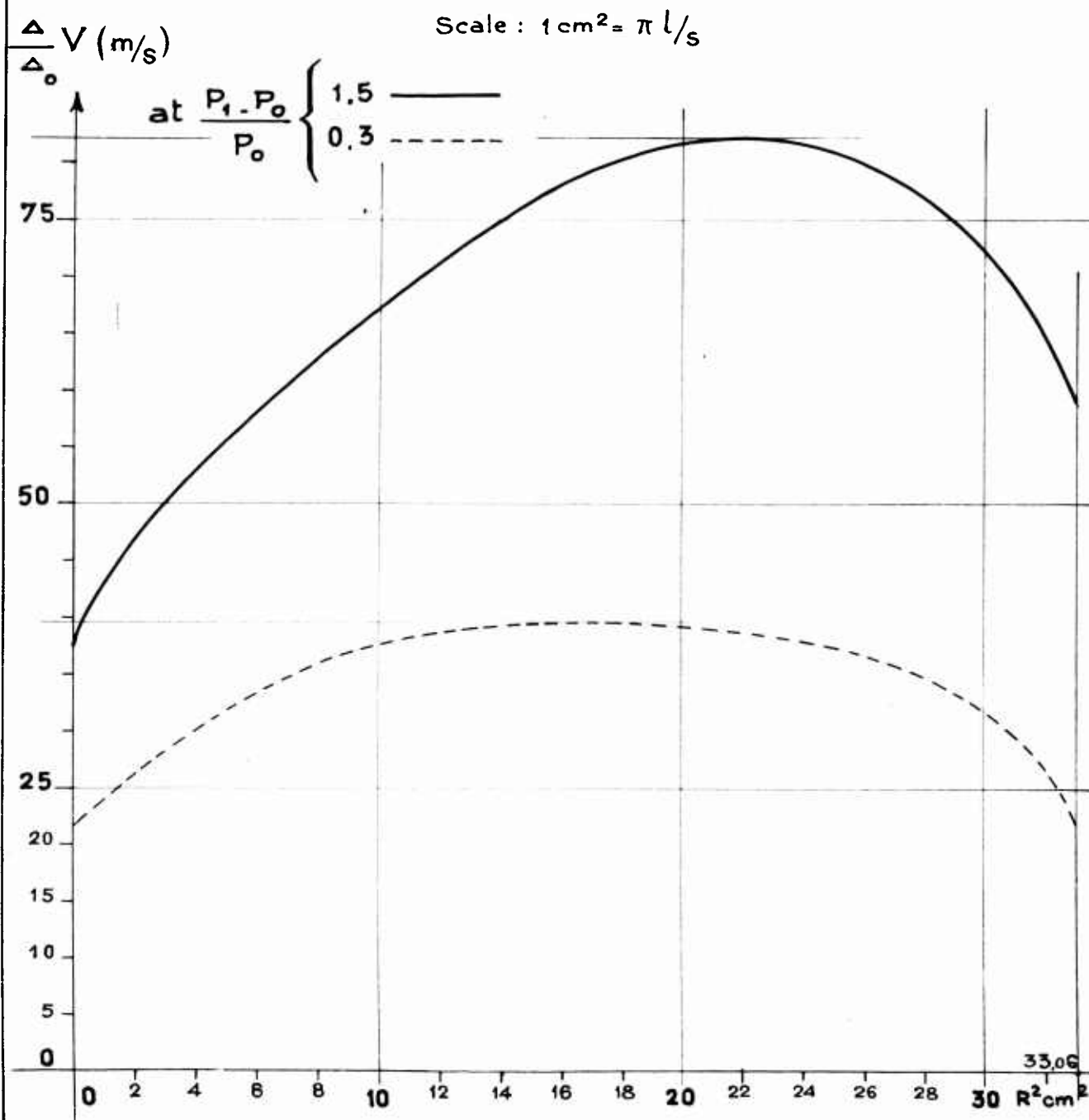


SFERI COANDA

FIG.29

## EXIT SECTION (VI)

Computation of the corrected air discharge  
through the section  $\int_{R^2=0}^{R^2=(Rm)^2} \frac{\Delta}{\Delta_0} V dA$



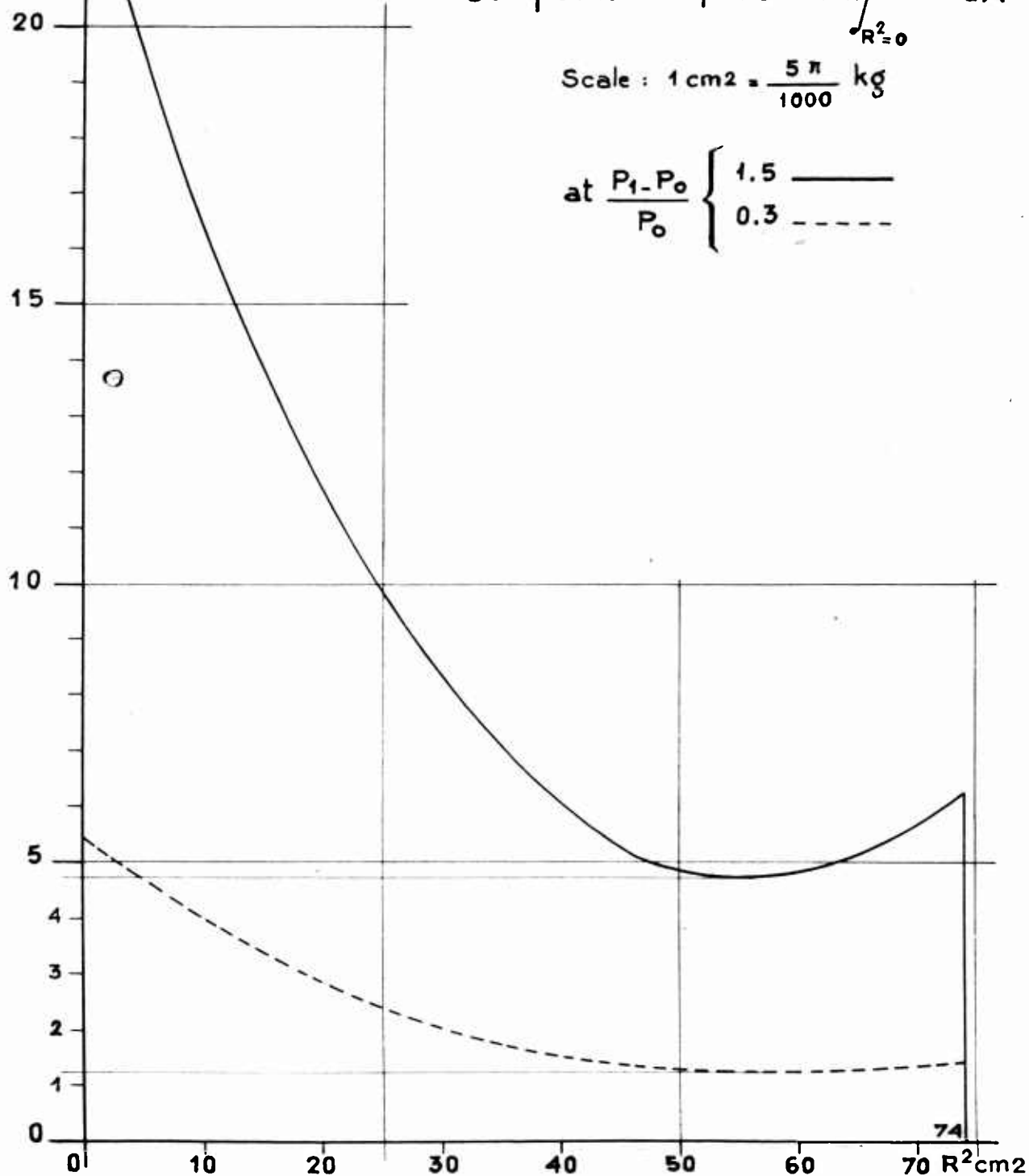
SFERI COANDA

FIG.30

 $(P_s - P_0)$  g/cm<sup>2</sup>

ENTRANCE SECTION

I

Computation of the term  $\int_{R^2=0}^{R^2=(R_m)^2} P dA$ Scale :  $1 \text{ cm}^2 = \frac{5 \pi}{1000} \text{ kg}$ at  $\frac{P_1 - P_0}{P_0} \begin{cases} 1.5 \text{ ———} \\ 0.3 \text{ - - - -} \end{cases}$ 

SFERI COANDA

FIG.31

UPSTREAM THE SLOT

SECTION **II**

Computation of the term  $\int_{R^2=0}^{R^2=(R_m)^2} (P_s - P_o) dA$

Scale :  $1 \text{ cm}^2 = \frac{4 \pi}{1000} \text{ kg}$

at  $\frac{P_1 - P_o}{P_o} \begin{cases} 1.5 \text{ —————} \\ 0.3 \text{ - - - - -} \end{cases}$

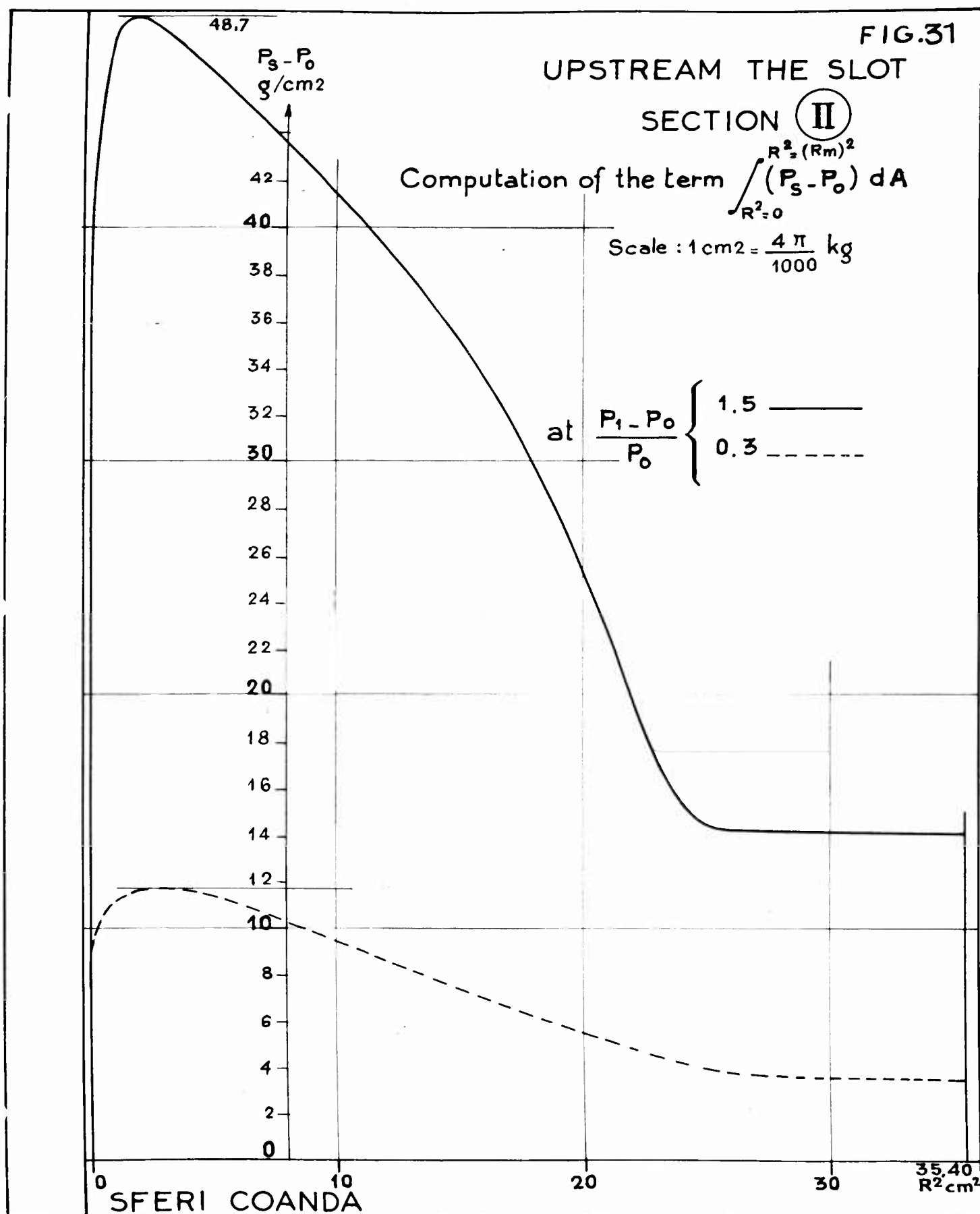
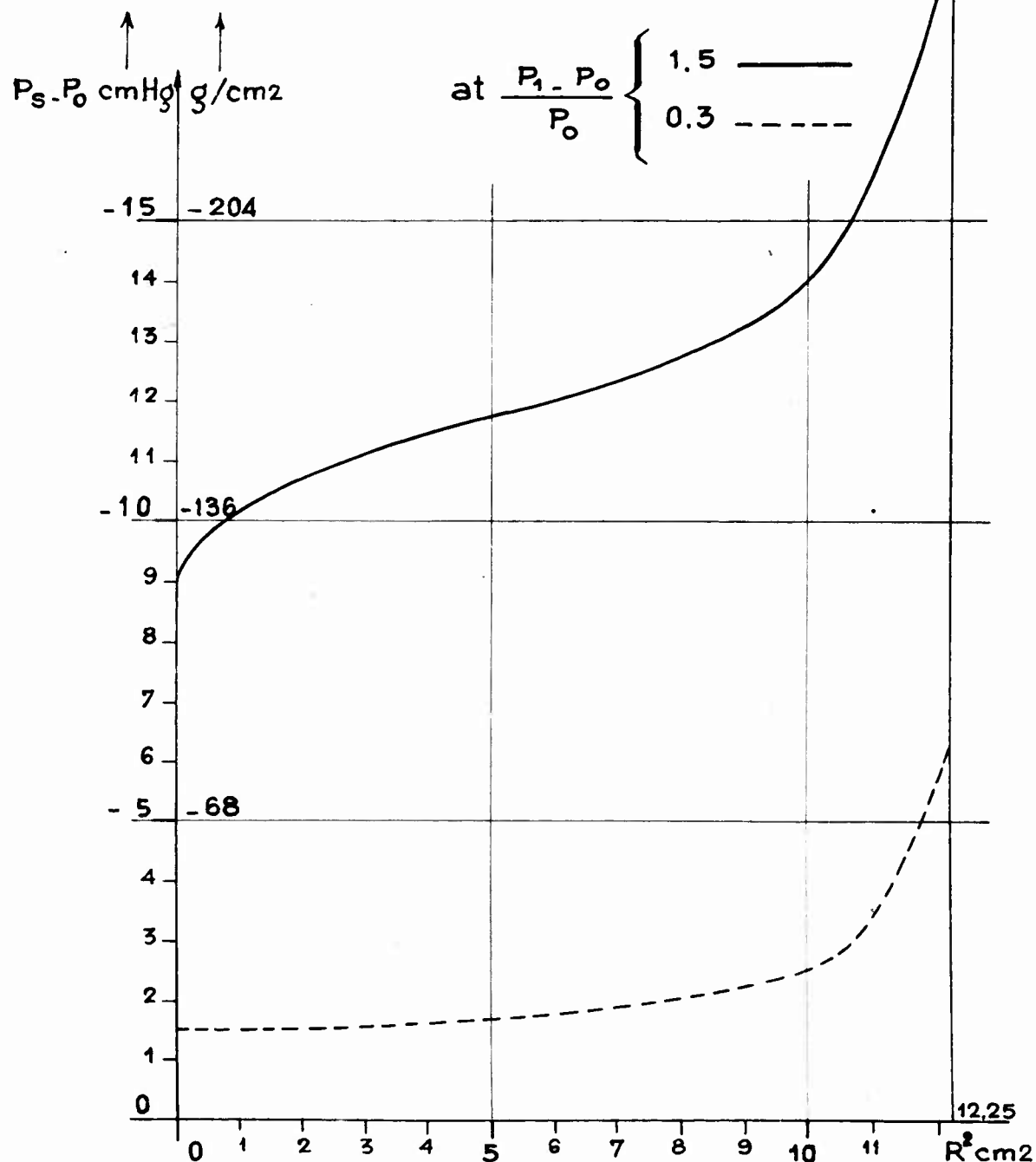


FIG.32

THROAT SECTION

III

Computation of the term  $\int_{R^2=0}^{R^2=(R_m)^2} (P_s - P_0) dA$ Scale : 1 cm<sup>2</sup> = 0.0428 kg

SFERI COANDA

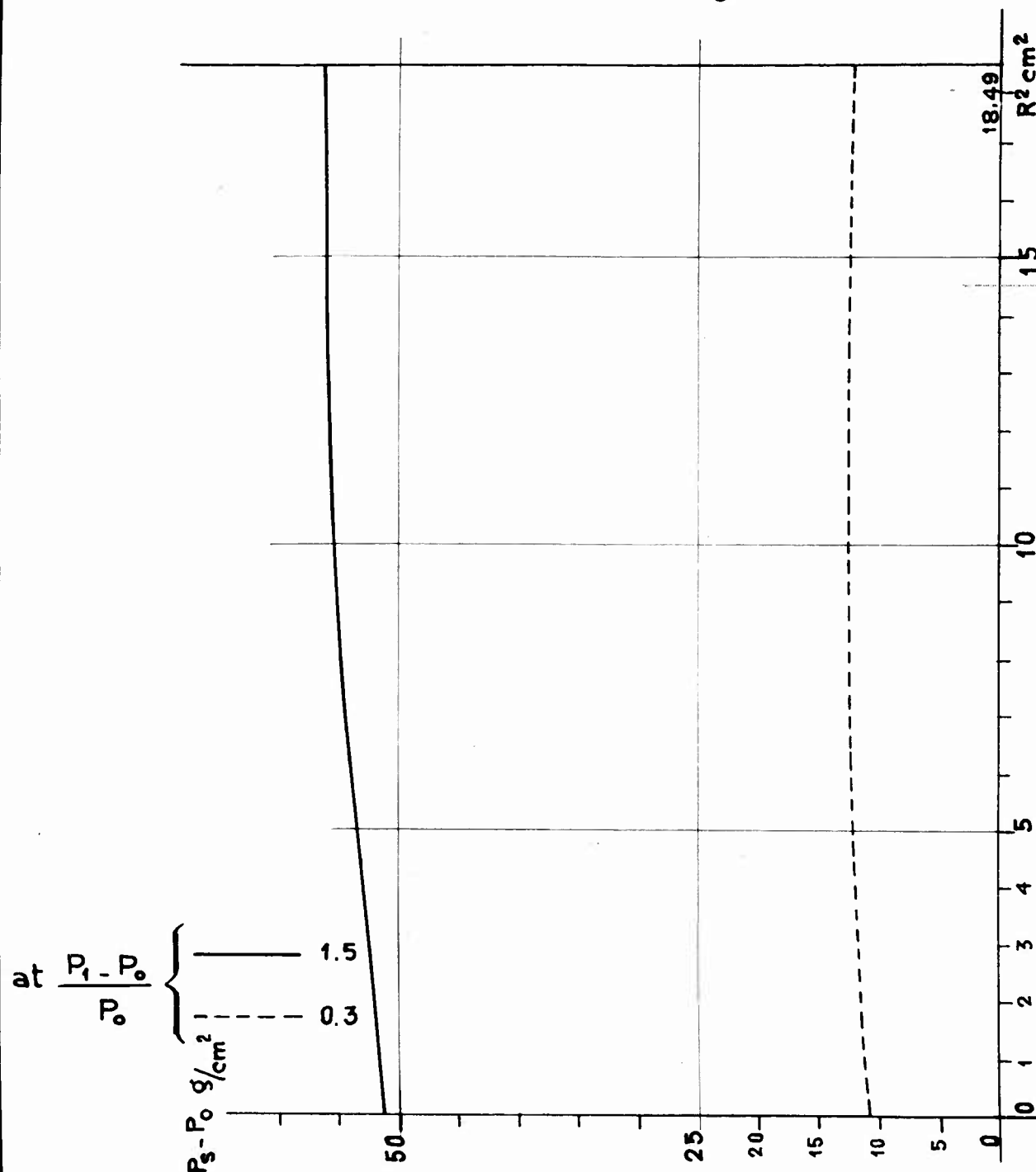
FIG.33

# UPSTREAM SECTION IN THE DIVERGENT

IV

Effective static pressures plotted versus  $R^2$

Scale :  $1 \text{ cm}^2 = 5 \pi 10^{-3} \text{ kg}$



SFERI COANDA

# DOWNSTREAM SECTION OF THE DIVERGENT

(V)

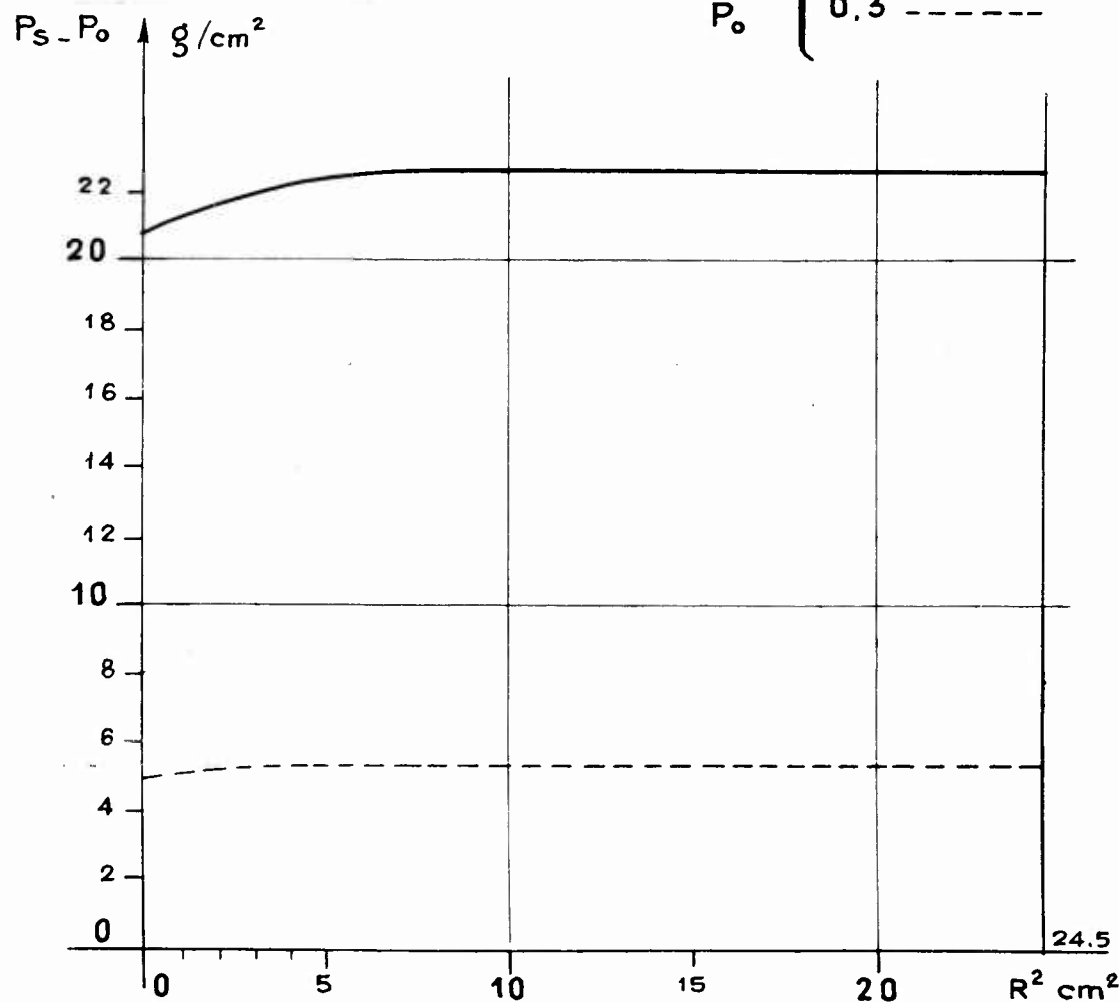
Computation of the pressure term

$$\int_{R=0}^{R^2=(R_m)^2} (P_s - P_o) dA$$

$P_s - P_o$  g/cm<sup>2</sup> versus  $R^2$  cm<sup>2</sup>

Scale: 1 cm<sup>2</sup> =  $4 \pi 10^{-3}$  kg

at  $\frac{P_1 - P_o}{P_o} \begin{cases} 1.5 \text{ ———} \\ 0.3 \text{ - - - -} \end{cases}$



SFERI COANDA

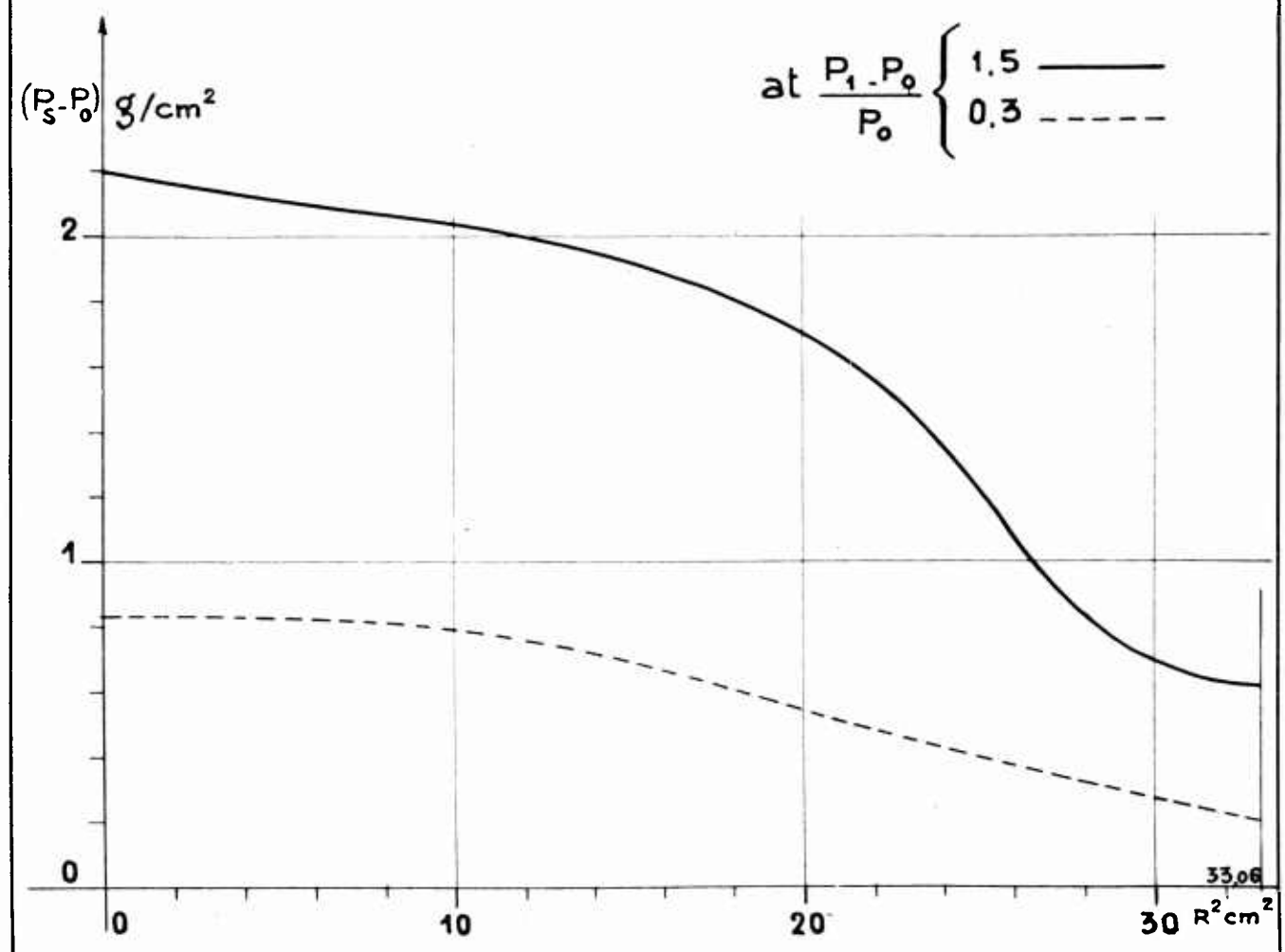
# EXIT SECTION (VI)

Computation of the pressure term

$$\int_{R^2=0}^{R^2=(R_m)^2} (P_s - P_o) dA$$

$P_s - P_o$  g/cm<sup>2</sup> versus  $R^2$  cm<sup>2</sup>

Scale: 1 cm<sup>2</sup> = 4π10<sup>-4</sup> kg

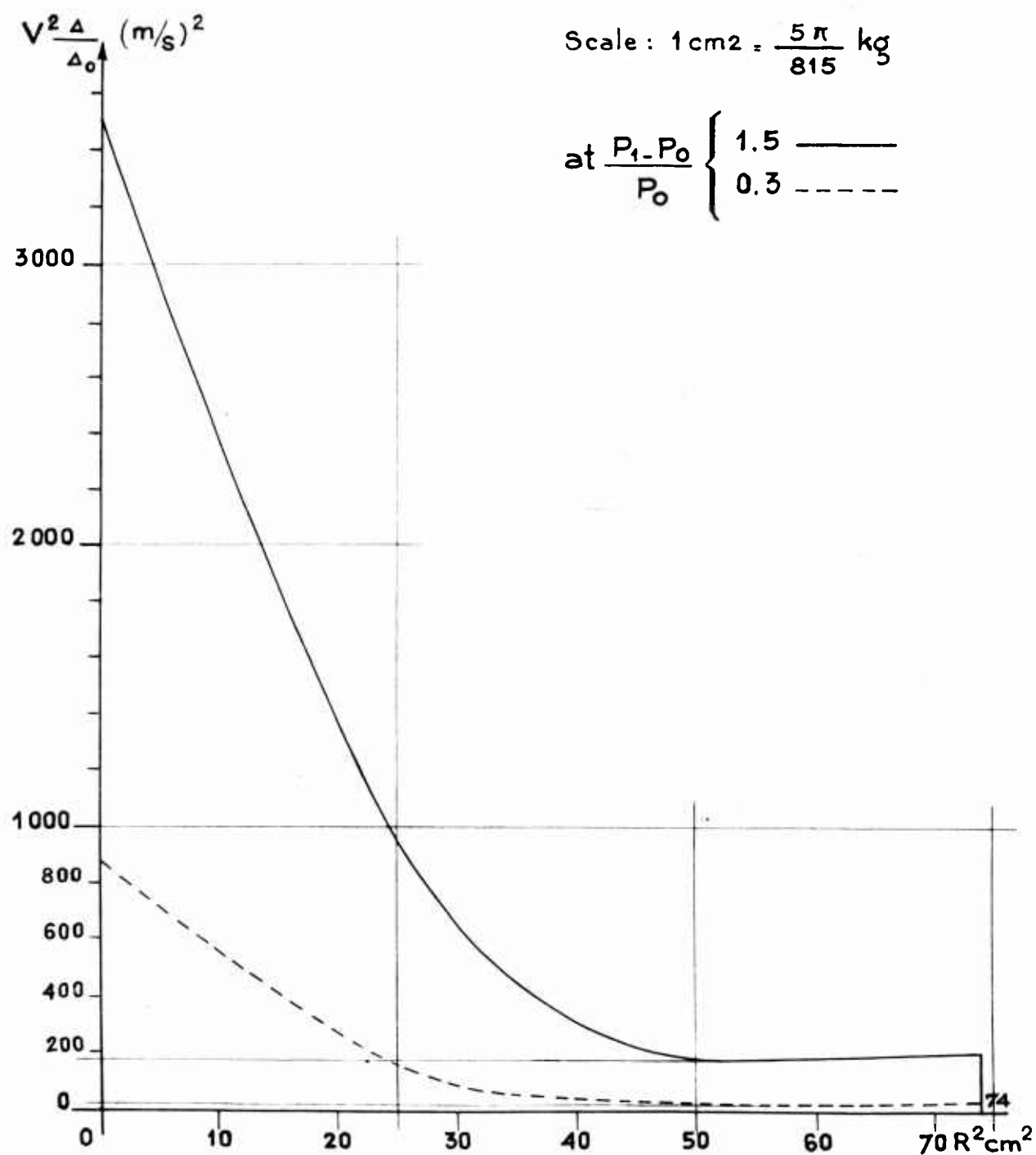


SFERI COANDA

FIG.36

## ENTRANCE SECTION (I)

Computation of momentum MV



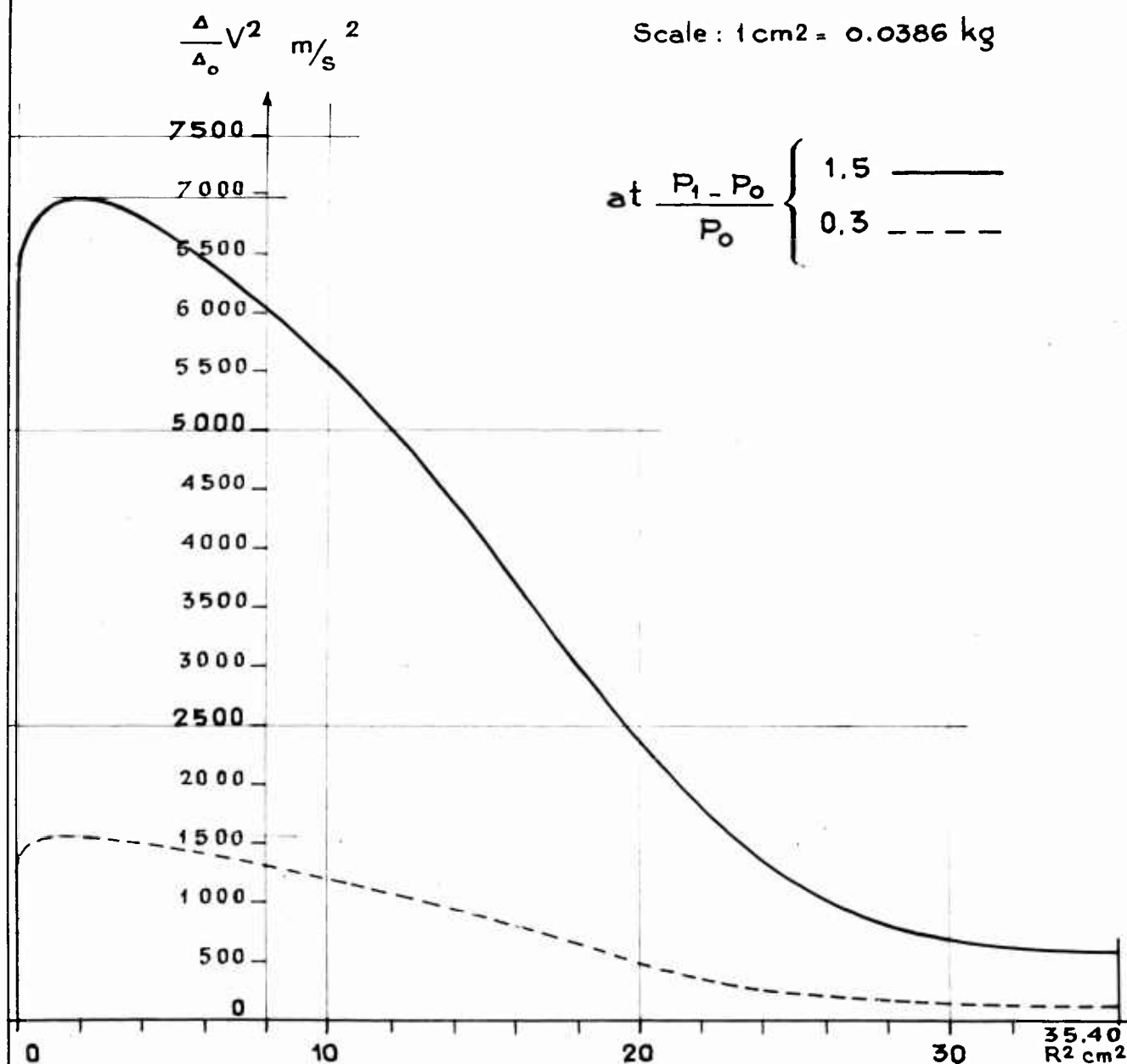
SFERI COANDA

FIG.37

UPSTREAM THE SLOT  
SECTION (II)

Computation of momentum MV

Scale : 1 cm<sup>2</sup> = 0.0386 kg



SFERI COANDA

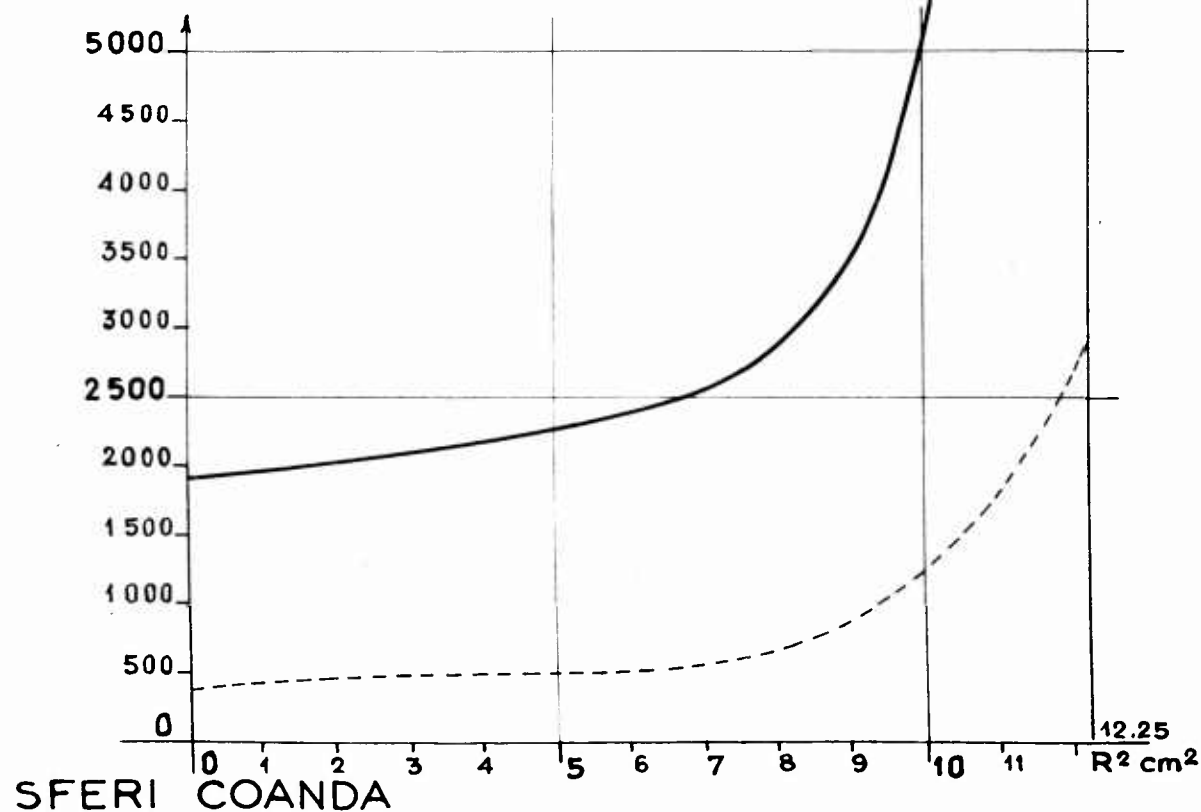
FIG.38

## THROAT SECTION (III)

Computation of the momentum  $MV$ Scale :  $1 \text{ cm}^2, 0.0194 \text{ kg}$ 

$$\text{at } \frac{P_1 - P_0}{P_0} \begin{cases} 1.5 \text{ ————} \\ 0.3 \text{ - - - -} \end{cases}$$

$$\frac{\Delta}{A_0} V^2 \text{ (m/s)}^2$$



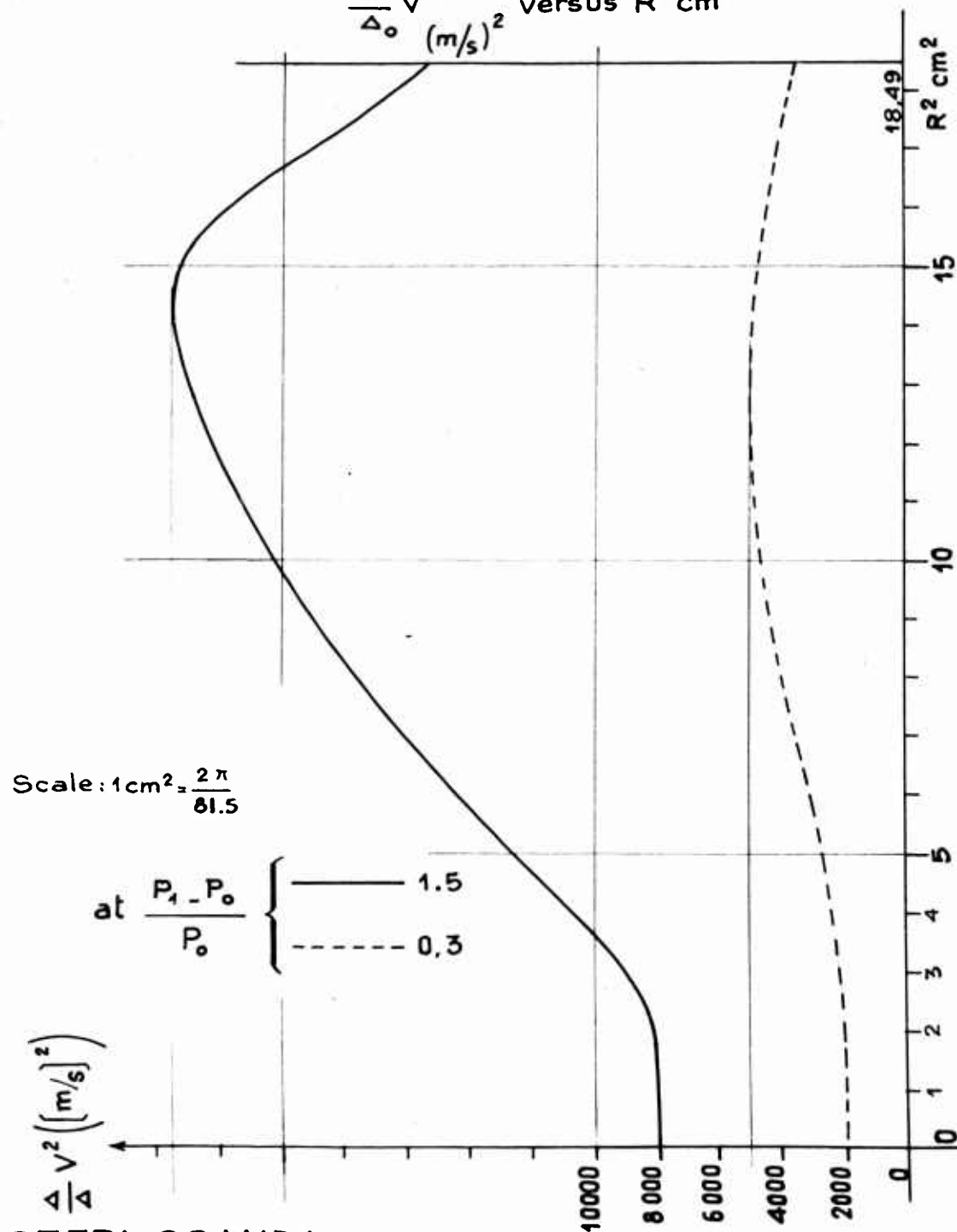
SFERI COANDA

FIG.39

## UPSTREAM SECTION IN THE DIVERGENT (IV)

Computation of the momentum  $MV = \int_{R^2=0}^{R^2=(Rm)^2} V dm = \frac{\Delta_0}{g} \int_{R^2=0}^{R^2=(Rm)^2} \frac{\Delta}{\Delta_0} V^2 dA$

$\frac{\Delta}{\Delta_0} V^2$  versus  $R^2 \text{ cm}^2$



SFERI COANDA

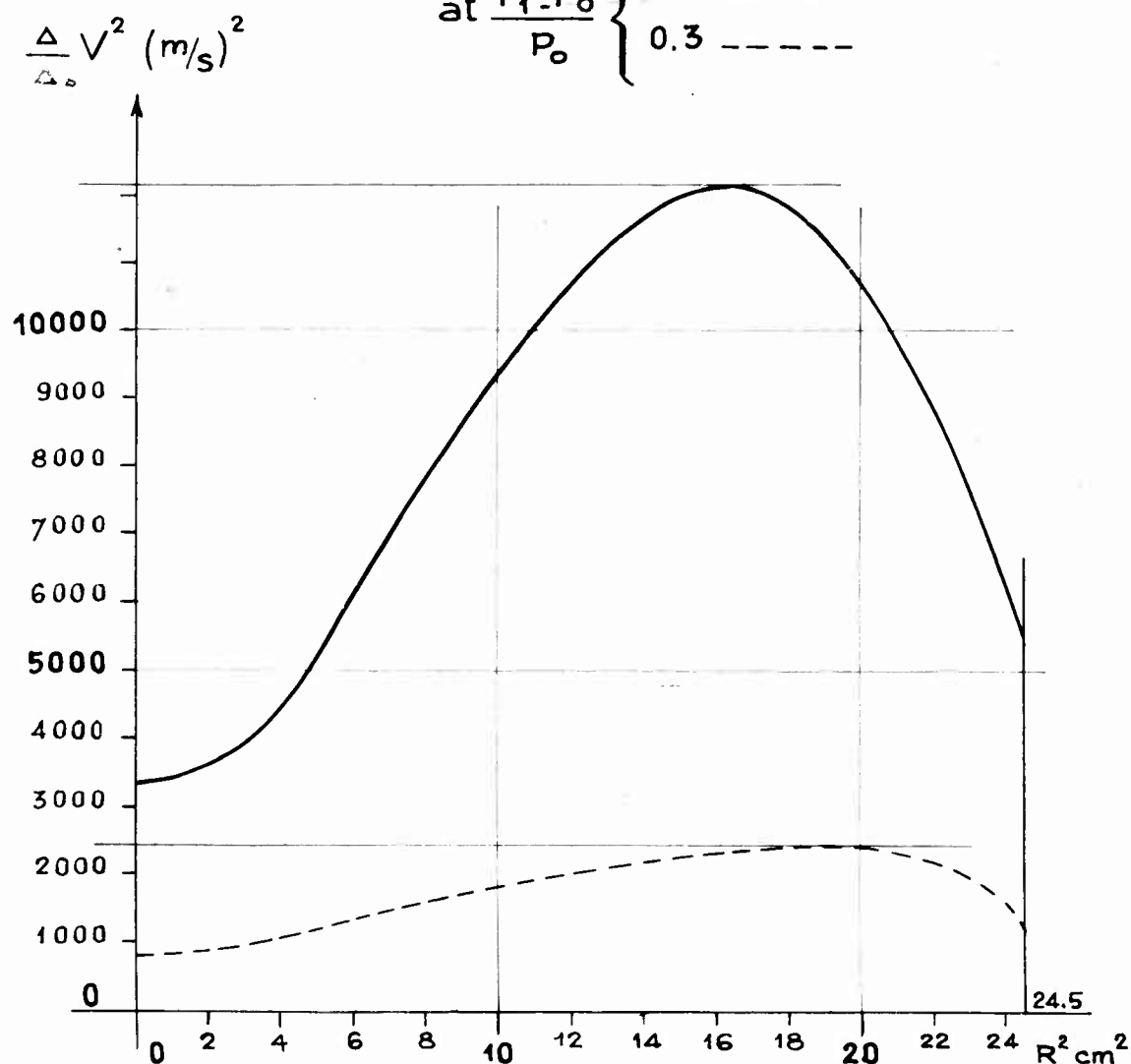
## DOWNSTREAM SECTION OF THE DIVERGENT

(V)

Computation of  $\frac{\Delta_o}{g} \int_{R^2=0}^{R^2=(Rm)^2} \frac{\Delta}{\Delta_o} V^2 dA$

Scale :  $1 \text{ cm}^2 = \frac{2\pi}{8.15} 10^{-2} \text{ kg}$

at  $\frac{P_1 - P_o}{P_o} \begin{cases} 1.5 \text{ ———} \\ 0.3 \text{ - - - -} \end{cases}$



SFERI COANDA

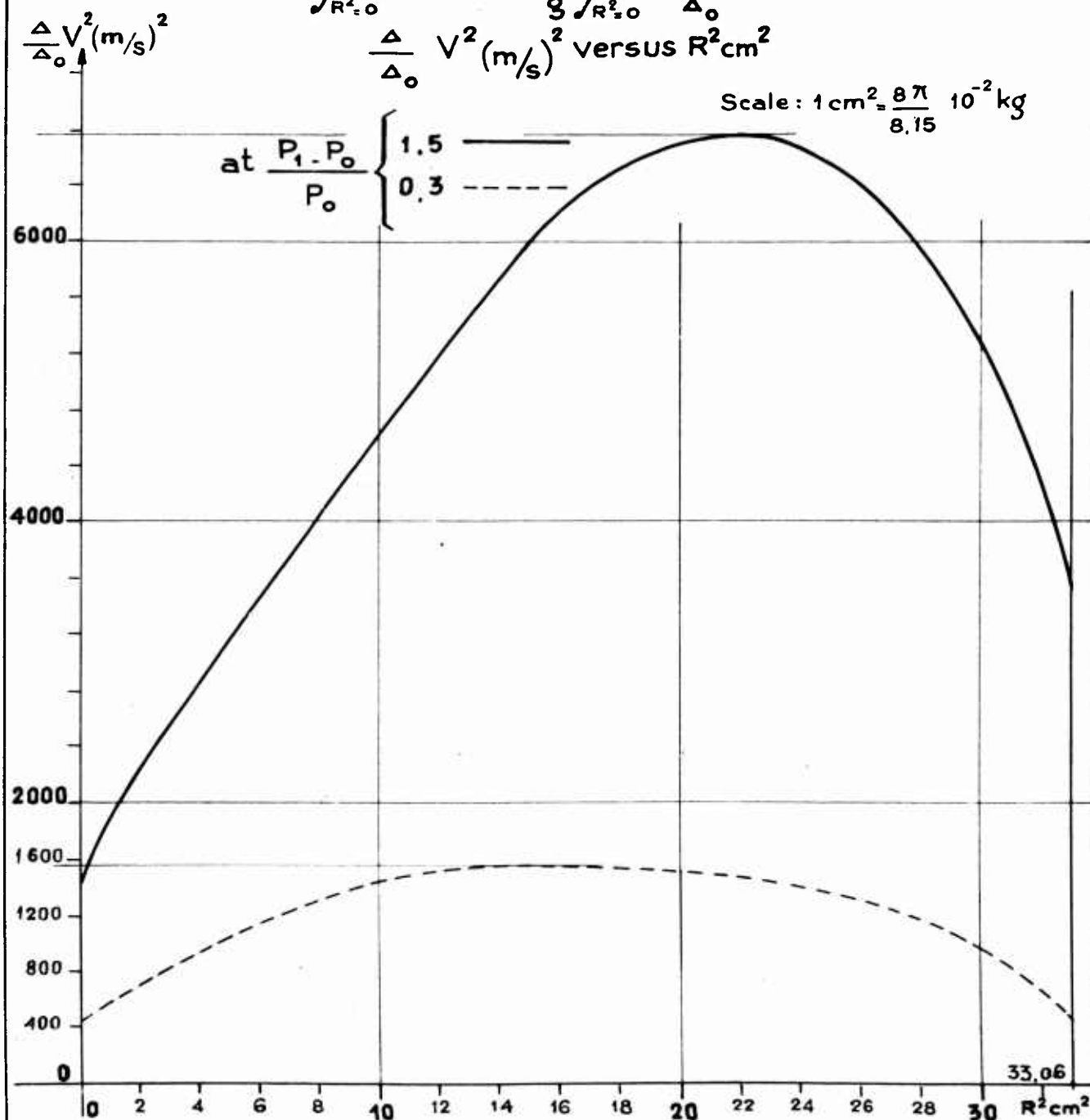
FIG.41

## EXIT SECTION (VI)

Computation of the momentum

$$MV = \int_{R^2=0}^{R^2=(R_m)^2} V dm = \frac{\Delta_o}{g} \int_{R^2=0}^{R^2=(R_m)^2} \frac{\Delta}{\Delta_o} V^2 dA$$

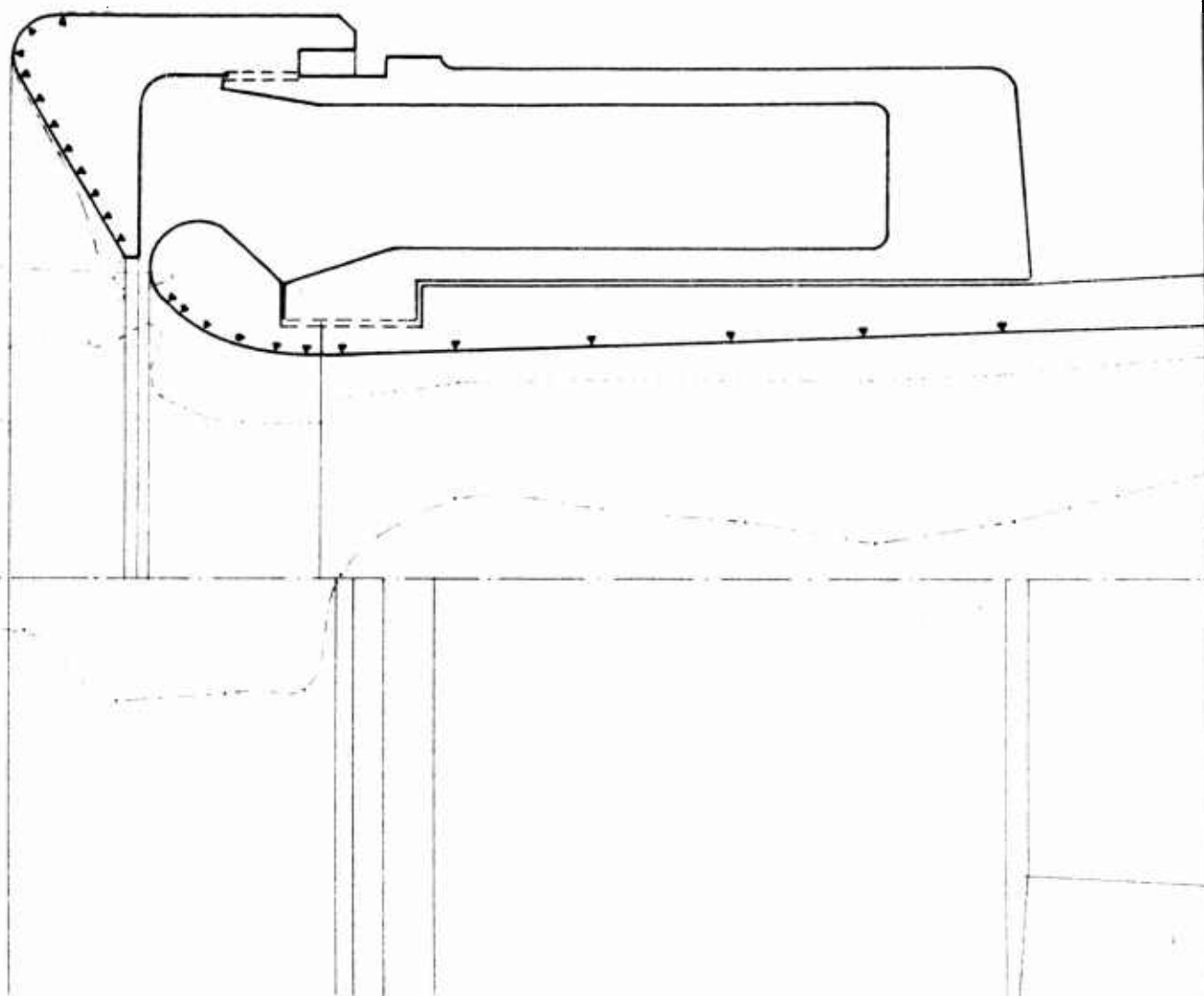
$$\frac{\Delta}{\Delta_o} V^2 (\text{m/s})^2 \text{ versus } R^2 \text{ cm}^2$$



SFERI COANDA

General view of the distribution of the depressions  
( $P_w - P_0$ ) along the internal profile of the nozzle

1



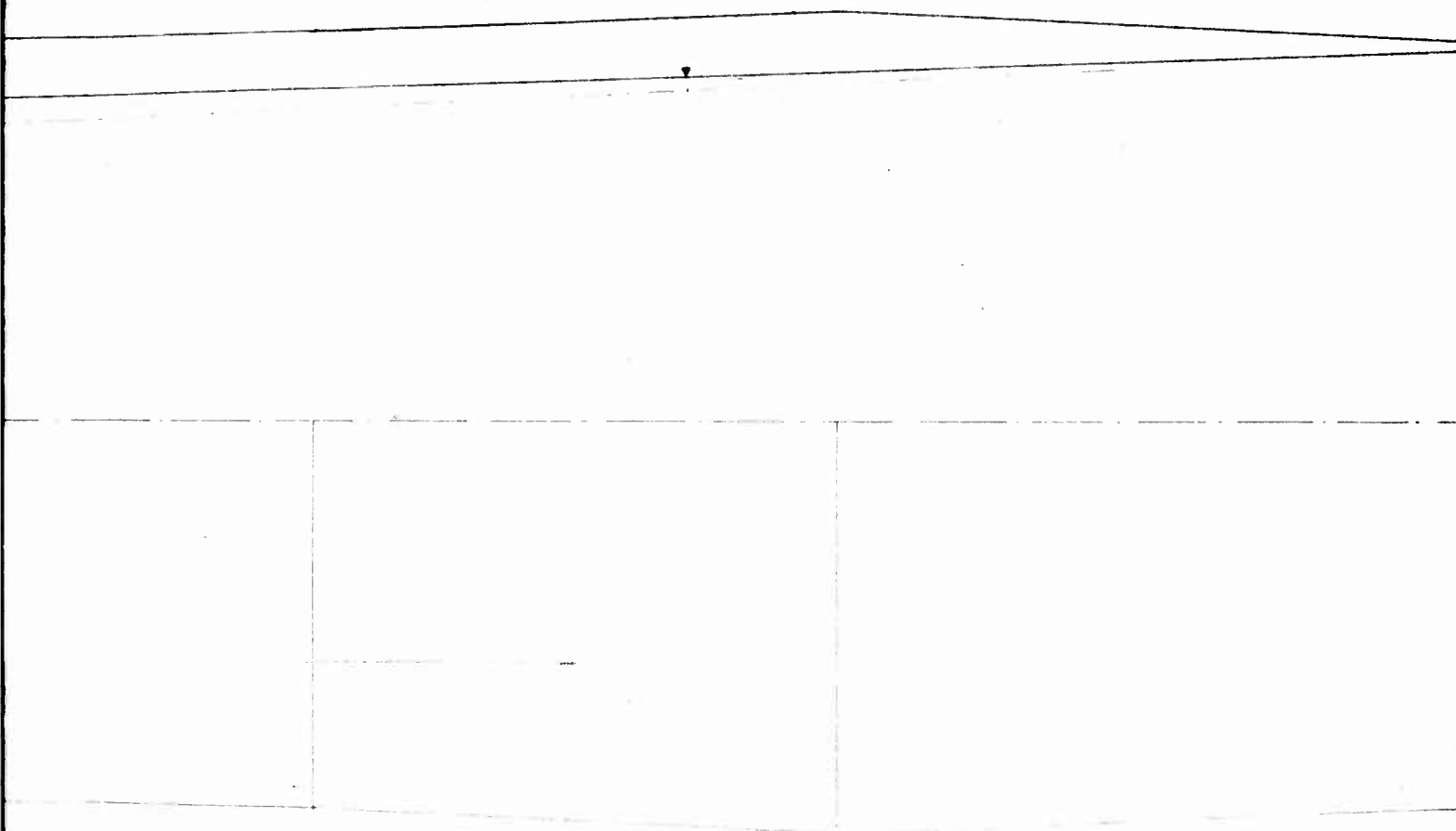
General scale :  $1 \text{ cm} = 50 \text{ gr/cm}^2$   
at this scale the pressures on the cap at  $\frac{P_i - P_0}{P_0} = 0.3$  are not visible

SFERI-COANDA.

**2**

3

4

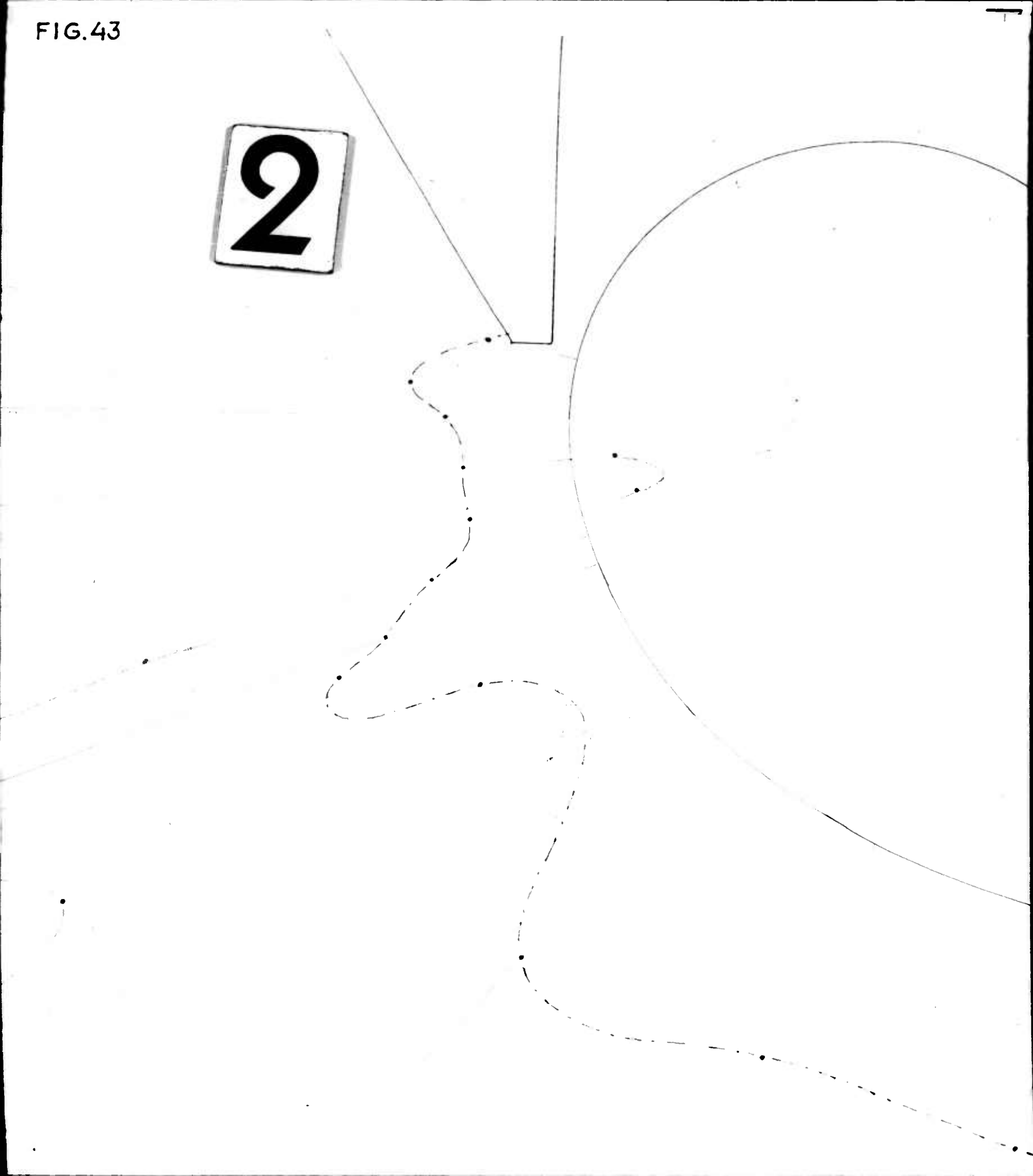


Detailed view of the depressions ( $P_w - P_o$ ) FIG.43  
on the lip.

1

FIG.43

2



3

4

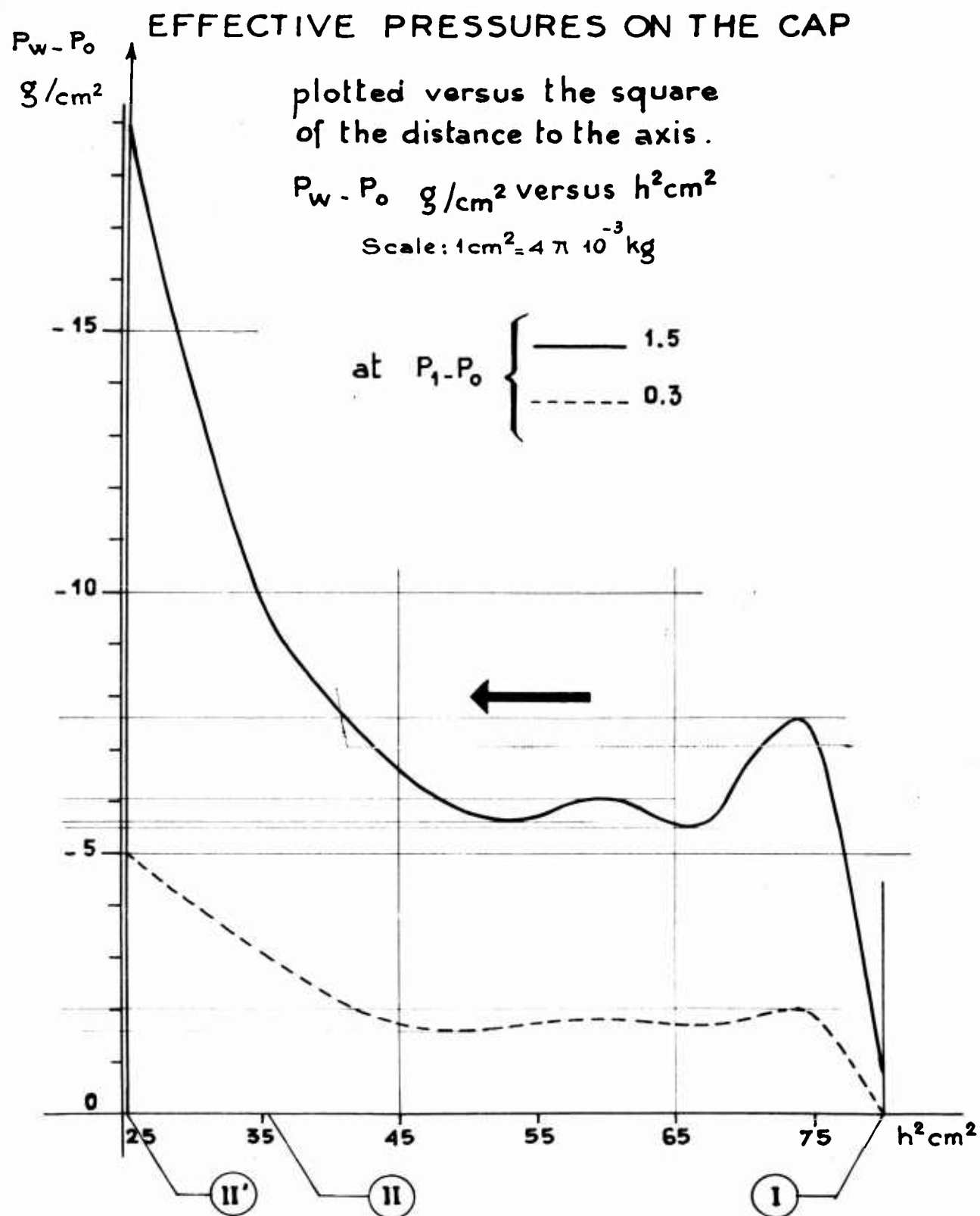
$$\frac{P_1 - P_0}{P_0} \left\{ \begin{array}{l} \text{---} 1.5 \text{ Kg/cm}^2 \\ \text{---} 0.3 \text{ Kg/cm}^2 \end{array} \right.$$

Scale 1 cm = 10 gr/cm<sup>2</sup>

5

6

FIG.44



SFERI COANDA

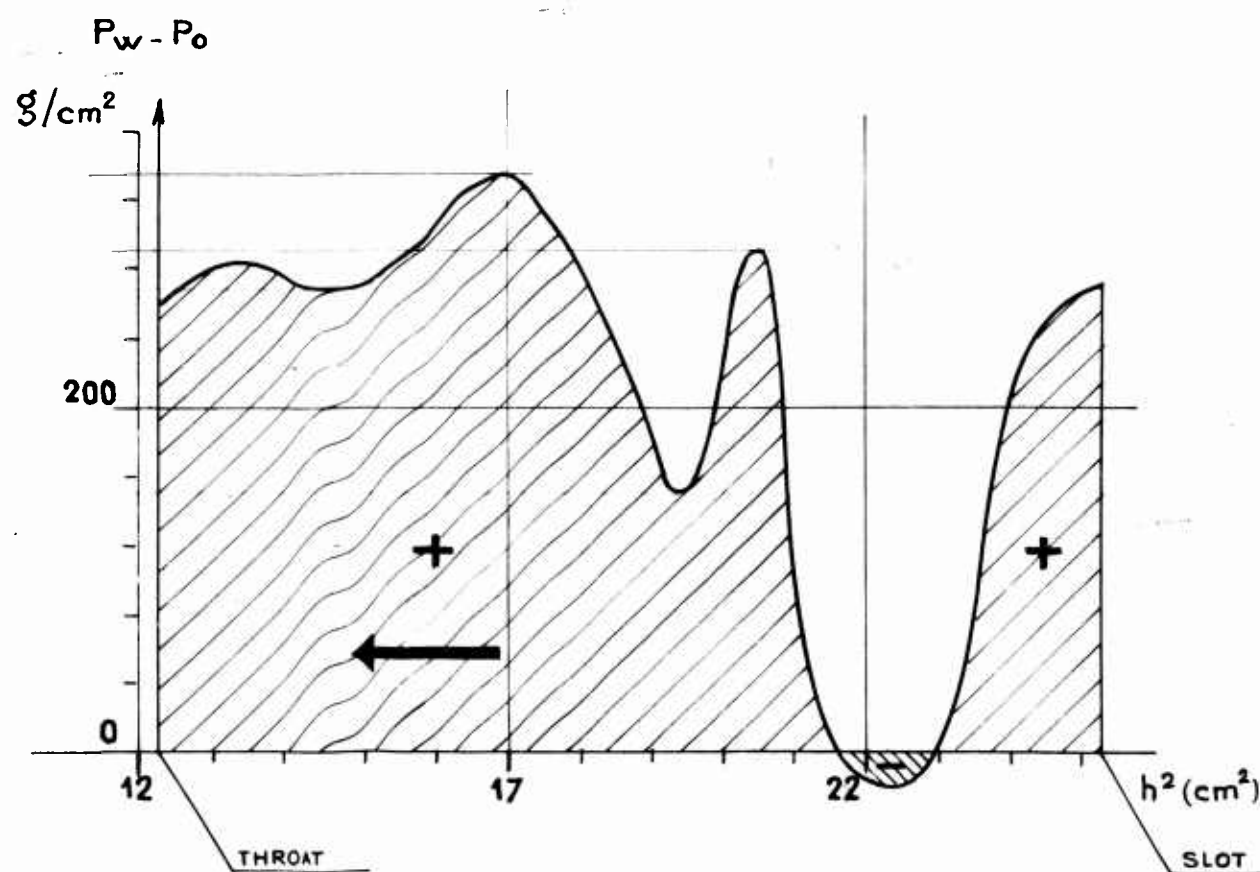
## EFFECTIVE PRESSURES ON THE LIP

plotted versus the square  
of the distance to the axis.

$P_w - P_o$  g/cm<sup>2</sup> versus  $h^2$  cm<sup>2</sup>

Scale :  $1 \text{ cm}^2 = 4 \pi 10^{-2} \text{ kg}$

at  $P_1 - P_o = 1.5$



SFERI COANDA

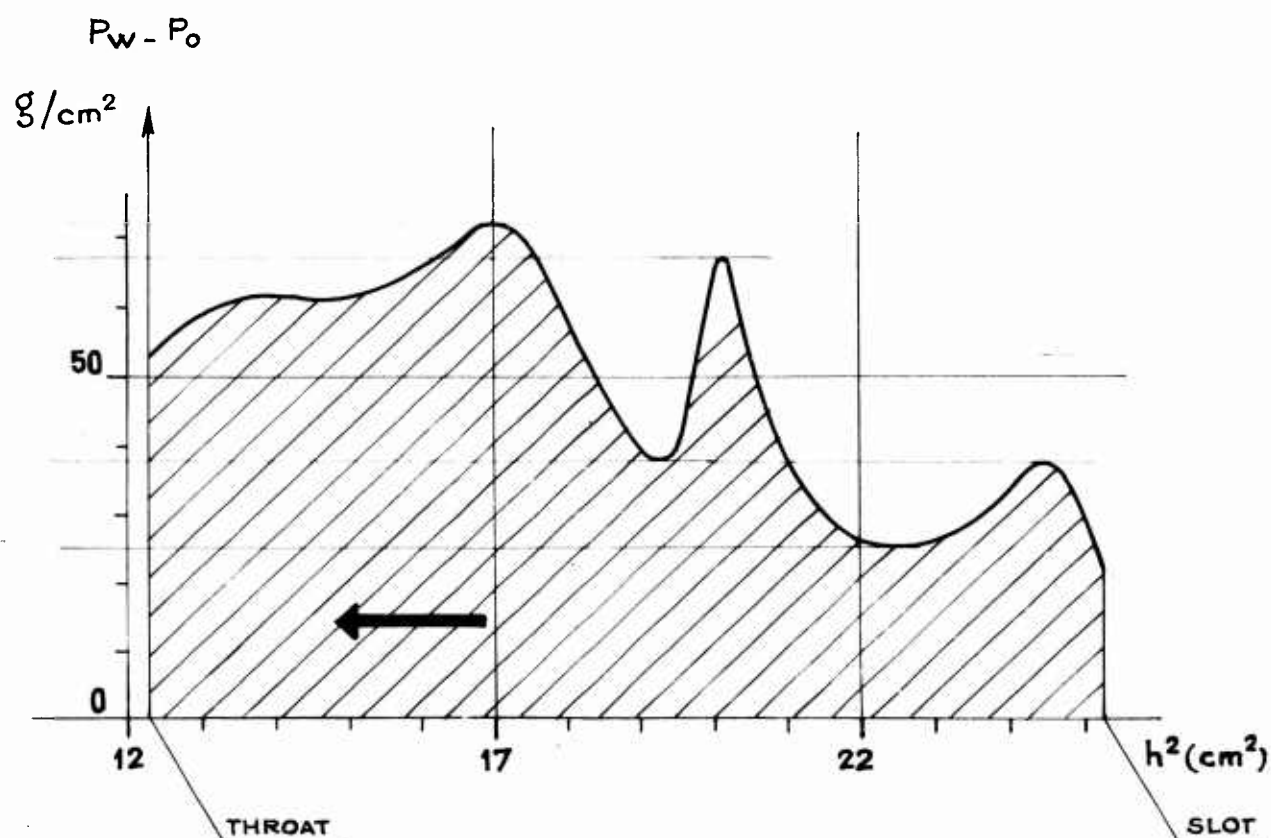
## EFFECTIVE PRESSURES ON THE LIP

plotted versus the square  
of the distance to the axis.

$P_w - P_o$  g/cm<sup>2</sup> versus  $h^2$  cm<sup>2</sup>

Scale :  $1 \text{ cm}^2 = \frac{\pi}{100} \text{ kg}$

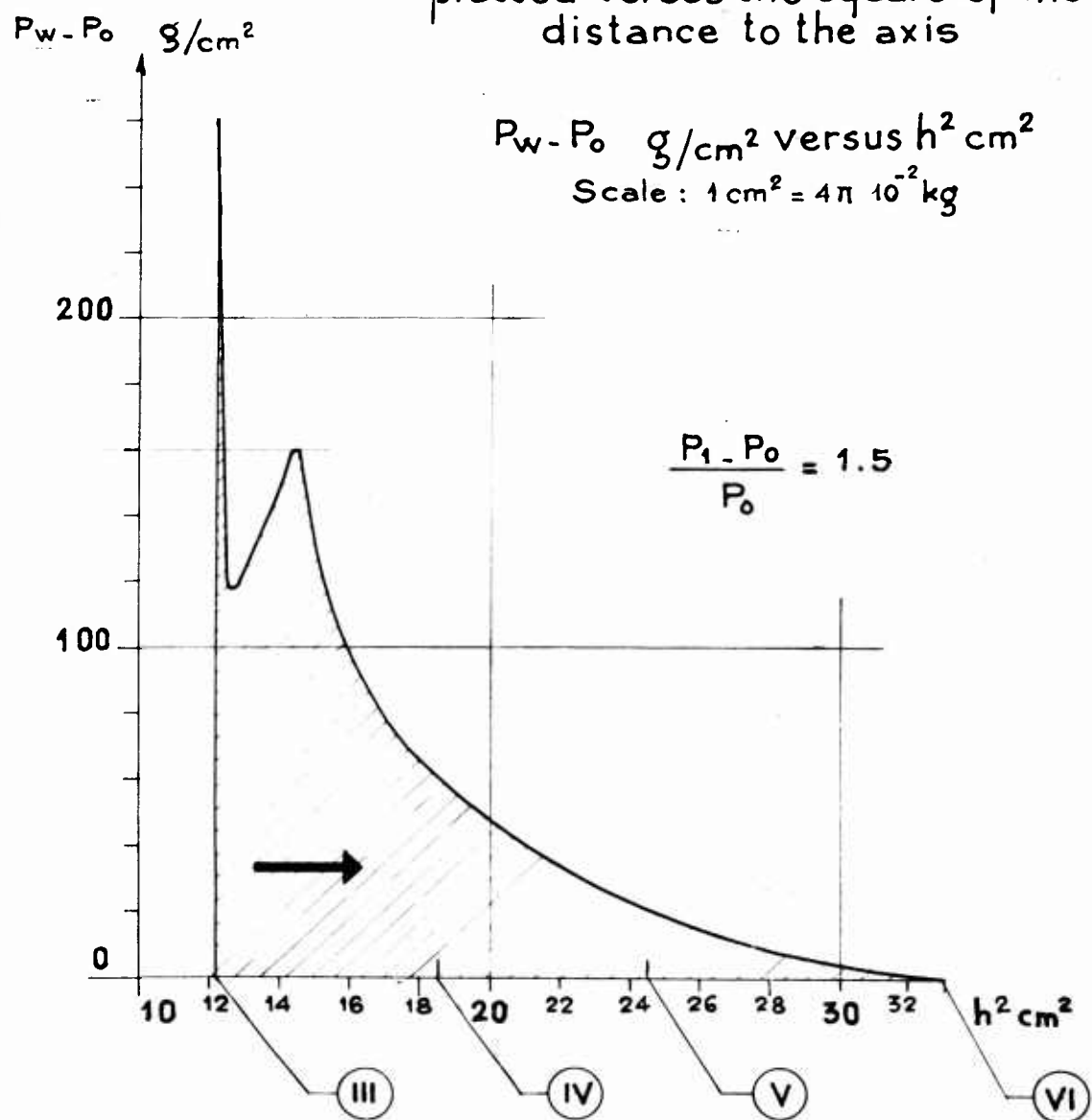
at  $P_1 - P_o = 0.3$



SFERI COANDA

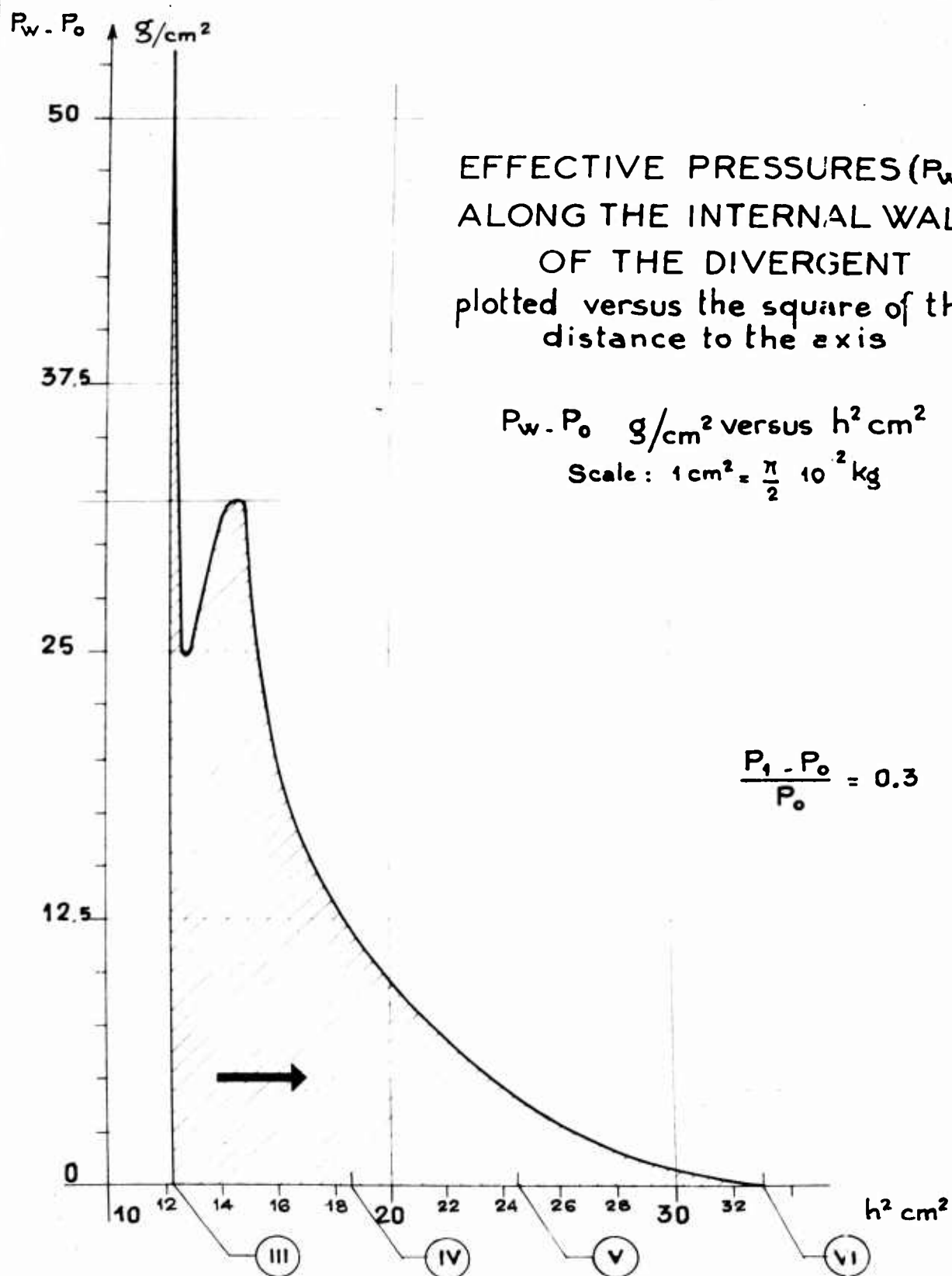
FIG.46

EFFECTIVE PRESSURES ( $P_w - P_0$ )  
ALONG THE INTERNAL WALL  
OF THE DIVERGENT  
plotted versus the square of the  
distance to the axis



SFERI COANDA

FIG. 46bis



SFERI COANDA

**UNCLASSIFIED**

**UNCLASSIFIED**